



THE EFFECTS OF ANKLE-FOOT ORTHOSES ON GAIT
DEVIATIONS ASSOCIATED WITH UNTREATED
DEVELOPMENTAL DYSPLASIA OF THE HIP DURING
WALKING: CASE STUDY

A Thesis submitted by

Redha Burhan Salman Alrikabi

For the award of

Doctor of Philosophy

2019

ABSTRACT

Developmental dysplasia of the hip (DDH) is considered to be one of the most common orthopaedic disorders, referring to a range of conditions from mild to severe dislocation of the hip joint. Knowledge of ankle-foot orthosis (AFO) use in patients with severe developmental dysplasia of the hip bone is crucial and may help improve the gait cycle during walking. The plantar pressure-sensing mat and insole plantar sensor pad are ideal low-cost alternatives to the force plate for capturing plantar centre pressure excursion during gait. Acquired centre of pressure (COP) traces are favoured by many medical clinicians and allied health professionals evaluating foot loading and body balance with respect to foot biomechanics, foot injury, foot deformation and foot ulceration. Researchers have recommended the use of COP traces for the study of the deformed foot and deformed lower limb to improve orthosis assessment and orthosis performance testing. Knowledge of the COP and plantar pressure characteristics such as peak pressure, contact pressure and pressure time integral during walking can help identify possible foot pathology, help determine the most effective foot orthosis, and allow for the appropriate calculation of balance control and joint kinetics and kinematics during gait.

However, there are unclear gait alterations in individuals with DDH which have clinical implications such as the investigation of AFOs and their effect on lower limb kinematics and kinetics, and their impact on the plantar pressure characteristics of the joints during walking and running. This research aimed to provide a better understanding of the gait characteristics of patients with severe DDH.

The first set of objectives was to study and evaluate the kinematics and kinetics of the ankle, knee and hip joints during walking in the sagittal plane for a patient aged 27 years (the author of this research) with severe dysplasia of the left hip, using two different types of ankle-foot orthosis (custom-made, and leaf-AFO). The data were collected using ten cameras and one force plate under four conditions: barefoot, custom-made AFO, leaf AFO, and shoes only. The angles between every two segments were calculated using the Euler rotation sequence. An inverse dynamic approach was used to calculate sagittal joint moments and power. The results showed that the planter flexion angle reached its maximum during the time between the toes-off, the ground phase and the initial swing phase with a mean difference of 21.1° and 14° , respectively.

Moreover, the results indicated that the fabricated orthosis decreased both the right and left extensor moments significantly during the load-bearing phase in comparison to barefoot by a mean difference of 0.29, and 0.43 Nm/kg respectively for both limbs. Results showed that the custom-orthosis had a higher moment during the late stance of the gait cycle compared to barefoot, with the data showing significant change by a mean difference of 0.1604 Nm/kg. However, the Leaf Spring AFO had little impact on the flexion moment during the late stance phase.

The second set of objectives of this study was to evaluate the effect of wearing the two ankle-foot orthosis on the plantar pressure distribution of specific foot regions for the patient with DDH. These objectives were achieved by developing a correlation technique between the COP trajectory and the lower limb trajectory during the three main phases of gait (heel strike, midstance and push off). The lower limb trajectory data were collected using a new close-range photogrammetry system that employed six HD video cameras to capture the lower limb trajectory. The COP trace and

pressure data were collected using 3000E F-scan in-shoe sensors sampling at 100 Hz inserted inside the patient's shoes. Six walking trials (ten steps per trial) were recorded for each condition (barefoot, custom-made orthosis, and Leaf-AFO). The average of the three middle steps was taken out of the ten steps for each trial under each condition. The corresponding results showed that the highest values of the pressure-time integral for the left foot barefoot condition were registered under the lateral heel (LH) 115.92 ± 2.91 kPa.sec, medial heel (MH) 101.66 ± 2.55 kPa.sec, first toe (T1) 73.79 ± 1.85 kPa.sec, fourth and fifth toes (T45) 49.90 ± 1.25 kPa.sec and second toe (T2) 42.94 ± 1.08 kPa.sec.

The research concluded that the kinematics and kinetics of the ankle and hip joint were improved by the custom-made orthosis more than that of the Leaf AFO-Spring Orthoses. The current work also concluded that both AFOs did not much change the kinematics of the knee joint however, there were some improvements in the moments and power generated. Finally, the researcher concluded that both orthoses enhanced body stability, minimized foot pain, and minimizing the risk of injury beneath specific foot regions. More investigations are required in the future, such as the investigation of the customized Knee-Ankle-Foot Orthosis (KAFOs) and increasing the number of samples.

CERTIFICATION OF THESIS

This Thesis is entirely the work of Redha Burhan Salman Alrikabi except where otherwise acknowledged. The work is original and has not previously been submitted for any other award, except where acknowledged.

Principal Supervisor: DR Sharifian-Barforoush

Associate Supervisor: DR ALBERT CHONG _____

Student and supervisor's signatures of endorsement are held at the University.

LIST OF PUBLICATIONS

- 1- Studying the effects of using two types of Ankle Foot Orthoses (AFO) on the hip joint kinematics and kinetics during walking in the sagittal plane for patient with Severe Developmental Dysplasia of the hip; part 1, Submitted and accepted for publication by the International journal of materials, mechanics and manufacturing <http://www.ijmmm.org/>
- 2- Studying and evaluating the effect of using multiple types of AFOs on the kinematics and kinetics of ankle and knee joints while walking as exhibit in the sagittal plane, for a patient with severe untreated dysplasia of the left hip joint. Submitted and accepted for publication by the International journal of materials, mechanics and manufacturing <http://www.ijmmm.org/>
- 3- Gait COP trajectory of left side hip-dislocation and scoliotic patient using ankle-foot orthoses, Proceedings Ninth International Conference on Digital Image Processing (ICDIP 2017); Volume 10420, 104204S (2017) <https://doi.org/10.1117/12.2281547>
- 4- Correlating COP trajectory and 3D lower limb-foot movement for the study of biomechanics in human movement. Prepared and ready to be submitted

ACKNOWLEDGEMENTS

I would like to thank all the people who helped me throughout my PhD journey without whom this thesis would have been tough to complete. I would like to thank my supervisor Dr. Albert Chong for his outstanding contribution despite all the difficult times he went through fighting for his life. Thank you very much Dr. Albert, it was such a pleasure to have you as my supervisor, I have such a great friend for life now.

I would also like to express my gratitude to my supervisor Dr. Ahmad Sharifian-Barforoush for his valuable feedback and help during my time as a PhD student. Thank you very much, your support will always be appreciated and mentioned. I would like, as well, to thank all my colleagues for helping me throughout the experimental work, thank you very much for your valuable effort Dr Kadhem, Mr Ammar, and Mrs Nibras.

I would like to express my gratitude to the Graduate Research School at USQ for supporting me throughout and providing me with a Disability Action Plan Stipend Scholarship for an 18 months period. I would also acknowledge the Research Training Program (RTP) and the Iraqi Government sponsor for their support covering the study fees for the entire three and a half years of my journey at USQ.

To all my family in Baghdad, Iraq, thank you very much. To my friends, Mahmood, Adnan, Ali, Usama, Mustafa, Mohammed, Haraz, Raed, Chris, and Dhriti, thank you for being such great helpers to me.

TABLE OF CONTENTS

ABSTRACT.....	i
CERTIFICATION OF THESIS.....	iv
LIST OF PUBLICATIONS	v
ACKNOWLEDGEMENTS	vi
TABLE OF CONTENTS.....	vii
LIST OF FIGURES.....	xi
LIST OF TABLES	xvi
1 CHAPTER 1: INTRODUCTION.....	1
1.1 background.....	1
1.2 Research problem and aim.....	5
1.3 Research objective	6
1.4 Significance of the research	6
1.5 The selection and evaluation of the related publications.....	7
1.6 The structure of the thesis	8
2 CHAPTER 2: BACKGROUND AND LITERATURE REVIEW	10
2.1 Able-bodied gait cycle.....	13
2.1.1 Phases of the gait cycle.....	13
2.1.2 Temporal and Stride Parameters.....	18
2.1.3 Kinematic Parameters	20

2.1.4	Kinetics Parameters	22
2.2	Image processing technique	26
2.3	GAIT PARAMETERS ASSOCIATED WITH DDH PATIENTS	28
2.3.1	SPATIOTEMPORAL PARAMETERS	28
2.3.2	Lower limbs Kinematics and Kinetics of DDH patients	30
2.4	Types of Orthosis	31
2.4.1	The effects of foot orthosis on Pathological gait parameters	33
2.5	An overview of foot pressure distribution	37
2.6	Foot pressure analysis technique evolution	38
2.6.1	In shoe-plantar pressure system	41
2.7	Foot posture is associated with plantar pressure distribution characteristics 43	
2.8	The effect of walking speed and footwear types on plantar pressure characteristics	51
2.9	Conclusion	56
3	CHAPTER 3: METHODOLOGY	58
3.1	An overview	58
3.2	The limitations of previous methods and justification for using the current method	58
3.3	KINEMATICS AND KINETICS	60
3.3.1	Subjects and case description	60
3.3.2	Measurement system	61

3.3.3	Test protocol and system calibration.....	62
3.3.4	Digitizing and modeling	66
3.3.5	Calculations.....	69
3.3.6	Statistics	73
3.4	Correlation between lower limb movements and plantar pressure characteristics.....	74
3.4.1	Introduction.....	74
3.4.2	The plantar pressure measurement system	74
3.4.3	Low-cost photogrammetry measurement system	75
3.4.4	Data Processing of the correlation technique.....	77
4	CHAPTER 4: RESULTS	85
4.1	An overview.....	85
4.2	The kinematics and kinetics of the lower limbs	86
4.2.1	Ankle joint kinematics and kinetics in the sagittal plane.....	87
4.2.2	Knee joint kinematics and kinetics in the sagittal plane under four conditions	95
4.3	HIP joint kinematics and kinetics in the sagittal plane under four conditions	102
4.4	Plantar pressure distribution.....	109
4.4.1	Right foot characteristics during the three main phases of the gait	109
4.4.2	Left foot characteristics.....	119
4.5	Foot regions characteristics.....	129

4.5.1	Contact area	129
4.5.2	PEAK PRESSURE.....	133
4.5.3	Pressure time integral (PTI).....	137
5	chapter 5 Discussions.....	142
5.1	An overview.....	142
5.2	kinemAtics and kinetics.....	142
5.3	Plantar Pressure Characteristics.....	148
6	CHAPTER 6: CONCLUSIONS	157
7	REFERENCES	160
	Appendix.....	180
7.1	2-in sole shoes F-scan system specifications.....	186

LIST OF FIGURES

Figure 2.1: Healthy hip joint with the femoral head placed correctly in the acetabulum, adapted from	12
Figure 2.2: Patient with hip dislocation, which occurs with the exit of the femoral head from the acetabulum, adapted from	13
Figure 2.3: Main and sub-phases during human locomotion (Burnfield 2010)	14
Figure 2.4: Sub-phases of the swing during human locomotion (initial swing, mid-swing, and terminal swing) (Burnfield 2010)	17
Figure 2.5: Spatiotemporal parameters (Janež et al. 2017).....	19
Figure 2.6: Knee moments and knee power during walking in the sagittal plane for able-bodied individuals (Burnfield 2010)	24
Figure 2.7: Ankle forces: describes the ankle moments and ankle powers during walking in the sagittal plane for able-bodied individuals (Burnfield2010).....	26
Figure 2.8: Experimental setup for healthy participants during barefoot and shod tests, adapted from Najafi et al. (2012).....	43
Figure 2.9: Comparison of maximum force readings between the normal arch and high arch American football players, adapted from (Carson et al. 2012)	50
Figure 3.1: X-ray image of the dislocated area of the patient's left hip joint.....	59
Figure 3.2 (a) Right and left foot shape for the patient with DDH,(b) the leaf- AFO, (c), and the custom-made AFO	60
Figure 3.3: Subject with DDH standing on the force plate during the static trial	61
Figure 3.4: Qualisys PAF package: Istituti Ortopedici Rizzoli (IOR) lower body marker set (Leardini et al. 2007)	63
Figure 3.5: Calibrated volume of the space, which represents the walkway area ...	64

Figure 3.6: Digitized model for a Subject with DDH stepping on the force plate during standing (a) and dynamic trial (b). The red arrow shows the direction of the ground reaction force GRF	66
Figure 3.7: Musculoskeletal model generated by the visual 3D modelling System. Example of a patient with a DDH Stepping on the force plate with the right foot during a dynamic trial (a), and both feet stepping on the force plate during a standing trial (b)	68
Figure 3.8: Musculoskeletal model generated by the visual 3D modelling System, Example of a patient with DDH Stepping on the force plate with the right foot during the five sub-phases of the walking stance trials (initial strike, loading response, mid-stance, push-off, and toe-off). The figure shows the same moments as well for each phase exerted from the video camera.....	70
Figure 3.9: Musculoskeletal model generated by the visual 3D modeling System, Example of a patient with DDH Stepping on the force plate with the left foot affected with DDH during the five sub-phases of the walking stance trials (initial strike, loading response, mid-stance, push-off, and toe-off). The figure shows the same moments as well for each phase exerted from the video camera	71
Figure 3.10: COP trajectory and target imprints' location of the right foot	78
Figure 3.11: Definition of the thirteen main regions according to F-scan software classification	79
Figure 3.12: Example 3D plot of the lower limb coordinates.....	81
Figure 3.13: Examples of the correlation between the lower limb and plantar centre of pressure	82
Figure 4.1: Ankle joint angles for the right limb (a) and left limb(b) during walking in the sagittal plane	88

Figure 4.2: Ankle joint moments for the right limb (a) and left limb (b) during walking in the sagittal plane	90
Figure 4.3: Ankle joint power for the right limb (a) and left limb (b) during walking in the sagittal plane.....	92
Figure 4.4: Knee joint angles for the right limb (a) and left limb (b) during walking in the sagittal plane	96
Figure 4.5: Knee joint Flexion-Extension moments for the right limb (a) and left limb (b) during walking in the sagittal plane.....	98
Figure 4.6: Knee joint Flexion-Extension power generation and absorption for the right limb (a) and left limb(b) during walking in the sagittal plane	99
Figure 4.7: Hip joint angles for the right limb (a) and left limb (b) during walking in the sagittal plane	104
Figure 4.8: Hip joint Flexion-Extension moments for the right limb (a) and left limb(b) during walking in the sagittal plane	106
Figure 4.9: Hip joint Flexion-Extension power generation and absorption for the right limb (a) and left limb (b) during walking in the sagittal plane.....	107
Figure 4.10: Correlation between the COP (b) trajectory and lower limb movement (a) during barefoot walking for a patient with severe developmental dysplasia of the hip joint.....	110
Figure 4.11: The correlation between the center of pressure trajectory (b) and lower limb movements (a) during custom-made-orthosis trial for the patient with severe DDH.....	113
Figure 4.12: The correlation between the plantar centre of pressure trajectory (b) and lower limb movements (a) during walking while the patient is wearing the Leaf -AFO-Spring orthosis	116

Figure 4.13 Ground reaction force along with the entire stance phase for DDH patient right foot under the three conditions; barefoot, custom-made, and Leaf AFO spring orthosis.....	117
Figure 4.14: Peak pressure readings registered under the total foot during the whole stance phase of the gait under three conditions; barefoot, custom-made, and Leaf-AFO-orthosis.....	117
Figure 4.15: Correlation between the COP trajectory (a) and lower limb movement (b) during barefoot walking for a patient with severe developmental dysplasia of the hip joint.....	120
Figure 4.16: Integrating the COP (b) and KC trajectory (a) during walking while the patient is putting on the custom-made orthosis on the left foot	123
Figure 4.17: Integrating the COP (b) and KC trajectory (a) during walking while the patient is putting on the Leaf-AFO orthosis on the left foot	125
Figure 4.18: Peak pressure readings registered under the total left foot during the whole stance phase of the gait under three conditions; barefoot, custom-made, and Leaf-AFO-orthosis	127
Figure 4.19 showing the ground reaction force along the entire stance phase for DDH patient left foot under the three conditions; barefoot, custom-made, and Leaf AFO spring orthosis.....	127
Figure 4.20 Shows Mean, standard deviation (S.D.), and mean differences between each two condition of contact area (CA) for the 13 regions of the left foot with DDH.	130
Figure 4.21:Mean, standard deviation (S.D.) and mean differences between each two condition of contact area (CA) for the 13 regions of the right foot.....	133

Figure 4.22: Mean, standard deviation (S.D.) and mean differences between each two condition peak pressure (PP) for the 13 regions of the left foot with DDH .
..... 135

Figure 4.23 Mean, standard deviation (S.D.) and mean differences between each two-condition peak pressure (PP) for the 13 regions of the right foot137

Figure 4.24 Mean, standard deviation (S.D.) and mean differences between each two condition of pressure time integral for the 13 regions of the left foot139

Figure 4.25 Mean, standard deviation (S.D.) and mean differences between each two condition of pressure time integral (PTI) for the 13 regions of the right foot
..... 141

LIST OF TABLES

Table 2.1 Comparison between active and control groups with and without orthoses in participants with Pes Cavus. adapted from (Najafi et al. 2012)	44
Table 2.2 Comparison of plantar pressure mean values (kPa) in the various areas of the foot for 34 subjects (n=34), adapted from (Fernández-Seguín et al. 2014).....	45
Table 2-3 Pressure–time integral (N s/cm ²) characteristics for the normal foot type group, compared to the idiopathic pes cavus and neurogenic pes cavus groups adapted from (Burns et al. 2005).....	47
Table 2.4 : Mean, standard deviation (S.D.) and coefficient of repeatability (CR) for the peak pressure (PP), contact area (CA), contact time (CT), pressure-time integral (PTI), force-time integral (FTI) and instant of peak pressure (IPP) for the 10 regions of the foot, left and right sides combined. adapted from (Putti, A. et al. 2007)	48
Table 2.5 Widely reported spatiotemporal and plantar pressure variables for children, adolescents, adults and older adults, adapted from (McKay et al. 2017)	49
Table 2.6 Average peak pressure of twenty healthy individuals adapted from the studies of (Segal et al. 2004).....	53
Table 4.1 Shows ankle kinematics and kinetics for the right limb during walking in the sagittal plane for the patient with DDH under four conditions; barefoot, custom-made, and Leaf-AFO. Note, the bold numbers showing the mean difference between conditions is significant, and the P-value is less than 0.025. B vs C refers to the mean difference between barefoot and custom-AFO	93
Table 4.2 Shows ankle kinematics and kinetics for the left limb during walking in the sagittal plane for the patient with DDH under four conditions; barefoot, custom-made,	

and Leaf-AFO. Note, the bold numbers showing the mean difference between conditions is significant and the P value is less than 0.025 B vs C refers to the mean difference between barefoot and custom-AFO 94

Table 4.3 Shows knee kinematics and kinetics for the left limb during walking in the sagittal plane for the patient with DDH under four conditions; barefoot, custom-made, and Leaf-AFO. Note, the bold numbers showing the mean difference between conditions is significant, and the P-value is less than 0.025. B vs. C refers to the mean difference between barefoot and custom-AFO 100

Table 4.4 Shows knee kinematics and kinetics for the left limb during walking in the sagittal plane for the patient with DDH under four conditions; barefoot, custom-made, and Leaf-AFO. Note, the bold numbers showing the mean difference between conditions is significant, and the P-value is less than 0.025. B vs. C refers to the mean difference between barefoot and custom-AFO 101

Table 4.5 Shows hip joint kinematics and kinetics for the right limb during walking in the sagittal plane for the patient with DDH under four conditions; barefoot, custom-made, and Leaf-AFO. Note, the bold numbers showing the mean difference between conditions is significant, and the P-value is less than 0.025. B vs. C refers to the mean difference between barefoot and custom-AFO 107

Table 4.6 Shows hip joint kinematics and kinetics for the left limb during walking in the sagittal plane for the patient with DDH under four conditions; barefoot, custom-made, and Leaf-AFO. Note, the bold numbers showing the mean difference between conditions is significant and the P value is less than 0.025. B vs C refers to the mean difference between barefoot and custom-AFO 108

Table 4.7 the correlation between the COP trajectory and lower limb movement during barefoot walking for a patient with severe developmental dysplasia of the hip joint.	111
Table 4.8 The correlation between the center of pressure trajectory and lower limb movements during custom-made-orthosis trail for the patient with severe DDH...	113
Table 4.9 The correlation between the plantar centre of pressure trajectory and lower limb movements during walking while the patient is wearing the Leaf -AFO-Spring orthosis.....	115
Table 4.10: Right foot characteristics during the main three phases of the gait; heel strike, midstance, and push off under three conditions of barefoot, custom-Made-Orthosis and Leaf-AFO Orthosis	118
Table 4.11 the correlation between the COP trajectory and the lower limb movement during barefoot walking for a patient with severe developmental dysplasia of the hip joint	121
Table 4.12 The correlation between the COP trajectory and lower limb movement for the left foot under custom-made-AFO condition walking for a patient with severe developmental dysplasia of the hip joint.....	122
Table 4.13 the correlation between the COP trajectory and lower limb movement for the left foot under Leaf-AFO-orthosis condition walking for a patient with severe developmental dysplasia of the hip joint.....	126
Table 4.14 left foot characteristics during the main three phases of the gait; heel strike, midstance, and push off under three conditions of barefoot, custom-Made-Orthosis and Leaf-AFO Orthosis	128
Table 4.15 Mean, standard deviation (S.D.) and mean differences between each two condition of contact area (CA) for the 13 regions of the left foot with DDH	130

Table 4.16 Mean, standard deviation (S.D.) and mean differences between each two condition of contact area (CA) for the 13 regions of the right foot132

Table 4.17 Mean, standard deviation (S.D.) and mean differences between each two condition of peak pressure (PP) for the 13 regions of the left foot with DDH134

Table 4.18 Mean, standard deviation (S.D.) and mean differences between each two condition of peak pressure (PP) for the 13 regions of the right foot136

Table 4.19 Mean, standard deviation (S.D.) and mean differences between each two condition of the pressure-time integral (PTI) for the 13 regions of the left foot.....138

Table 4.20 Mean, standard deviation (S.D.) and mean differences between each two condition of the pressure time integral (PTI) for the 13 regions of the right foot140

CHAPTER 1: INTRODUCTION

1.1 BACKGROUND

The hip dysplasia disorder refers to the inadequate progression of the femoral head, the acetabulum, or both. The prognosis for developmental dysplasia of the hip (DDH) is positive if diagnosed early and treated according to a fixed protocol. If diagnosed late or left without treatment, it will progress to early secondary osteoarthritis (Singh et al. 2014). One of the popular treatment options in adults is total hip arthroplasty (THA) combined with an anatomical reconstruction of the acetabulum. The performance of a subtrochanteric shortening osteotomy is sometimes considered a necessary process to prevent nerve palsy in patients with severe hip dislocation (Marangoz et al. 2010). It is essential to detect DDH and intervene to achieve good results. However, there is a huge number of DDH adult patients who have had no treatment at an early age. Patients with untreated DDH face long-term morbidities such as avascular necrosis of the femoral head, degenerative hip osteoarthritis (OA), muscular fatigue and chronic pain, and gait deviations (Maeyama et al. 2009; Shorter, Hong & Osborn 2013; Lewis, Khuu & Marinko 2015; Hartofilakidis & Lampropoulou-Adamidou 2016).

Gait analysis is commonly performed to assess patients' walking patterns, including the study of the kinematics and kinetics of the lower limb in all three planes: sagittal, frontal, and transverse (Williams et al. 2010; Fernando et al. 2013; Nix et al. 2013). This evaluation technique has been regarded as a useful supplement to clinical and radiologic assessment (Williams et al. 2010; Fernando et al. 2013; Nix et al. 2013).

Many studies have investigated the gait patterns of patients who have received various operative treatments DDH. Most of these research studies have reported that the treated patients had an improvement in the gait patterns after the therapy, but they did not return to their normal level of walking (Chang et al. 2005; Hjorth et al. 2014; Sucato et al. 2015). However, there is a limited number of studies investigating the gait pattern of untreated DDH groups (Romano et al. 1996a; Jacobsen et al. 2013). Moreover, several studies have considered lower limb kinematics and kinetics for patients with DDH during walking in the sagittal plane. Several studies have probed reducing the hip flexion angle of the DDH limb and compared the reduced hip extension angle with a healthy group (Romano et al. 1996a; Lai, Lin & Su 1997; Pedersen et al. 2004). Lai et al. (1997) reported that the pelvic kinematics of DDH patients had a smaller maximum anterior tilting of the pelvis compared to the healthy control group. They also stated that during the entire gait cycle, the diseased side of the pelvis in the unilateral DDH group stayed lower than the unaffected side. A few researchers have also investigated the kinetics of the lower limb in the sagittal plane. They stated that the affected limb had a smaller maximum external extension moment of the hip joint and a smaller maximum external flexion moment of the knee than those of the healthy control group (Romano et al. 1996a; Lai, Lin & Su 1997; Pedersen et al. 2004). In terms of power, two studies reported that the diseased limbs had less peak hip power than the those reported from the healthy control group (Romano et al. 1996a; Pedersen et al. 2004).

Many patients with developmental dysplasia of the hip joint disorders experience some gait limitations such as drop foot during the swing phase, mediolateral instability of the ankle joint in the stance phase, and insufficient plantar flexor activity.

These problems result in an asymmetrical gait pattern, decreased gait speed, and affect postural stability and balance (Marangoz et al. 2010). Previous findings suggest that ankle-foot orthoses (AFOs) can manage various lower limb and neuromuscular disorders. These assisted devices had positive impacts on kinematics, balance, and spatiotemporal gait parameters (Franceschini et al. 2003; Desloovere et al. 2006; Enzinger et al. 2008; Damiano, Alter & Chambers 2009; Fatone, Gard & Malas 2009; De Sèze et al. 2011). The custom-molded ankle-foot orthosis is the most commonly used device for patients with inadequate gait cycles, such as cerebral palsy and excessive ankle plantar flexion. The orthosis provides safe ambulation by facilitating toe clearance during the swing phase, decreasing body weight and improving mediolateral stability in the stance phase (Franceschini et al. 2003). The AFO Leaf Spring is a prefabricated polypropylene ankle-foot orthosis designed to support flaccid drop foot. It provides a semi-rigid section for toe clearance and support. The absence of a heel section makes the Leaf Spring more comfortable to wear and provides a better fit in shoes. The AFO Leaf Spring Orthosis has many features such as injection-moulded polypropylene which is lightweight, variable thickness throughout the orthosis providing strength, good toe clearance and support, and excellent fit for most types of shoes.

Several studies have investigated the effects of AFO use on cerebral palsy, stroke and scoliosis rehabilitation (Beckung et al. 2002). Ankle-foot orthoses (AFOs) have been introduced to improve the dynamic efficiency of the gait of children with cerebral palsy to such a degree that gait is well controlled and energy efficient (Figueiredo et al. 2008). Few studies report positive effects of various types of AFOs on the gait kinetics and kinematics of the children with cerebral palsy (Radtka et al. 2005;

Lam WK et al.2005). These effects include increased ground reaction force and plantar flexion moment, increased stride length, and improvement in walking, and running. Franceschini et al (2003) suggested a reduction in stance time and double support combined with increases in walking speed and cadence. Gök et al. (2003) found that custom-molded and metallic AFO orthosis provided an increase in step length, cadence and walking speed combined with a decrease in double support time. They stated that the more solid molded AFO could provide a better outcome than the plastic over the counter AFO orthosis. Simons et al (2009) found that rigid custom-molded AFOs offer significant improvements in the balance scale, timed up and go, and increase the walking and functional ambulatory category (Simons et al. 2009). Some studies have compared the use of Chicagon articulated AFOs with off-the-shelf AFOs. The authors indicated that the Articulated Chicagon Brace provided a high level of improvement in walking speed, measured kinematics parameters such as balance, angle of ankle dorsiflexion, and a massive reduction in spasticity measures over three months for people with stroke and cerebral Palsy (Parvataneni, Olney & Brouwer 2007).

Moreover, some studies have advocated that the combination of shoes and AFO orthosis could have a positive effect on balance performance (Arvin et al. 2013). Fewer studies have compared several non-articulating, polypropylene AFOs of different degrees of stiffness. These studies found that all orthoses increased dorsiflexion in swing, except for the stiffest design which added more stability during the stance phase (Wang et al. 2005; Mulroy et al. 2010). Mulroy et al. (2010) studied and compared the effects of three different types of AFO on walking after stroke. The results pointed out that all three AFOs increased the level of ankle dorsiflexion in the swing and

early stance phases of gait. Both the posterior and rigid AFOs have increased knee flexion and restrict ankle plantar flexion in the loading portion of gait (Mulroy et al. 2010). Only in participants without a plantar flexion contracture, rigid AFO tended to restrict knee flexion in swing and dorsiflexion in the stance phases. The results also showed that those individuals with quadricep weakness could easily tolerate an AFO with plantar flexion mobility in loading. An AFO that permits dorsiflexion mobility in stance can benefit participants without a contracture.

1.2 RESEARCH PROBLEM AND AIM

The literature shows that there is a lack of research regarding the investigation of orthosis devices and their effects on gait pattern plantar pressure distribution for patients with developmental dysplasia of the hip. Thus, this research aims to provide a better understanding of gait characteristics for patients with severe developmental dysplasia of the hip while wearing multiple types of AFO. First, the research will study the kinematics and kinetics of the lower limbs under four conditions (barefoot, custom-made-orthosis, Leaf AFO Spring, and shoes only), and compare these with the published data of healthy individuals. Second, the research will investigate the effect of the two mentioned AFOs on the plantar pressure distribution characteristics during the three main phases of gait: initial strike, midstance, and push off under three conditions: barefoot, custom-made-orthosis, and Leaf AFO Spring.

1.3 RESEARCH OBJECTIVES

- 1- Studying the effect of custom-made and Leaf Spring AFOs on the kinematics of the lower limb for a patient with severe DDH
- 2- Investigating the effect of custom-made and Leaf Spring AFOs on the kinetics of the lower limbs for a patient with severe developmental dysplasia of the left hip in comparison with published data of healthy people
- 3- Studying the plantar pressure characteristics during the primary three phases of the gait under three conditions: barefoot, custom-made AFO, and Leaf Spring AFO
- 4- Studying the pressure distribution under specific regions of both feet during walking under three conditions: barefoot, custom-made AFO, Leaf Spring AFO
- 5- To develop low-cost advanced photogrammetric techniques to correlate the lower limb movements' and centre of pressure trajectory.

1.4 SIGNIFICANCE OF THE RESEARCH

- 1- Understanding the correlation of lower limb movement and plantar pressure data helps to develop new ways to improve the quality of drop foot AFOs for hip dislocation patients
- 2- Improving the understanding of the gait characteristics of patients with severe developmental dysplasia of the hip joint for doctors, podiatrists, and physiotherapists
- 3- Providing a better understanding of various types of AFOs and their effects on the gait parameters during walking in the sagittal plane
- 4- Improved 3D stereo lower limb/foot movement capture system.

1.5 THE SELECTION AND EVALUATION OF RELATED PUBLICATIONS

A literature review was undertaken to select the appropriate and eligible articles for this study. The author used the following resources and publication records (Google Scholar and the USQ Library to retrieve the titles and abstracts of related journal papers. All articles are from quality and peer-reviewed journals. These articles were screened for eligibility according to the following questions: Did the researchers investigate the gait parameters of young healthy adult individuals with developmental dysplasia of the hip, and individuals with lower limb disorders such cerebral palsy?, Did the research investigate the use of AFOs on the gait cycle of healthy and abnormal individuals?, Did the study discuss the kinematics and kinetics of DDH and healthy individuals?, Did the author discuss the plantar pressure characteristics of young healthy individuals and individuals with lower limb abnormalities?.

Then, the author obtained the full articles for detailed assessment and the final decision on inclusion according to the following criteria: 1) Studies which investigated the gait cycle of untreated developmental dysplasia of the hip patients in comparison to healthy individuals, 2) Studies which investigated multiple types of AFOs and their influence on the gait parameters of patients with lower limb abnormalities , 3) Studies of pressure distribution beneath the foot of young, healthy individuals? and 4) Studies written in English.

1.6 THE STRUCTURE OF THE THESIS

The thesis is structured as follows:

- Chapter 1 is the introductory chapter, explaining the background and definition of developmental dysplasia of the hip disorder, research problems and aims, research objectives, the significance of the research, the selection and evaluation of the related publications, and the structure of the thesis
- Chapter 2 forms the literature review, presenting the anatomy of developmental dysplasia of the hip, the gait cycle and phases of gait, the types of orthoses and their effect on pathological gait parameters, foot pressure distribution, and conclusion
- Chapter 3 describes the instrumentation used to perform the study's experiments. The first part shows the measurement system used to calculate the kinetics and kinematics of the lower limb joints, the test protocol, the digitizing and modelling process using visual 3D, calculation, and statistics. In this part, the creation of the author's own musculoskeletal model for a DDH patient is introduced. The second part describes the foot pressure measurement system, image process technique utilized to calculate the 3D coordination of the knee joint, and the correlation between plantar pressure data and lower limb movements
- Chapter 4 presents the ankle, knee and hip joint kinematics and kinetics results while walking in the sagittal plane for the patient with DDH under the mentioned conditions, plantar pressure distribution during the three primary phases of the gait, and foot region characteristics including contact pressure, contact area and pressure time integral parameters
- Chapter 5 presents the main discussions points of the research conducted

- Chapter 6 presents the conclusion of the Thesis

CHAPTER 2: BACKGROUND AND LITERATURE REVIEW

The term developmental dysplasia of the hip (DDH) refers to a range of dislocations from mild dysplasia of the acetabulum or femur to high dislocation of the hip joint. The femoral head must lie in the acetabulum to encourage the healthy development of the hip joint. Secondary osteoarthritis commonly causes DDH disorders in young adults. It is more frequently encountered in women, and in countries such as Japan.

The term DDH replaced the previous name of “congenital hip dislocation” (CHD). DDH is a generic term that refers to a wide range of anatomical abnormalities of the hip, which may be dislocated or may be developed in the first months of a child’s life. This new name has been endorsed by the American Academy of Orthopaedic Surgeons (AAOS), American Academy of Pediatrics (AAP), Pediatric Orthopaedic Society of North America (POSNA), European Paediatric Orthopaedic Society (EPOS) and Brazilian Society of Pediatric Orthopaedics (SBOP) (Guille, Pizzutillo & MacEwen 2000; Martin & Petruneac 2017).

There are three classifications for DDH in adults: 1) low range of dislocation in which the femoral head articulates with a false acetabulum which covers part of the true acetabulum, 2) A dysplasia in which the femoral head lies in the right acetabulum and 3) high range of dislocation in which the right acetabulum is not in contact with the super-posteriorly femoral head (Hartofilakidis et al. 1996; Hartofilakidis, Karachalios & Stamos 2000; Hartofilakidis, Yiannakopoulos & Babis 2008).

The natural history of DDH encompasses many factors such as the presence of a false acetabulum; bilateral or unilateral. Increased contact stresses were thought to be a result of the development of secondary osteoarthritis (OA) (Murphy, Ganz & Müller 1995; Xu et al. 2010). The presence of a false acetabulum can be altered and associated with early development of OA, and may occur as a result of altered loading patterns (Xu et al. 2010). The mean age at onset of hip pain symptoms of Type A DDH is 34.5 years, Type B DDH is 31.2 years, and Type C is 46.4 years (Hartofilakidis, Karachalios & Stamos 2000). Individuals with bilateral Type C DDH may stay free from OA for a long time. Patients with the unilateral disorder may experience difficulties related to leg inequality and other symptoms of the ipsilateral and contralateral knee (Weinstein 1997). Patients with severe hip dislocation may develop lower back pain and compensatory lordosis (Weinstein 1997).

In DDH patients, the acetabulum is ovoid, shallow low cavity and, with the increasing the degree of dysplasia, the superolateral bone stock diminishes (Hartofilakidis et al. 1996). The roof of the acetabular often shows excessive obliquity accompanied by an increase in the acetabular angle (Jacobsen, Rømer & Søballe 2005). Additionally, the containment of the femoral head is reduced, as seen on the coronal plane CT imaging (Jacobsen, Rømer & Søballe 2005). The increasing severity of DDH results in increasing bone stock in the medial acetabular wall, and has been shown to correlate with a degree of subluxation and acetabular depth (Liu et al. 2009). The combination of the above abnormalities results in decreasing acetabular coverage of the femoral head, as shown in Figures 2.1 and 2.2. Moreover, the increase of the acetabular anteversion is somewhat similar to controls, however this increase is not similar to that seen at the femoral neck (Akiyama et al. 2012).

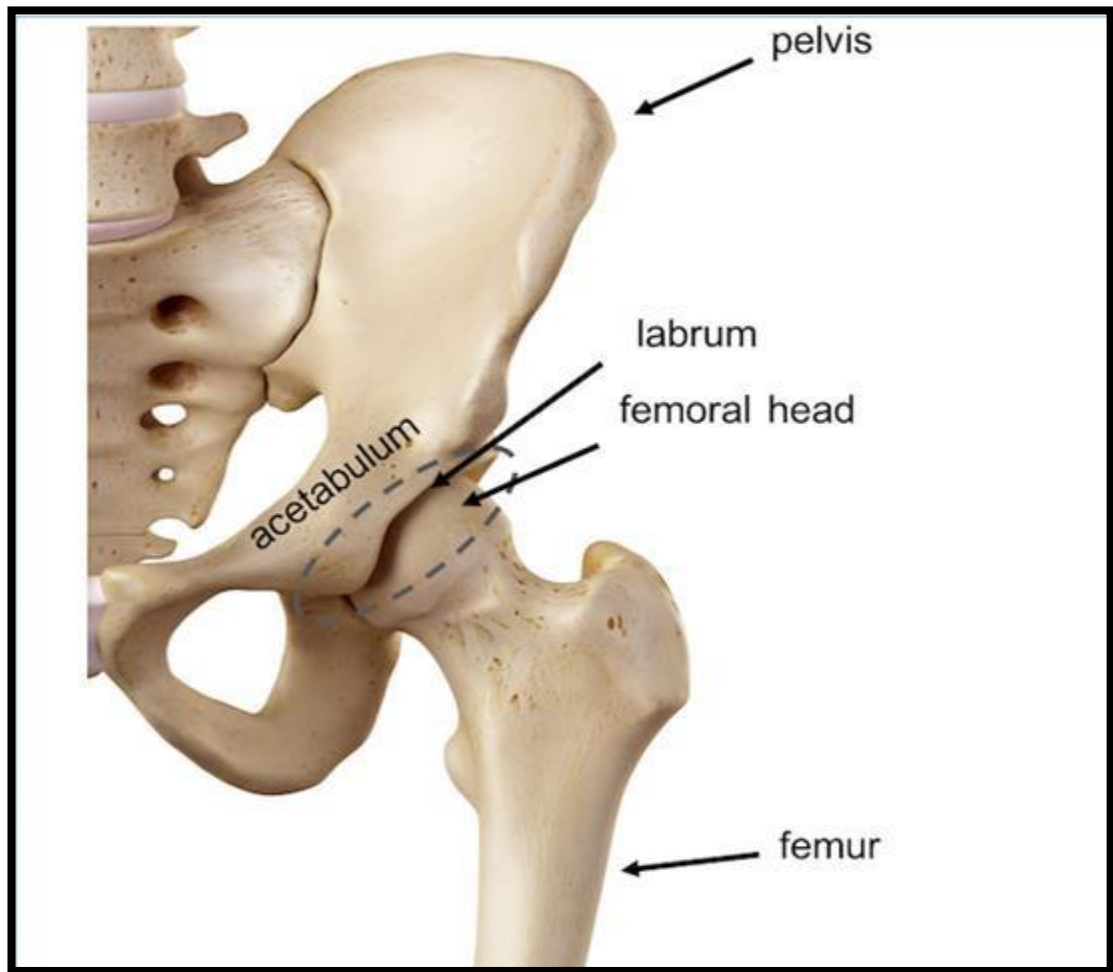


Figure 2.1: Healthy hip joint with the femoral had placed correctly in the acetabulum, adapted from <http://pathologies.lexmedicus.com.au/pathologies/hip-dislocation-luxation>

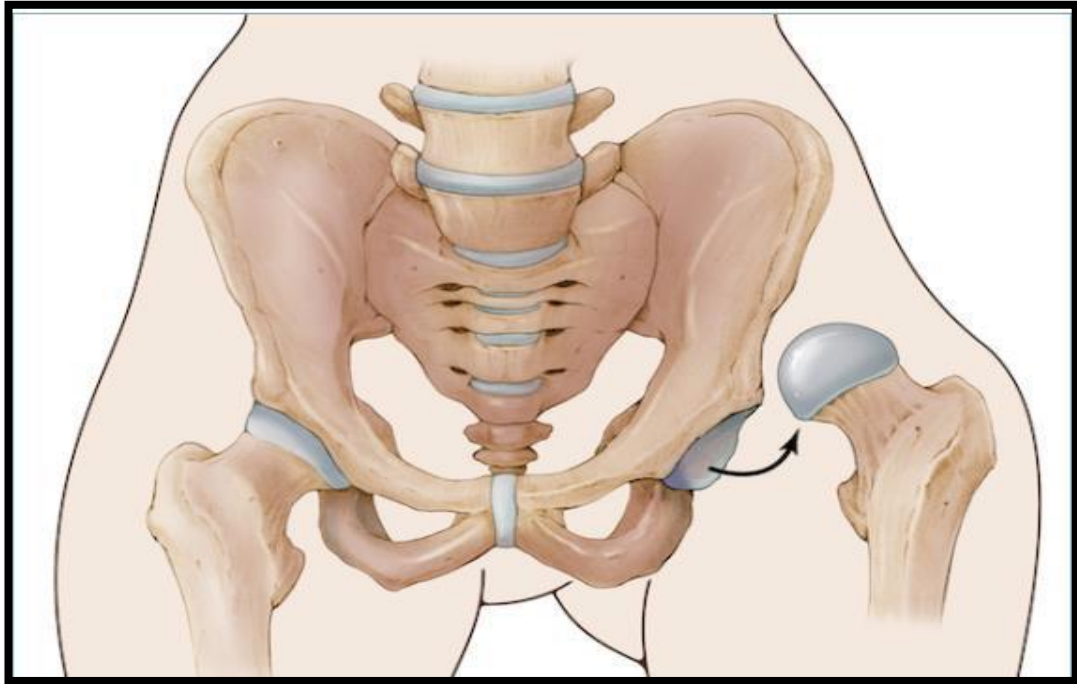


Figure 2.2: Patient with hip dislocation, which occurs with the exit of the femoral head from the acetabulum, adapted from <http://pathologies.lexmedicus.com.au/pathologies/hip-dislocation-luxation>

2.1 ABLE-BODIED GAIT CYCLE

It is necessary to review the gait cycle of healthy individuals, in particular the phases of the gait cycle, the temporal and spatial parameters, and lower limb joint kinematics and kinetics.

2.1.1 Phases of the gait cycle

The successive recurrence of events defines the gait cycle. Healthy individuals' gait is defined by two consecutive heel strikes. The gait cycle is divided into two main phases: stance, and swing. The period between the initial foot contact (heel strikes the ground) and ipsilateral toe-off (same foot pushes off the ground) defines the stance phase. For unimpaired healthy individuals, the stance phase forms approximately 62%

of the whole gait cycle. The swing phase is defined by the time between the ipsilateral toe-off and the ipsilateral heel strike when the foot is no longer in contact with the ground. This second phase forms the remaining 38% of the gait cycle. These two main phases can be subdivided into another eight functional portions as shown in Figure 2.3. These functional phases are initial contact, loading response, and mid-stance, terminal stance, pre-swing, and swing: initial swing, mid-swing and terminal swing (Whittle 1996; Levangie & Norkin 2000; Kaufman & Sutherland 2006; Burnfield 2010; Everett & Kell 2010).

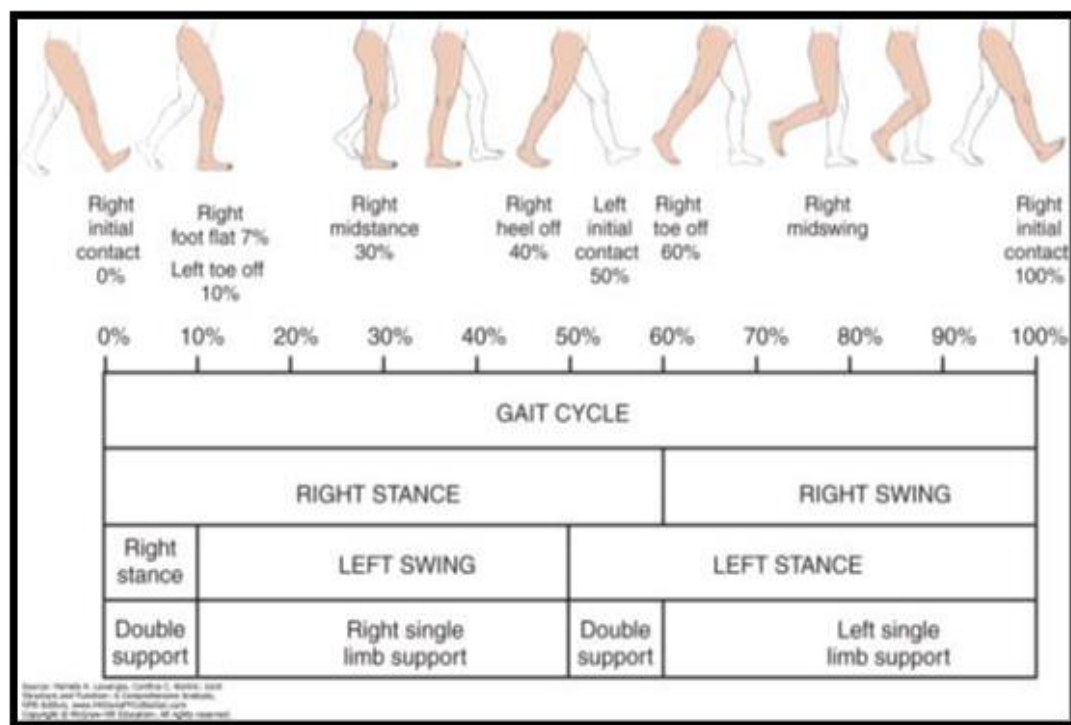


Figure 2.3: Main and sub-phases during human locomotion (Burnfield 2010)

The initial contact phase is defined by the moment the foot first strikes the ground. Although short, this phase is crucial because the lower limb joint orients during the initial contact with the floor affecting the lower limb's loading response. This phase plays a vital role in positioning the limb for stance and load-bearing. The heel acts as a fulcrum by creating a rocker during the moment the heel first contacts the ground. This heel rocker continues into the next portion or the sub-phase, loading response (Burnfield 2010).

Load bearing starts with heel strike and continues as the opposite foot is pushed off the ground (i.e. contralateral toe off). The duration of the loading response phase for healthy bodied individuals is 2-10% of the total gait cycle. The loading response is defined as the first period of double limb support. During this time, several key events occur to achieve the three main objectives: preservation of progression, shock absorption and weight-bearing stability. As previously illustrated, when the heel first touches the ground, it acts as a fulcrum, allowing the foot to rotate at the ankle. The rapid loading of approximately 60% body weight onto the stance phase produces an external plantar flexion moment. This dorsiflexor contracts eccentrically, adjusting the foot as it is lowered to the ground, avoiding foot slap, and prolonging heel support. The prolonged heel support and the advancement of the tibia help to preserve the forward progression of the limb. Shock absorption is another benefit of the dorsiflexor muscle activity since some of the body's downward movement is absorbed by the tibialis anterior as it resists the external plantar flexion moment. During the loading response phase, the knee flexion transmits part of the energy to the contracting quadriceps, providing additional shock absorption. The quadriceps have many responsibilities such as providing weight-bearing stability, resisting the

internal rotation of the tibia, and preventing external knee flexion torque (knee bucking) (Burnfield 2010).

The mid-stance phase forms approximately 10-30% of the gait cycle, occurs during the first half of the single limb support when the contralateral foot is lifted off the ground, and continues until the body is aligned vertically over the ipsilateral forefoot. Passive ankle dorsiflexion results from the forward fall of the body as well as the momentum of the contralateral limb. This passive dorsiflexion moment allows the tibia to transition over the foot, creating what it is called second rocker. Furthermore, the soleus plantar flexor contracts eccentrically to control the rate of dorsiflexion and give more stabilization to the ankle joint.

The second half of the single-limb (terminal stance phase) occurs from 30-50% of the whole gait cycle. This phase starts when the ipsilateral heel rises, and finishes when the contralateral foot strikes the foot again. Moreover, the body advances beyond the supporting foot during the terminal stance, contracting the gastrocnemius and soleus muscles to stabilise heel rise, allowing the body to transition forward over the forefoot creating the third rocker (Burnfield 2010).

The pre-swing phase is considered the last phase of the stance, starting when the contralateral heel strikes the ground and finishes with ipsilateral toe off the ground, which is the second interval of double limb support. At this phase, the bodyweight is fully transferred to the opposite limb to prepare the ipsilateral limb for swing, resulting in decreased loading on the limb and producing rapid plantar flexion of approximately 20%. Thus, this flexion allows the tibia to rotate anteriorly, stabilising the toe on the ground, and resulting knee flexion. Eventually, the toe extensor muscles are active preparing for swing (Burnfield 2010) .

The initial swing phase, which is approximately 60-73% of the gait cycle, begins when the toes are lifted off the ground and ends when the ipsilateral foot is opposite. The main aim of this swing phase is toe clearance. The toe clearance is achieved when the ankle dorsiflexes from its initial 20° plantar flexion to a more neutral position due to toe extensor activity and tibialis anterior. Both dorsiflexion and knee flexion (nearly 60°) result in toe clearance (Burnfield 2010).

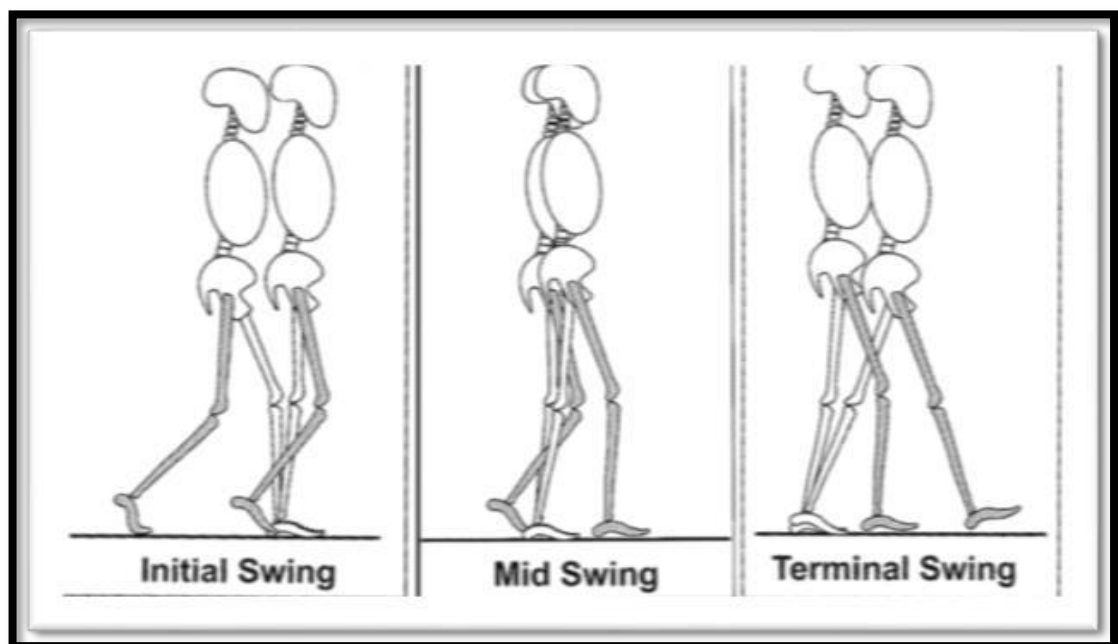


Figure 2.4: Sub-phases of the swing during human locomotion (initial swing, mid-swing, and terminal swing) (Burnfield 2010)

The second portion of the swing phase is the mid-swing (approximately 73-87% of the whole gait cycle). This phase begins when the ipsilateral swinging foot is positioned next to the contralateral stance foot and finishes when the tibia of the ipsilateral foot is vertical (Figure 2.4). The mass of the foot is at higher demand on the ankle when the tibia approaches a vertical position, resulting in increased activity of the tibialis anterior extensor hallucis longus (Burnfield 2010).

The final phase of the gait cycle refers to the terminal swing (approximately 87 - 100%). This phase starts with the ipsilateral tibia located vertically and finishes with the ipsilateral foot touching the ground. During the terminal swing, the limb begins to prepare for the initial contact moment. Pretibial muscle action, especially the tibialis anterior contraction, increases to counteract the inertia of the swinging leg, ensuring that the ankle is neutrally positioned for subsequent heel contact. The knee extends in preparation for this initial contact (Burnfield 2010).

2.1.2 Temporal and Stride Parameters

Many standard temporal and stride parameters are used to evaluate the time of specific events and phase durations of the gait cycle such as cadence, stance and swing duration, as well as the duration of single limb and double limb support. The number of steps taken per unit time (steps/minute) defines cadence. As previously pointed out, for healthy individuals, stance duration is about 62% of the gait cycle, and the swing phase is about 38% of the remainder of the gait cycle. These time percentages are dependent on the individual and velocity.

There are two periods of double limb support for the stance phase, separated by one period of single-limb support. The swing phase happens during single-limb support. The period when only one limb is in contact with the floor defines the single limb support period. During the double limb support period, both ipsilateral and contralateral feet are in contact with the floor. The first 12% of the whole gait cycle, including the period from ipsilateral initial contact to contralateral toe off (loading response), defines the initial period of double limb support. The single-limb support starts over the subsequent 38% of the gait cycle through the contralateral heel strike

(mid- and terminal stance phases). The second limb support (50-62%) occurs during the late stance phase of gait, starting from the contralateral heel strike and ending with the ipsilateral toe-off (pre-swing phase). The final single limb support period spans the entire swing phase (initial, mid- and terminal swing), from ipsilateral toe-off through to ipsilateral heel strike (Figure 2.5).

The most common stride parameters tested during gait are stride length, step length and velocity. The distance between the heel strike of one limb and heel strike of the other limb defines the step length. The stride length is determined by the distance between subsequent heel strikes of the same limb, as shown in Figure 5.2. Finally, velocity is defined as the distance travelled per period (m/sec).

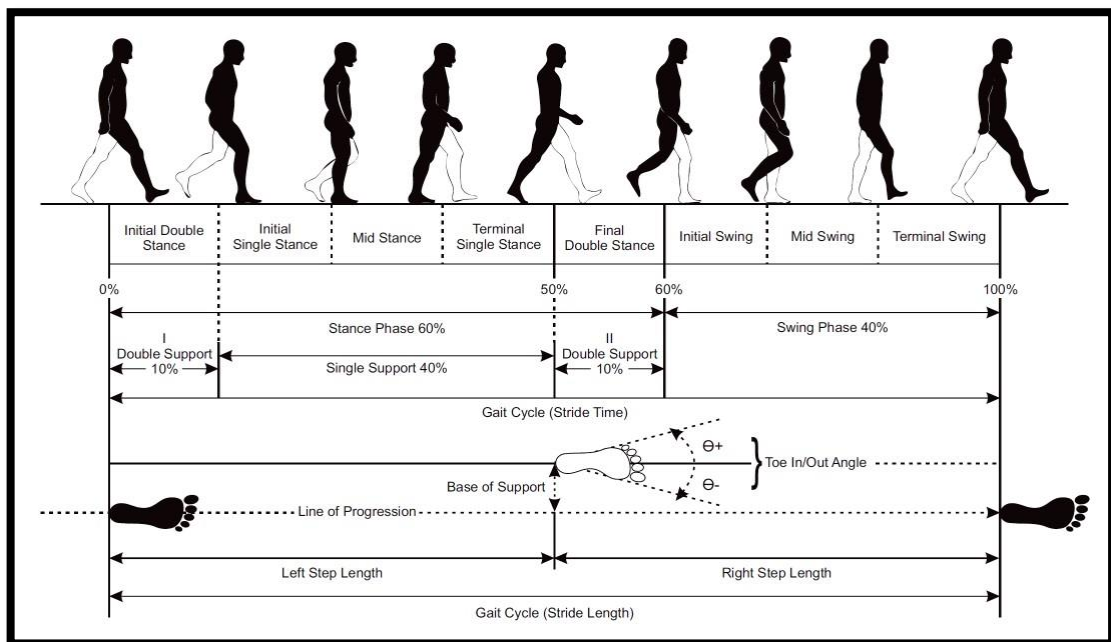


Figure 2.5: Spatiotemporal parameters (Janeh et al.2017)

2.1.3 Kinematic Parameters

The movement of the lower extremities during walking refers to gait kinematics. The kinetic parameters are presented in terms of lower limb joint (i.e. hip, knee, and ankle) angles in the three main planes of motion (sagittal, coronal and transverse). The only sagittal kinematics reviewed in this section are due to the largest ranges of motion observed in this plane during walking gait (Burnfield 2010).

During walking in the sagittal plane (for healthy able-bodied individuals) each lower limb joint shows a characteristic waveform. Each joint transition occurs between periods of flexion and extension along the entire gait cycle (Burnfield 2010).

The normal hip joint range of motion during walking in the sagittal plane at self-selected speed is 40° . At the heel strike phase of the gait, the degree of hip flexion is about 30° . The hip starts to extend until the contralateral foot strikes the ground. Then the ipsilateral hip flexes in preparation for swing as bodyweight is transferred to the contralateral limb during the pre-swing phase of gait. During the terminal swing phase of gait, the ipsilateral hip extensor muscles decelerate the limb in preparation for weight acceptance (Burnfield 2010).

As shown in Figure 2.5, the knee displays two periods of flexion, and it has the most extensive range of motion of the lower extremity joints (approximately 60°). The first knee flexion period occurs during early stance, showing maximum knee flexion of 20° during the moment of transitioning between the loading response phase and the mid-stance phase. The initial knee flexion is a reflection of shock absorption that aids weight acceptance. The knee slowly starts to extend to approximately 5° of flexion during terminal stance (single-limb support). Then, the degree of knee flexion rapidly

increases following contralateral heel strike. During the initial swing phase of gait, the knee flexion moves to approximately 60° to allow the limb to shorten and facilitate toe clearance. A rapid knee extension results from the combination of the inertial shank/foot forces and activation of the quadriceps muscles. Finally, full knee extension occurs just prior to heel strike (Burnfield 2010).

The ankle sagittal plane range of motion has four periods of plantar-flexion and dorsiflexion which relate to the three ankle rockers. Ankle range of motion is about approximately 25° . During loading response (weight acceptance), the neutral position of the ankle joint allows the heel to contact the ground. The foot uses the heel as a fulcrum, rotating to achieve foot flat (heel rocker). Then the plantar flexes to about 5° to provide both shock absorption and deceleration of the tibia. Followed by the rotation of the tibia around the ankle (ankle rocker) just after the forefoot contacts the ground, resulting in what it is called passive dorsiflexion. The maximum angle of approximately 10° dorsiflexion occurs during single-limb support. The centre of mass of the body is located over the metatarsal heads after the contralateral heel strikes the ground, causing the ipsilateral heel to rise. The foot then transitions from 10° dorsiflexion to 15° plantar flexion, rotating over the metatarsal-phalangeal joint (forefoot rocker). Eventually, the ankle rapidly dorsiflexes during the swing phase of the gait, providing foot and toe clearance. At the end of the swing phase, the ankle is back to its neutral position in preparation for heel strike (Burnfield 2010).

2.1.4 Kinetics Parameters

At the time of initial contact, the hip flexes to about 20° , and the bodyweight vector is located anteriorly to the hip joint centre. The impact that results from the abrupt drop of body weight onto the foot requires an instant peak in the extensor hip moment (0.84 N.m/kg). The replacement of the initial inertia with the developing shear forces allows the body weight vector to rapidly realign itself towards the body's centre of mass (COM) and move backwards towards the hip joint. Even though the moment's arm length decreases during the remainder of the loading response phase, a rapid increase in the magnitude of the ground reaction force preserves the need for an extensor moment throughout weight acceptance. The extensor moment becomes half its magnitude (0.44 N.m/kg) towards the end of the loading response portion of gait. During the moment of transitioning from the loading response phase to the mid-stance phase of, the first spike of power generation occurs (0.72 W/kg.m) at approximately 12% of the whole gait cycle, contributing to hip extension (Burnfield 2010).

During the mid-stance phase (25% of GC), the thigh is progressively extended and the hip joint centre moves in front of the bodyweight vector, contributing to a flexor moment. The primary resistance provided by the flexor moment during mid- and terminal stance is the passive resistance from the Y ligament. Throughout the terminal stance phase of gait, the flexor moment increases and reaches its peak towards the beginning of the pre-swing period (1.06 N.m/kg) at approximately 51% of the whole gait cycle. When the body shifts towards the contralateral limb, the flexor moment rapidly declines, generating a second short burst of power (peak 1.14 W/kg.m) at approximately 60% of the entire gait cycle. The rate and magnitude of thigh extension

are controlled by a low-level extensor moment during the latter half of mid-swing and terminal swing phases (Burnfield 2010).

The impact of initial floor contact creates a vector which is vertically oriented and anteriorly aligned to the knee joint. After 1% of the gait cycle, a low magnitude flexor moment (0.35N.m/kg) is produced to prevent knee hyperextension as energy is generated (1.0 W/kg.m). During the loading response phase, the knee is rapidly flexed, and an extensor moment is produced to ensure stability across the joint (0.52 N.m/kg), and power is absorbed due to the eccentric activity of the vastii (peak 0.8 W/kg.m) at approximately 8% of the entire GC (Figure 2.6). In the early mid-stance phase, at about 16% of the gait cycle, the knee extension is augmented by the peak power generation of 0.5 W/kg.m . Then, the knee extensor moment is rapidly diminished by the end of the mid-stance phase, presenting a small flexor moment which persists through terminal stance (peak 0.36 N.m/kg) at approximately 38% of the entire gait. During the pre-swing and terminal swing phases, the rate of rapid knee flexion is modulated by a low amplitude extensor moment (peak 0.21 N.m/kg) at approximately 58% of the GC. During the same period, peak power absorption of 1.2W/kg.m occurs with the knee at about 59% of the entire gait. During the late swing phase, the knee is extended, the flexor moment is increased again to peak magnitude of 0.26 N.m/kg at approximately 93% of the entire gait cycle, and power is absorbed to peak amplitude of 0.9W/kg.m at 90% of the gait as the hamstrings eccentrically control the rate of knee extension (Burnfield 2010).

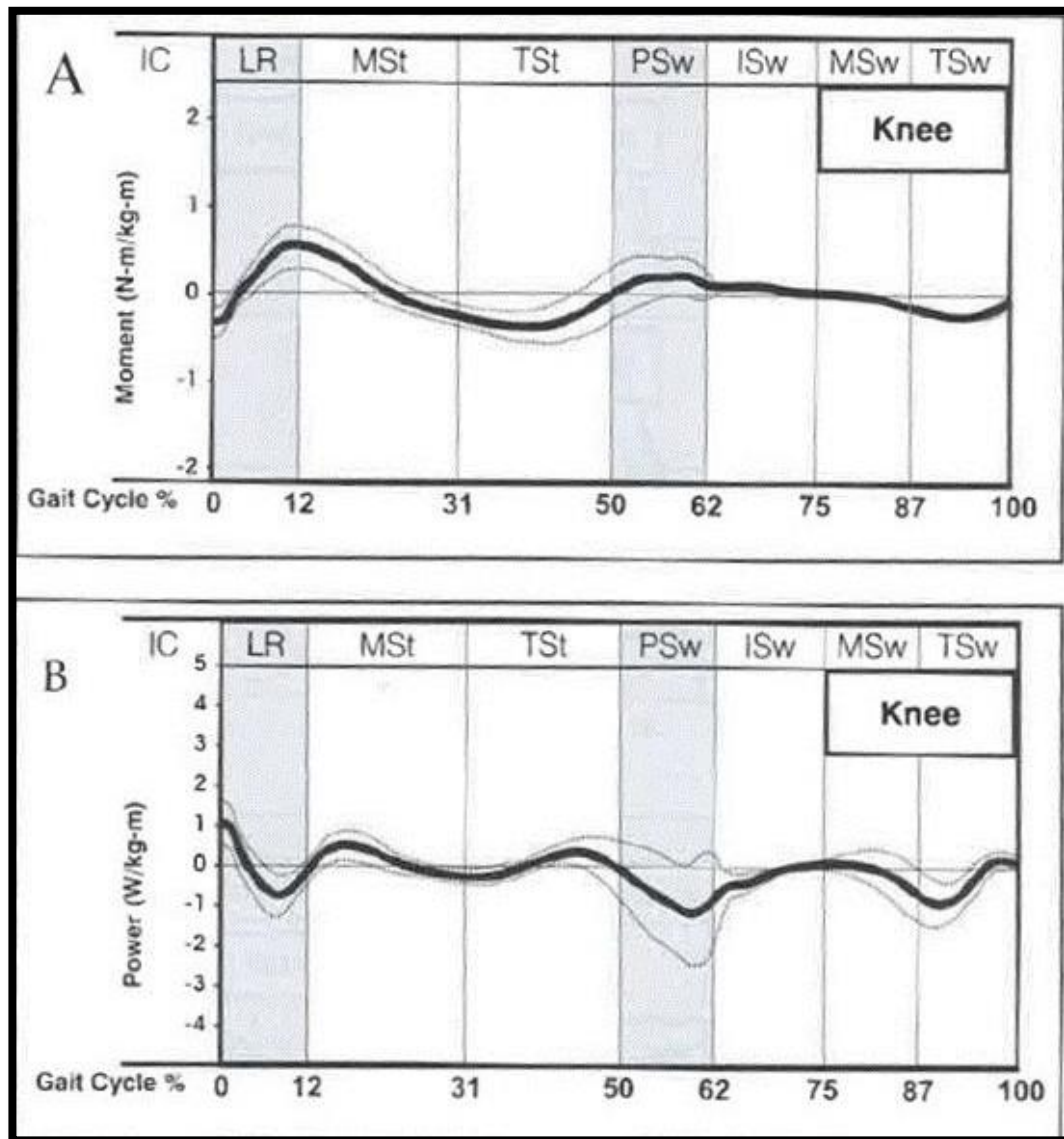


Figure 2.6: Knee moments and knee power during walking in the sagittal plane for able-bodied individuals (Burnfield 2010)

During the initial contact phase of gait, the body vector is placed posteriorly to the ankle joint, and a low magnitude dorsiflexor moment is needed early in this phase to control foot lowering ($0.18\text{N}\cdot\text{m}/\text{kg}$) at approximately 4% of the entire gait cycle, thus generating an immediate peak of absorptive power ($0.15\text{W}/\text{kg}\cdot\text{m}$). By the end of the loading response, the centre of pressure rapidly advances, the body vector is positioned anteriorly to the ankle joint, and the ankle dorsiflexor moment is reduced to zero at 12% of the entire gait. The generation of low amplitude power at the end

of the weight acceptance portion of the stride reflects concentric control of the pretibial as they function to draw the tibia forwards. The plantar flexor moment increases during the period of transitioning to SLS as the centre of pressure is progressively moved ahead of the ankle joint (Burnfield 2010).

Approaching the end of the terminal stance phase just before the contralateral foot strikes the ground, the plantar flexor moment reaches its peak magnitude of 1.40N.m/kg at approximately 47% of the entire gait cycle. Therefore, limiting the ankle dorsiflexion to 10 degrees, thus preserving the height of the centre of mass and the position of the vector over the metatarsal heads. The power absorption peak of 0.54W/kg.m predominates until the latter half of the terminal stance at approximately 40% of the GC, which reflects the eccentric control provided by the flexors at the plantar during the entire single limb support (Burnfield 2010).

During the pre-swing phase of gait, tension in the gastrocnemius and soleus musculotendinous unit is released by the rapid unloading of the trailing limb that follows ground contact by the contralateral foot thus, generating a strong burst of 3.7W/kg.m power at approximately 54% of the GC. This is called a push-off event. At the onset of the swing phase, the foot is lifted for clearance by a small generated moment of 0.03 N.m/kg at 62 % of GC (Burnfield 2010).

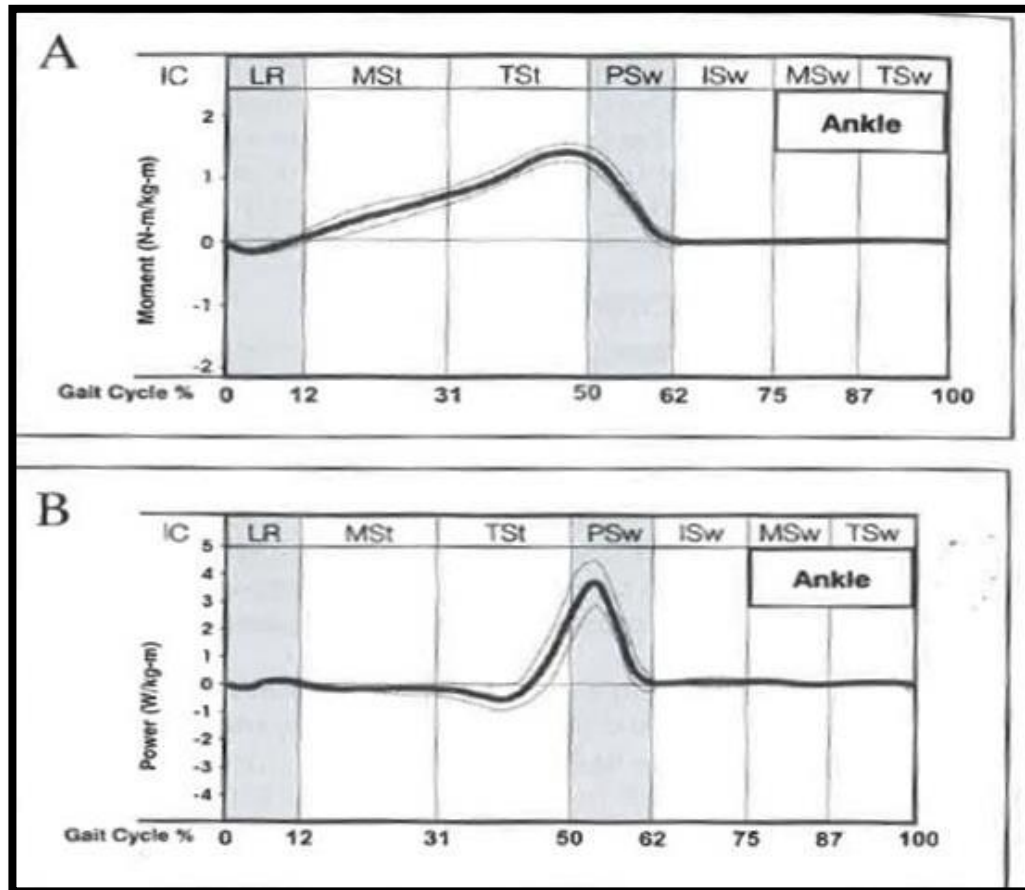


Figure 2.7: Ankle forces: describes the ankle moments and ankle powers during walking in the sagittal plane for able-bodied individuals(Burnfield 2010)

2.2 IMAGE PROCESSING TECHNIQUE

Image-based motion capture and photogrammetry image processing methods have been used widely for the creation of a 3D movement model of the lower limb and foot. These models are utilized by doctors, podiatrists, and physiotherapists to develop reliable treatment strategies for individuals suffering from physical disorders such as drop foot, spinal cord injuries and joint dislocation (Peter 2007). While several technologies such as electromagnetic sensors and inertial systems have been utilized to address fast human movement tracking, the optical imaging system utilizing photogrammetric targets on the object is still considered one of the most accurate and reliable techniques (Chong 2012, Al-Baghdadi 2013). The method has a few limitations. These include: (1) suitable imaging sensor geometry or

configuration (Chong 2012), (2) definition of axes associated with each bony segment incorporated in the model and (3) preparation time for imaging target placement (Cappozzo et al. 2005). However, photogrammetric techniques are still considered practical for this research. Therefore, further study: 1) to determine the suitability of photogrammetric methods for capturing the 3D movement of the lower limb and the foot plantar pressure .

3D object modelling systems and techniques create a 3D surface model, and these models can be animated into 3D solid or stick models for a straightforward interpretation of human movement based on anthropometric markers. Nevertheless, some efficient 3D capturing systems, such as flat-bed scanners and laser scanners, are only suitable for static or slow movement of the body. In the study of scoliotic subject gait, knowing the dynamic change of the lower-limb and foot shape at normal gait speed is crucial. Thus, these two techniques are not suitable for this investigation. Recently, Chong et al. (2012; 2015) developed precision techniques for correlating force plate recording and foot shape using close-up imaging sensors. The approach was based on accurate time stamps for synchronizing between video recording and force plate recording.

The analysis of joint kinetic data, including muscle force and joint reaction force, has enhanced the dynamic study of sport and exercise of both healthy and lower limb pathological individuals (Adouni & Shirazi-Adl 2014). Understanding the pathomechanics of individuals can be achieved by analysing COP spatial relationships relative to the location of primary joints in normal gait. In previous research, COP has been an excellent index to calculate the balance of individuals in

gait, and undertaking exercise and sport (Carpenter et al. 2001; Karlsson & Frykberg 2000). COP would be suitable for motion evaluation and rehabilitation applications (Jamshidi et al. 2009). Other studies have shown the use of COP trace to provide a set of references to evaluate the function of orthoses during walking Aboutorabi et al. (2014) and Chockalingam et al. (2008) assessed the COP pattern and moments in scoliotic subjects during normal walking. They showed wide variations in the mediolateral direction COP which could be related to the laterality of both the primary and compensation curves. The authors argued that individuals with a higher left compensation curve had more significant displacement to the left.

2.3 GAIT PARAMETERS ASSOCIATED WITH DDH PATIENTS.

2.3.1 SPATIOTEMPORAL PARAMETERS

Many studies have investigated the spatiotemporal parameters in untreated DDH compared with a healthy control group. Several studies pointed out that patients with hip dislocation had a slower walking speed than those with an able-bodied gait cycle. However, the study of Pedersen et al. (2004) showed that there is no significant change in walking speed between the healthy controls and patients with severe untreated DDH. Their results pointed out a walking speed-reading of 4.5km/h for DDH individuals. Also, the studies of Jacobsen, Rømer and Søballe (2005) stated that there is no significant difference in the running speed of DDH patients and people in a healthy control.

In terms of stride length parameters, the study of Romano et al. (1996a) reported that individuals with DDH walked with a shorter stride length than those of healthy

individuals. The authors also found no significant difference in the duration of the stride cycle between the DDH and healthy control. Moreover, the results of the same study found no significant difference between the affected limb and the healthy control regarding the duration of the stance phase however, the unaffected side had a longer stance phase duration than the affected side and healthy control. Lai, Lin and Su (1997) investigated walking cadence and proved that there is no significant difference between the healthy group and DDH group. Their results also pointed out that the diseased side with hip dislocation had a shorter single support time than both the unaffected side and healthy control.

Finally, the diseased limb had a longer double support time than the healthy control according to some studies. The studies of Romano et al. (1996a) showed that both the limb affected by DDH and the unaffected limb had a slower foot velocity than those of the healthy control. They also found that the diseased limb had a slower foot velocity than the healthy limb. Of relevance to our project, the literature shows no study investigating the walking parameters and spatiotemporal time parameters of patients with severe DDH while using an AFO. Thus, in this research, we are aiming to look at the differences in these parameters for four conditions: barefoot, custom-made AFO, and Leaf Spring AFO and shoes only.

2.3.2 Lower limbs Kinematics and Kinetics of DDH patients

Romano et al. (1996a) reported that the diseased hip had a smaller maximum flexion angle than the healthy control during single limb stance phase. The results of their studies showed a reduction in the diseased hip maximum extension angle in comparison to the healthy control group. Moreover, they found that the diseased hip showed a greater maximum external rotation angle than the healthy control however, the healthy unaffected hip had a greater maximum internal rotation angle than those of healthy individuals. A few studies showed that the limb with DDH had a greater maximum knee flexion angle, greater maximum ankle plantar flexion, and greater maximum ankle dorsiflexion angle than the healthy group. The studies of Lai, Lin and Su (1997) pointed out that healthy individuals had a higher maximum anterior tilting of the pelvis than the limb affected with DDH along the entire gait cycle. The same study found that the diseased limb of unilateral hip dislocation patients showed an increased pelvic drop during the whole stance phase than the healthy side.

In terms of the kinetic parameters findings, the investigation of Romano et al. (1996a) on subjects with different degrees of dysplasia (from mild to severe degree of dysplasia) showed that the affected limb had a smaller maximum flexion moment of the hip joint than the healthy control. The authors also found that healthy individuals had a greater maximum extension moment of the hip joint, greater maximum flexion moment of the knee joint, and higher ground reaction force readings than those of DDH individuals. Few studies have investigated the peak power in the lower extremity joints (hip, knee). They found that the hip with DDH has less reading of power generation and power absorption in the hip joint “the period from late stance to early swing phase,” and less peak of power absorption in the knee joint (the period from

middle to late stance phase of the gait) than that of healthy individuals (Romano et al. 1996a). However, the results of the peak ankle power readings during the stance phase showed no significant difference between the diseased limb and healthy controls data.

2.4 TYPES OF ORTHOSIS

The AFO is a device used to control the knee joint in weight-bearing because of weakness, absence of muscle function or deformation in the knee joint, and to provide stability for individuals with lower limb weaknesses in walking and standing phases. KAFO is prescribed as a solution for many disorders, which cause muscular weakness of the lower limb such as peripheral neurological diseases (poliomyelitis and post-polio syndrome, spina bifida, polyneuropathy), muscular diseases and central neurological diseases (spinal cord injury and multiple sclerosis) (Cullell et al. 2009). AFO devices provide control for ankle and knee joints and can be worn unilaterally or bilaterally depending on the requirements (Fatone 2006). Several types of knee ankle-foot orthoses have been developed: passive devices and active devices (Stance control KAFO and Dynamic KAFO) (Tian, Hefzy & Elahinia 2015).

Passive AFOs do not require any power system. These devices lock the knee joint throughout the extension in both stance and swing phases. There are three types of passive AFO joint: polycentric knee joint, posterior offset knee joint, and straight-set knee joint. The straight-set knee joint with drop lock consists of a simple hinge joint and a sleeve that moves over to unlock/lock the joint automatically. The individuals can easily reposition their centre of mass by using the posterior offset joint KAFO. The polycentric knee joint provides more stability as the knee's centre of rotation keeps the body weight anterior (Tian, Hefzy & Elahinia 2015).

Various types of assistive devices have been developed to improve the walking and standing parameters for spinal cord injuries (Motloch et al 1992). HKAFO is essentially a KAFO device which extends along the hip joint to provide more trunk stability and support the spine (Nenel et al. 1996). These mechanical orthoses are divided into: traditional orthosis hip knee AFO (HKAFO) and HGO the hip guidance orthosis, RGO reciprocating gait orthosis, ARGO the advanced reciprocal gait orthosis, the isentropic reciprocating gait orthosis (IRGO) and the medial linkage orthosis (MLOs), and the walkabout orthosis (WO) (Moore and Stallard 1991). The hybrid system of ARGO-FES was developed to improve the gait parameters of SCI individuals (Jaspers et al. 1995). The factors of energy expenditure, weight, size and lack of cosmetics have limited the use of these devices by paraplegic patients included in the studies of Kim et al. (2009) and Bernardi et al. (1995). The hip abduction device generally consists of a pelvic harness (right and left) which is connected with joint support by four clip fasteners supplied and with a connector plate that can be adjusted to five different settings depending on pelvic girth and the upper part of device which surrounds the hip. The upper part is connected with an assembly joint (bar) by two bolts where the last is attached onto the lower side of the bar and covered by a thigh shell using two bolts.

2.4.1 The effects of foot orthosis on Pathological gait parameters

SCKAFO flexes the knee during the stance phase and rotates the knee joint freely during the swing phase. Irby, Bernhardt and Kaufman (2005) developed an electronically controlled dynamic knee brace system and later commercialized it as the Ottobock's Sensor Walk. Irby showed the difference between thirteen subjects of experienced KAFO users and eight of novice users. Novice users tended to have high velocity (55 vs. 71 cm/s, $p=0.048$) and increased cadence to (85 steps/min, $p<0.05$). Arazpour et al. (2015a) developed an electrically powered knee ankle foot orthosis which locks the knee during the stance phase and provides active assistance for both knee flexion and extension during the swing phase.

The outcomes of gait symmetry for poliomyelitis patients were improved for the symmetry index in step width ($p = 0.037$), swing time ($p = 0.014$), stance phase percentage ($p = 0.008$), and knee flexion during swing phase ($p \leq 0.001$) and these results were better than using the normal one. Cadence is not significantly different between both of conditions ($p=0.751$) (Arazpour et al. 2016). Yakimovich et al. (2006) developed a friction belt clamping mechanism for SCKAFO. The kinematics gait analysis was performed on three male subjects suffering from quadriceps muscle weakness. The result showed that knee flexion increased by a mean of 21.1° for all subjects during the swing stage, knee range of motion increased by 23.2° as an overall average, less pelvic obliquity, and hip abduction angle abnormalities. The stance-flexion range of motion increased by a mean of 5.6° (Yakimovich, Lemaire & Kofman 2009). Continuing to this work, Lemaire et al. (2009) presented the angular-velocity control (the rotary-hydraulic device). The results showed that the new one gave more safety and body balance for people with lower extremity weakness. Shamaei et al.

(2013) developed a quasi-passive compliant stance SC, that can be fitted into a normal KAFO. The new CSCO displays various levels of stiffness during the engagement\ disengagement phases by using control algorithm depending on the linear spring, which implements in parallel with knee joint.

Hwang et al. (2008) presented in their work the biomechanical effect of an electromechanical knee ankle foot orthosis on four female KAFO users with poliomyelitis (37 years old, 159 cm height, 56 kg in weight). The results showed that that using the developed KAFO decreased the amount of energy consumed by 33% compared with the passive orthosis (locked-knee-joint).

Sawicki and Ferris (2009) presented a pneumatically powered KAFO with myoelectric activation and inhibition. By fitting the device on one individual with muscle weakness in the lower limb, the outcomes stated that the new KAFO produced approximately 22-23% of the peak knee flexor moment, 15-33% of the peak extensor moment, and 42-46% of the peak plantar flexor moment. McMillan et al. (2004) presented the preliminary evidence for the effectiveness of a stance control orthosis. Data was collected on three male subjects with significant weakness in at least one lower limb. All three subjects increased speed and cadence, increased stride and increased step lengths. Two subjects exhibited lower heart response and lower energy consumption. Lawn et al. (2015) presented the development of an actuation system for rotary hydraulic brake on a low-cost, lightweight knee ankle foot orthosis to rehabilitate stroke victims. Cullell et al. (2009) stated that the biologically based design of an actuator system for a knee-ankle-foot orthosis. By testing the device on two poliomyelitis patients, the results pointed out that by means of compensations applied by an actuated orthosis, the feasibility of improving gait pattern significantly in

patients with proximal leg weakness has been improved (Cullell et al. 2009).

Many types of HKAFO that have been developed to rehabilitate individuals with spinal cord injury. There are two groups of HKAFO: passive orthosis and active orthosis. The reciprocating gait orthosis (RGO) is a bilateral hip-knee-ankle-foot orthosis (HKAFO) which has been employed to rehabilitate patients with neuromuscular disorders (Douglas, Larson & McCall 1983). Butler, Major and Patrick (1984) developed a unique device, the hip guidance orthosis (HGO), which allows the leg to swing straight forward efficiently, reinforcing the leg braces that protect them from damage during a sudden bend or twist.

Stallard et al. (1986) designed a parawalker orthosis which is used to enable paraplegic patients to have better a walking gait and to provide enough support for the user's body. Patients with tetraplegia experienced a significant change in energy expenditure when the functional electrical stimulation (FES) interfaced with a RGO (Isakov et al., 1992). Massucci et al. (1998) evaluated the energy expenditure of six individuals with spinal cord injury walking with advanced reciprocating gait orthosis (ARGO). The authors stated that that high energy cost and slow walking were the main reasons for low utilization by paraplegic patients. Scivoletto et al. (2003) developed the prototype of an adjustable advanced reciprocating gait orthosis (ARGO) for SCI patients. They concluded that the device reduced the percentage of ARGO rejection.

Genda et al. (2004) designed a new walking orthosis for a paraplegic hip and ankle linkage system which keeps both feet parallel to the floor during walking. Nascimento et al. (2008) developed a new powered hip orthosis by Pneumatic Artificial Muscle.

They found that patients with poliovirus witnessed a huge gait improvement as the design of the new hip orthosis provided a satisfactory and comfortable use of the device throughout the gait cycle. Audu et al. (2010) stated that the variable constraint hip mechanism (VCHM) with controller provided more control of the hip joint. The device reduced the walking speed of patients with paraplegia by 25% due to the heavy weight of the mechanism and controller.

Onogi et al. (2010) compared the effects of sliding medial – hip joint (Primewalk system) and a hinge – type medial hip joint (Walkabout system). The authors stated that the average gait velocity of patients with paraplegia was higher, cadence was faster, and stride length was longer with the Primewalk than the Walkabout. Arazpour et al. (2012) designed a new powered orthosis for paraplegic patients. They suggested that this device could be a suitable for those individuals who have adequate ranges of motion and could be ideal for other impaired lower limb functions such as those associated with stroke, poliomyelitis and traumatic brain injury. Gait parameters in paraplegic patients have been improved by using the advanced reciprocating gait orthosis with solid versus dorsiflexion assist ankle-foot orthosis. These show an increase in mean walking speed, stride length and the mean ankle joint ranges of motion (Bani et al., 2013). Continuing this work, Arazpour et al. (2013) stated that the use of actuated movements of the hip and knee joints in the newly powered gait orthosis increased both of step length and gait speed.

Bani et al. (2015) designed a new medial reciprocal linkage orthosis (MLO) with lower-limb paralysis simulated. It showed improvements of kinematics and kinetic parameters for patients with paraplegia. Katsuhira et al. (2014) showed the increase in pre-swing gait parameters such as hip joint flexion when the adult patients with post-stroke hemiparesis used a new trunk orthosis providing resistive force. Arazpour et al.

(2015b) demonstrated that energy consumption is less when using an isocentre reciprocating gait orthosis (IRGO) with dorsiflexion–assisted AFOs.

2.5 AN OVERVIEW OF FOOT PRESSURE DISTRIBUTION

In the world of the biomechanics of human gait and posture analysis, foot pressure distribution plays a massive role in accessing the hidden information under the foot with the surface in contact. Pedobarography is referred to as the study of foot posture acting between the foot contactings with the supporting surface (Hughes 1993). The clinical diagnosis on foot deformities is considered to be the beginning of the revolution of foot posture, creating an understanding of concepts fundamental to static posture or dynamic foot pressure movements through different perspectives (Morton 1930; Elftman 1934). Few studies have investigated pressure distribution (Rupérez et al. 2012) qualitatively, while others worked on evaluating the foot pressure quantitatively by considering foot sensitivity aspects (Luo, Berglund & An 1998; Sánchez-Rodríguez et al. 2012).

Typical investigations of earlier studies focused on foot diseases and deformities. The enormous interest in foot posture and pressure studies led to the development of new tools and systems measurements for foot pressure distribution (Razak et al. 2012). The most recent studies have paved the way for new areas of sports biomechanics and biomedicine such as the development of medical and non-medical devices designed to enhance sport s performance.

The proper developmental foot pressure distribution analysis setups can produce accurate and reliable foot pressure measures for modelling analysis. The integration and relationship between independent (walking speed, footwear, surface contact and

inclination) and the dependent variables (peak pressure and the centre of pressure) were considered in most modelling for informative patterns and knowledge discovery used in the decision-making processes (Xiong et al. 2013). Foot pressure distribution characteristics are highly reliant on particular features with informative results integration. Foot pressure distribution pattern analysis was reported using data mining techniques like the Artificial Neural Network (ANN) to create a generic model which predicts the pressure distribution across the foot (Rupérez et al. 2012).

2.6 FOOT PRESSURE ANALYSIS TECHNIQUE EVOLUTION

The earliest studies on foot pressure distribution settings were conducted using simple equipment using ink (Soames 1985). To date, many researchers have aimed to develop an accurate modern technology with sensory foot measurement equipment (Klimiec et al. 2016). However, research using current scientific technology devices for pressure distribution across the foot only started from the 1985 (Soames 1985). The preliminary approach to foot pressure analysis discovered by (Soames 1985) was about integration between dependent variables, specifically the pressure time-integral. He indicated that the foot pressure distribution could be related to either peak pressure data or the temporal variables. Most importantly, only a minimum of two temporal variable measurements linking with foot pressure distribution can be generated. The advances in technology used has proven that foot pressure distribution measurements can be correlated with peak pressure and temporal paramours, as well as with walking velocity, loading, inclination, and surface foot contact (Soames 1985).

To our knowledge, foot pressure distribution has been investigated from two significant aspects: static and dynamic gait. Both aspects consider that data collection has a temporal effect, on either the postural basis or during dynamic movements such as gait analysis, respectively (Skopljak et al. 2014). The kinetograph was the device used during the earliest stage of foot pressure studies. This simple device was obtained from the elasticity of a rubber mat that measures the foot pressure during walking motion (Morton 1930). The kinetograph was validated by the images extracted from x-rays. It was even enhanced by placing a black rubber mat with reflecting pyramidal projecting fluid on a glass plate. The contact area between the foot and the glass created what it is called the footprint. The footprints were recoded underneath the underlying heavy glass (Elftman 1934).

Early studies only focused on foot deformities or foot illnesses only. From 1985 onwards researchers began to explore sports biomechanics, ergonomics and the footwear industry with the help of the growing advanced technology systems (Zulkifli & Ping 2018). The newest technology, such as the platform system and in-shoe system, offered electrical sensors to be connected with computer software to scan, generate and collect more accurate foot pressure data. Some studies used the MatScan (TekScan, USA) system on obese and non-obese individuals to examine foot pressure characteristics. The authors analysed the data of barefooted individuals walking at different speeds on plantar pressure platforms (Butterworth et al. 2015). A few researchers used in the shoe-pressure system (FScan, South Boston, MA, USA) to collect foot pressure data from walking at different speeds on a treadmill (Zhang & Li 2013).

The pressure distribution under the human foot can be classified according to the subject's posture and foot health status. The range of pressure data is different between the normal healthy foot and the abnormal diseased foot under similar conditions, whether using the pressure platform system or in-shoe system experiments (Zulkifli & Ping 2018). Some studies showed that the higher pressure recorded under the abnormal feet in specific regions compared with healthy normal feet due to various foot sensitivity and health conditions (Patil, Thatte & Chaskar 2009). For instance, foot ulcers can result in excessive foot plantar pressure in specific foot regions (Razak et al. 2012; Searle et al. 2017). Thus, higher foot pressure was mostly recorded and observed beneath the abnormal feet of unhealthy subjects such as patients with foot illness, diabetic and older people or those subjects performing heavy duties (Resch et al. 1997; Patil, Thatte & Chaskar 2009). Foot pressure distribution and peak pressure area of athletes depend on the type of activities and sports. Thus, the key for the assessment of the foot pressure data relates to many considerations such as the subject's foot health status, age and activities being performed (Zulkifli & Ping 2018).

2.6.1 In shoe-plantar pressure system

The in-shoe system can be embedded easily in the shoe to measure and assess the pressure distribution between the foot and shoe (Razak et al. 2012). Due to its high flexibility, mobility, simplicity and applicability to different types of footwear, the in-shoe system is favored over the plantar pressure platform system. The in-shoe system applies to different materials, features and heights of the heel section of the shoes. One of the most noticeable advantages is that the subjects can walk freely and have natural gait during the tests, avoiding the troubles of platform targeting (Ledoux et al. 2013). Hence, the in-shoe system is suited to multiple tests types such as indoor and outdoor uses, and can be used for a wider range of sports activities as the system is portable within the shoes and socks (Burnfield et al. 2004; Mei et al. 2015). The ergonomics of footwear or foot deformities can be easily analysed throughout the in-shoe system.

Plantar sensitivity is associated with posture control, so the one limitation of the in-shoe system is that the sensor's performance sensitivity may be perturbed while inserting insoles in the shoes (Machado et al. 2017). A few studies have found that inserting the insoles improperly during walking or running gait can result in tissue breakdown, leading to high pressure and discomfort on the foot contact area with the floor. Also, the number of sensors of the in-shoe system is just sufficient to cover the area inside the shoes, unlike the plantar platform system (Putti, A. B. et al. 2007). The replication of experiments and the heat and sweat trapped inside the shoes can also affect sensor performance and results analysis (Woodburn & Helliwell 1996). The slipping of the sensors while using the in-shoe system is another limitation mentioned of the studies of (Razak et al. 2012).

It is worth noting that the plantar pressure platform system has the advantage of performing barefooted motion experiments. However, it is dependent on the laboratory area to accommodate the various plantar pressure platforms lengths. Meanwhile, the in-shoe system can allow the study of subject's motions characteristics on different types of shoes (such as heel size, shoe materials, and shapes) to be tested on different footwear (Zulkifli & Ping 2018). The weakness is that the number of sensors placed within the shoe coverage is limited from as few as three according to the studies of Putti et al. (2007) and Pataky et al. (2011), and up to 10 placements according to another study conducted by Soames (1985). Hence, the previously mentioned features of the plantar pressure platform system and in-shoe system have their advantages and weaknesses. Therefore, deciding which method is suitable to be selected for a particular experiment can be crucial and dependant on the patient's status. Real-time measurement of natural gait is crucial factor for ensuring ideal and accurate foot pressure readings. Unfortunately, none of the two systems have a standard guideline to ensure natural gait of the foot pressure measurements. Thus, during tests, the individuals have to be verbally instructed to walk at a self-selected comfortable speed (Zulkifli & Ping 2018).

The plantar platform system and in-shoe devices system require various types of force sensors such as the semiconductor strain gauge transducers, critical light deflection Dynamic Foot Morphology, Lion System S.A., Foetz, Luxembourg, capacitive strain gauge, capacitive sensors –emed1 platform systems and Pedar1 in-shoe system (Novel, Germany), resistive sensors (also known as a force-sensing resistor, FSR), MatScan1 platform system and F-Scan1 in-shoe system (TekScan, Boston, MA) and force sensor with light deflection Biokinetics dynamic optical pedobarograph

(Biokinetics Inc., Bethesda, USA) (Zulkifli & Ping 2018).

2.7 FOOT POSTURE IS ASSOCIATED WITH PLANTAR PRESSURE DISTRIBUTION CHARACTERISTICS

A study investigated the effect of the custom foot orthosis on the dynamic plantar pressure loading of 154 individuals with painful pes cavus feet (Najafi et al. 2012), the experimental setup is shown in Figure 2.8. The authors indicated that peak pressure magnitude in pes cavus was significantly higher than those of healthy able-bodied individuals by 51% on average. Moreover, the authors suggest that the increase in peak pressure magnitude was due to the higher body mass index (BMI) of pes cavus individuals. The authors illustrated that wearing the custom-made foot orthosis decreased the second peak pressure magnitude and redistributed the pressure across the foot, thus minimizing foot pain and reducing the risk of injury, as shown in Table 2.1 below (Najafi et al. 2012)..

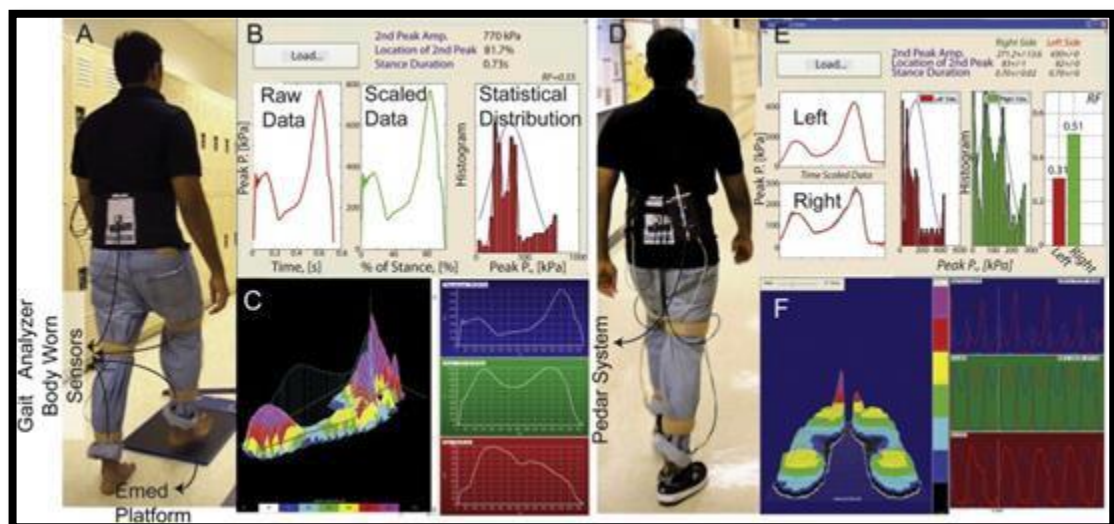


Figure 2.8: Experimental setup for healthy participants during barefoot and shod tests, adapted from Najafi et al. (2012)

Table 2.1: Comparison between active and control groups with and without orthoses in participants with pes cavus, adapted from Najafi et al. (2012)

	Shod without orthoses				Shod with orthoses			
	RF Index	2 nd Peak Mag. [kPa]	2 nd Peak Location [% of stance]	Stance duration [s]	RF Index	2 nd Peak Mag. [kPa]	2 nd Peak Location [% of stance]	Stance duration [s]
Active	0.30±0.15	405±90	78.3±3.2	0.75±0.07	0.46±0.15	348±97	79.3±2.9	0.74±0.08
Control	0.30±0.15	402±98	78.0±3.3	0.76±0.10	0.32±0.16	376±102	78.4±2.8	0.76±0.09
% of Change	-	-	-	-	44%	-8%	1.1%	-2.6%
p-Value	0.77	0.75	0.39	0.20	<10 ⁻⁷	0.02	<0.005	0.17
Mean difference and its 95% CI	0 [-0.03,0.04]	3 kP [-18,25]	0.3% [-0.4,1.1]	-0.01 s [-0.03,0.01]	0.14 [0.09,0.20]	-28 kPa [5,50]	0.9% [0.3,1.6]	-0.02 s [-0.3,-0.01]

The studies of (Fernández-Seguín et al. 2014) showed that the second and third metatarsal heads had the highest pressure readings in both neutral feet and cavus feet in the study. The authors indicated the high pressure readings were due to the anatomical structure of the two zones supported by the reviews of De Doncker and Kowalski (1976), with the M2 and M3 bones being wedged between the cuneiform joints, thus having less degree motion freedom (Table 2.2). The authors observed that in pes cavus feet, the load was significantly higher than neutral feet under the entire metatarsal heads region except for the fifth metatarsal, considering the forefoot as the most vulnerable area in cavus feet individuals (Fernández-Seguín et al. 2014).

Table 2.2: Comparison of plantar pressure mean values (kPa) in the various areas of the foot for 34 subjects (n=34), adapted from Fernández-Seguín et al. (2014)

	Normal foot (n = 34)	Pes cavus (n = 34)	p
Pressure 1st toe	100.14 (± 3.46)	56.69 (± 3.05)	<0.001
Pressure other toes	27.51 (± 2.41)	15.95 (± 1.53)	0.02
Pressure 1st metatarsal	55.56 (± 3.53)	99.12 (± 4.25)	<0.001
Pressure 2nd metatarsal	123.03 (± 4.86)	158.36 (± 6.08)	0.01
Pressure 3rd metatarsal	157.44 (± 3.06)	186.44 (± 6.72)	0.03
Pressure 4th metatarsal	114.98 (± 3.22)	147.21 (± 7.26)	0.02
Pressure 5th metatarsal	52.89 (± 2.66)	65.01 (± 4.26)	0.11
Pressure forefoot	631.36 (± 9.61)	728.69 (± 24.14)	0.03
Pressure metatarsal	503.79 (± 9.32)	656.12 (± 22.39)	<0.001
Pressure midfoot	28.62 (± 1.48)	34.08 (± 2.48)	0.28
Pressure hindfoot	270.13 (± 6.15)	300.45 (± 8.07)	0.23
Contact area	165.04 (± 20.68)	118.26 (± 30.31)	<0.001

Noticeably, the most important finding of their studies was that the structure of the foot showed only an increase in the pressure readings of the first four metatarsal regions with no alteration in the load distribution under the mentioned regions (Fernández- Seguín et al. 2014). Also, the authors pointed out a reduction in the pressure readings on the toes of cavus feet in comparison to neutral feet (Statler & Tullis 2005; Fernández-Seguín et al. 2014). According to (Statler & Tullis 2005), the alterations of the intrinsic stabilizers of the toes in the long extensor and long flexor muscles cause what it is called “claw toe-deformities”. This claw toe decreases the pressure readings under the first toe.

Regarding the contact area in pes cavus feet, the results of few studies indicated a smaller contact area reading, which is structurally accepted due to the associated deformities and that they are more rigid and less capable of absorbing impact during strike than normal feet (Franco 1987; Benedetti et al. 1997; Williams III et al. 2001). Moreover, few research studies illustrated that the reduction in the of the plantar contact area is highly related to the greater load per unit area in both forefoot and hindfoot regions, and that could be a risk for many lower limb injuries (Gravante et al. 2005). A significant reduction was observed in the study regarding the weight-bearing area of cavus feet in comparison to neutral feet (Fernández-Seguín et al. 2014). It has been reported that the better redistribution of the foot pressure under all the regions of the foot can be the result of a greater area of contact between the foot and the floor during strike, especially the areas that are subjected to the highest loads. Similarly, the poorer redistribution of foot pressure under the midfoot area in pes cavus was implied by a reduction in the contact area (Sneyers et al. 1995).

Another study was conducted with seventy subjects: thirty subjects with pes cavus unknown aetiology, ten subjects with pes cavus of neurological aetiology, and thirty subjects with normal foot type (Burns et al. 2005). The authors found that the recorded pressure-time integral magnitude was higher in the cavoid groups compared to the healthy normal individuals (Table 2.4). Therefore, the authors suggested that the higher-pressure time integrals registered in the idiopathic pes cavus group resulted from the increase in peak pressure beneath the forefoot and rearfoot regions (Burns et al. 2005). Such an increase in forefoot and rearfoot peak pressure may occur due to the lack of load-bearing beneath the midfoot area, and these findings are in line with other studies conducted by Rosenbaum et al. (1994). Moreover, the

authors illustrated that the increase in the pressure-time integral magnitude recorded under the neurogenic pes cavus group was the result of the longer foot contact time with the floor. The reason behind such an increase in the contact time could be due to the lower limb weakness of the participants recruited in this study which alters normal dynamics of the foot during walking gait cycle (Burns et al. 2005). This is supported by the studies of Benedetti et al. (1997).

Table 2-3: Pressure–time integral (N s/cm²) characteristics for the normal foot type group, compared to the idiopathic pes cavus and neurogenic pes cavus groups adapted from (Burns et al. 2005)

Foot region	Normal foot type (N = 30)	Idiopathic cavus (N = 30)	Neurogenic cavus (N = 10)
Whole foot	23.8 (5.1)	29.7 (7.4)*	37.2 (23.7)*
Rearfoot	8.5 (1.9)	10.4 (2.3)*	14.2 (5.7)*†
Midfoot	2.3 (1.0)	2.1 (1.7)	6.8 (8.7)*†
Forefoot	18.4 (5.5)	24.1 (8.0)*	31.4 (25.1)*

The study of Putti et al. (2007) pointed out that the highest peak pressure measurements in the shoe were in the area of the hallux, followed by pressures registered under the heel and the first, second, and third metatarsal regions. The authors indicated that the highest pressure in the big toe area was due to the pressure exerted throughout the toe-off phase of gait when the whole-body weight passes through it. So, wearing tight shoes with a narrow toe box could deform the pressures under the hallux. This could be the reason behind the high incidence of hallux valgus throughout the shod population. Noticeably, the largest contact area observed in the study was under the heel region, followed by the midfoot region, and the contact area of the hallux was only 8 cm². Moreover, the results showed the pressure-time integral of the healthy individuals who participated in the study was highest under the heel, first, second, third metatarsal region, then the great toe (Table 2.4) (Putti et al. 2007).

Table 2.4 : Mean, standard deviation (S.D.) and coefficient of repeatability (CR) for the peak pressure (PP), contact area (CA), contact time (CT), pressure-time integral (PTI), force-time integral (FTI) and instant of peak pressure (IPP) for the 10 regions of the foot, left and right sides combined, adapted from Putti et al. (2007)

Pedar ⁴⁰ masks	PP (kPa)		CA (cm ²)		CT (ms)		PTI (kPa s)		FTI (N s)		IPP (ms)	
	Mean (S.D.)	CR ^a	Mean (S.D.)	CR	Mean (S.D.)	CR	Mean (S.D.)	CR	Mean (S.D.)	CR	Mean (S.D.)	CR
Heel	264.3 (44.1)	2.4	41.54 (6.4)	1.2	470.1 (103.9)	3.6	64.58 (12.7)	3.5	145.03 (37.2)	3.9	78.92 (28.5)	8.0
Mid foot	109.0 (38.5)	5.4	21.58 (6.3)	2.5	511.3 (116.8)	4.2	39.18 (17.5)	5.7	43.08 (27.9)	5.5	250.0 (108)	9.8
1 MT ^b Head	248.0 (70.1)	3.9	12.29 (2.3)	2.7	498.9 (84.1)	4.4	65.43 (22.3)	4.8	48.05 (19.1)	4.9	502.8 (55.8)	2.8
2 MT Head	246.5 (48.3)	2.6	12.67 (2.0)	2.1	523.6 (73.7)	3.3	65.52 (16.3)	3.8	52.19 (16.2)	4.8	496.8 (55.5)	2.9
3 MT Head	224.7 (50.4)	2.9	6.79 (1.0)	1.2	549.3 (68.9)	3.6	62.96 (16.3)	4.0	28.97 (10.1)	4.4	487.7 (57.4)	2.8
4 MT Head	161.0 (49.7)	4.6	6.26 (1.1)	2.8	557.0 (76.8)	3.2	49.29 (17.1)	5.5	20.08 (8.8)	5.2	469.1 (62.5)	2.8
5 MT Head	141.6 (58.4)	7.7	6.23 (1.3)	3.0	543.9 (98.2)	2.8	46.53 (20.4)	7.6	18.93 (9.6)	7.1	445.2 (74.4)	3.5
Hallux	280.4 (83.0)	5.5	7.86 (1.4)	3.0	487.2 (112.3)	3.3	60.29 (20.6)	7.6	24.83 (10.7)	7.9	534.3 (60.1)	2.7
Second toe	138.9 (55.3)	10.5	7.72 (1.8)	4.5	394.5 (110.8)	4.3	28.93 (13.3)	13.6	9.89 (5.1)	14.7	530.4 (61.8)	3.1
3-5 Toe	121.3 (45.5)	8.7	7.48 (2.3)	6.0	429.2 (110.5)	6.7	29.52 (12.9)	9.7	9.19 (5.4)	10.8	523.1 (62.4)	2.9

The studies of McKay et al. (2017) established normative reference values for spatiotemporal and plantar pressure parameters. They investigated the influence of demographic, anthropometric and physical characteristics for one thousand individuals aged 3-101 years. The study showed the peak pressure magnitude increasing from childhood through to older adulthood (Table 2.5). The children experienced the highest pressure beneath the rearfoot, while adolescents, adults, and older adults recorded the highest pressure at the forefoot. There are many reasons behind the highest pressure in older adults such as aging effects on the mechanical properties of the ankle and foot leading to pronated foot posture, increasing plantar soft tissue stiffness, increasing plantar fascia thickness, and decreasing ankle joint ROM and strength. Thus, the changes in foot posture may reduce the ability of the ankle joint to respond quickly to such repetitive stresses and affect force attenuation as proven in the studies of Kwan, Zheng & Cheing (2010). Noticeably, an increase in the forefoot peak pressure in adults is associated with a decrease in the in-dorsiflexion ROM (Mueller et al. 1989; Morag & Cavanagh 1999).

Table 2.5: Widely reported spatiotemporal and plantar pressure variables for children, adolescents, adults and older adults, adapted from McKay et al. (2017)

	Male	Female	Male	Female	Male	Female	Male	Female
Spatiotemporal parameters								
Gait velocity (cm/s)	119.6 (21.0)	122.0 (20.5)	135.4 (16.7)	134.2 (14.3)	130.9 (15.0)	133.1 (14.6)	119.7 (17.5)	117.1 (21.8)
Stride length (cm)	99.5 (18.4)	99.9 (18.9)	141.8 (13.7)	134.4 (12.2)*	140.0 (13.3)	134.7 (11.8)*	129.0 (15.6)	120.7 (15.0)*
Stride width (cm)	7.2 (2.6)	7.0 (2.5)	7.7 (2.5)	7.2 (2.5)	9.0 (2.7)	8.1 (2.6)*	8.8 (3.0)	7.3 (92.9)*
Cadence (steps/min)	145.9 (18.8)	149.9 (26.0)	115.5 (10.4)	120.6 (8.0)*	112.5 (8.0)	119.4 (7.7)*	111.9 (9.8)	116.4 (11.5)*
Double support time (%GC)	18.1 (2.4)	18.7 (3.2)	20.6 (2.9)	20.5 (3.0)	23.3 (2.5)	22.0 (2.4)*	24.6 (3.6)	24.2 (3.7)
Maximum mean pressure (kPa)								
Rearfoot	67.0 (34.3)	76.1 (31.0)	99.2 (25.5)	102.1 (28.2)	105.6 (24.2)	99.5 (26.8)*	106.3 (37.4)	99.1 (32.1)
Midfoot	11.4 (8.8)	13.1 (12.0)	20.7 (14.6)	16.2 (12.6)*	26.2 (17.3)	22.0 (15.6)*	23.3 (22.0)	24.8 (17.9)
Forefoot	79.1 (35.3)	84.0 (30.0)	147.7 (51.0)	147.9 (40.5)	181.7 (55.8)	180.3 (45.7)	207.4 (73.9)	201.5 (74.0)
Whole foot	94.5 (4.9)	99.3 (31.9)	154.8 (49.1)	154.1 (38.1)	182.8 (55.2)	181.5 (44.7)	210.1 (73.0)	203.8 (72.5)
Peak pressure (kPa)								
Rearfoot	249.3 (129.3)	269.6 (120.1)	365.4 (129.2)	341.0 (92.3)	375.0 (122.6)	345.7 (113.5)*	356.7 (148.3)	319.9 (113.7)*
Midfoot	49.3 (26.9)	49.1 (34.0)	71.3 (41.1)	57.1 (35.5)*	80.6 (44.3)	74.4 (46.7)	75.9 (63.3)	84.7 (52.7)
Forefoot	230.0 (80.0)	245.1 (87.0)	433.4 (161.4)	431.0 (116.2)	523.9 (164.8)	527.7 (148.3)	576.1 (200.0)	570.3 (190.1)
Whole foot	290.9 (124.0)	310.8(120.3)	475.8 (163.9)	456.1 (111.9)	540.7 (168.0)	541.7 (147.0)	591.8 (203.5)	580.2 (186.4)

The studies of Carson et al. (2012) examined the difference in loading patterns on 26 American football players with high and normal arch structures. The results indicated that the players with high arch height experienced different loading patterns while walking than those players with typical arch structures (Figure 2.8). Most of these loading pattern differences were evident in the medial foot region and lateral heel region, resulting in a more rigid foot less capable of dissipating forces related to contact with the floor. In other studies, low arch feet were a better shock absorber than normal high arch feet (Simkin et al. 1989), and the low arch feet registered decreased force and peak pressure under the regions of normal arch (Nigg, Cole & Nachbauer 1993) as shown in the Figure 2.9. Furthermore, individuals with high arch structure experienced stiffer foot mechanics during dynamic loading and greater maximum force in comparison to normal arch individuals (Powell et al. 2011).

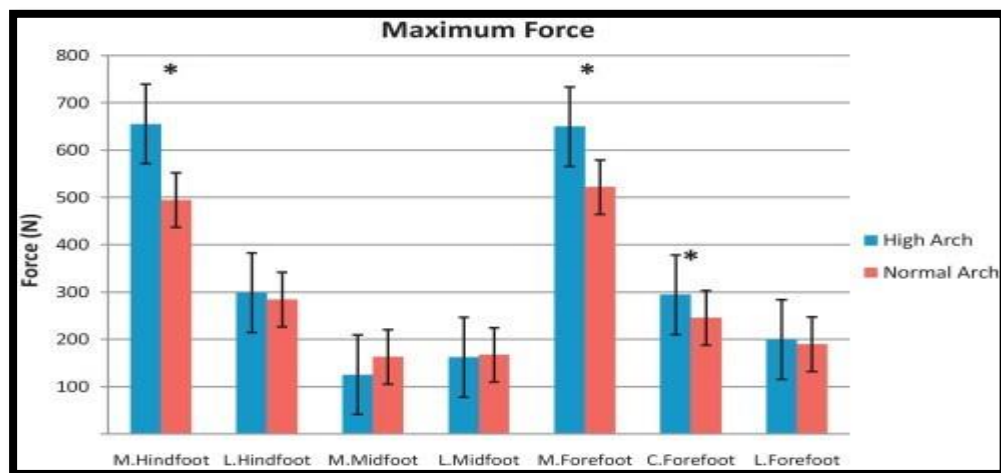


Figure 2.9: Comparison of maximum force readings between the normal arch and high arch of American football players, adapted from Carson et al. (2012)

2.8 THE EFFECT OF WALKING SPEED AND FOOTWEAR TYPES ON PLANTAR PRESSURE CHARACTERISTICS

The study of Burnfield et al. (2004) reported that the heel contact area did not significantly increase while walking with faster speed. However, the increase of cadence in young adults resulted in an increased heel contact area (Hughes et al. 1991). The logical reason behind why the heel contact of older people did not change with faster walking speeds is the age-related changes in the heel pad, according to the studies reported by (Jahss, Kummer & Michelson 1992). The dense fibrous septae support lattice to contain the fat globules, and prevent severe bulging and loss of support of the heel pad with loading (Jahss, Kummer & Michelson 1992). Moreover, the mechanical characteristics and structural changes in the older adult heel would allow more flattening under the lower forces associated with slower walking speeds (Jahss, Kummer & Michelson 1992). During barefoot waling, the total contact area value of older adults was lower than that of shod conditions by 16%.

In the investigation of Burnfield et al. (2004), the pressure-time integral values were decreased in six of the eight anatomic regions associated with the reduction in the stance time duration throughout faster barefoot walking.

Many studies investigated the differences in plantar pressure distribution between shod and barefoot conditions in various age groups. The investigations of Sarnow et al. (1994) showed higher peak pressure readings under the whole foot during barefoot walking in comparison to shod walking in a group of middle-aged adults (mean age =51). Sarnow et al. (1994) did not investigate the changes in the anatomical regions. However, the studies of Soames (1985) reported a significantly higher pressure reading registered under the posterior heel, fifth toe, and the lateral three metatarsal

heads in comparison to the shod condition during barefoot walking of younger adults. The effect of different kinds of footwear conditions (running shoes, leather-soled oxford shoes, barefoot) on the plantar pressure distribution in adults with and without diabetes were evaluated by the studies of Perry et al. (1995). The results of their studies documented significantly lower pressure values recorded under the regions of the heel, metatarsal heads and toes while wearing running shoes compared to the barefoot condition (Perry et al. 1995). Similarly, the results shown by Burnfield et al. (2004) indicated a reduction in the pressure values registered under the region of the heel, and central metatarsals while walking in shoes.

However, the pressure under the hallux (great toe) was higher during shod walking. The authors indicated that the toe box design and the level of the sole under the forefoot might have increased the pressure values under the toes region in older adults (Burnfield et al. 2004). Thus, wearing shoes and walking slowly can reduce peak pressure under the foot, especially under the heel and central metatarsal regions, resulting in the less painful heel, avoiding metatarsalgia, and fat pad atrophy in older people (Burnfield et al. 2004). Collectively, the findings of the previous study are also important for understanding the risk of ulceration due to diabetes mellitus in older adults. An increase in the risk of ulceration and amputation is associated with an increase in plantar pressure according to an investigation conducted by Stess, Jensen & Mirmiran (1997), Frykberg et al. (1998), and Ahroni, Boyko and Forsberg (1999). Reducing plantar pressure, educating patients to wear soft-soled shoes, fitting the patients to more appropriate shoe wear (particularly in the toe box region, and avoiding fast walking speeds are considered the most important suggestions that limit risk of injury and foot pain (Burnfield et al. 2004).

Many other investigations examined the effect of various types of footwear and walking speeds on plantar pressure distribution characteristics of the normal and pathological feet. The studies of Segal et al. (2004) on twenty healthy individuals revealed that foot regions responded differently to the changes in walking speeds throughout gait cycle phases (Table 2-6). The peak plantar pressure increased linearly at the hallux and heel regions as gait speed increased, and this finding is supported and consistent with other investigations conducted by Rosenbaum et al. (1994), Kernozek, LaMott and Dancisak (1996), Burnfield et al. (2004), and Warren, Maher & Higbie (2004).

Table 2.6: Average peak pressure of twenty healthy individuals, adapted from Segal et al. (2004)

Speed (m/s)	0.75	1.00	1.25	1.50	1.75	2.00
Hallux (T)	208.6 (42)	231.8 (53)	250.2 (56)	286.8 (69)	308.5 (79)	315.5 (77)
Medial FF (M)	155.7 (36)	172.6 (34)	180.1 (29)	196.2 (36)	196.2 (34)	194.2 (41)
Central FF (C)	168.4 (23)	186.8 (28)	202.1 (31)	211.5 (34)	210.0 (34)	200.4 (38)
Lateral FF (L)	137.1 (22)	151.7 (26)	158.9 (31)	159.0 (44)	155.4 (44)	149.8 (43)
Heel (H)	173.6 (34)	200.7 (34)	227.2 (34)	260.3 (36)	294.4 (45)	329.8 (52)

Average peak plantar pressure (kPa) with one standard deviation (in parentheses) of five plantar regions at six different walking speed (m/s).

The plantar pressure distribution response of specific regions may be correlated to the specific functions of these regions during walking. When the heel contacts the ground, the closed-cell structure of the heel pad absorbs the impact immediately (Jahss, Kummer & Michelson 1992). As speed increases to 4.0 m/s, the peak pressure following loading response increases linearly (Keller et al. 1996). Therefore, this linear increase relationship between the peak pressure at the heel region during walking at faster speeds seems to be associated with the velocity-vertical ground reaction force relationship as supported by the study of Keller et al. (1996). From the mid-stance to

the late stance phase of the gait, the vertical ground reaction forces start to increase again because the full-body weight passes beyond the stance limb (Keller et al. 1996) thus, leading to a simultaneous decrease in the contact area of the hallux region to accommodate the increasing load in preparation for the toe-off portion of gait (toe clearance) (Eils et al. 2002).

A shift of the body weight during the late stance phase of the gait (80% of the stance phase) towards the toes (40 % of the weight is present at the toes) is the reason behind the higher readings of plantar pressure distribution over a small contact area of hallux region (Hughes, Clark & Klenerman 1990; Kelly, Mueller & Sinacore 2000). During toe clearance (a toe-off portion of the stance), propulsive forces have been documented to increase with faster speeds according to the study conducted by Vaughan, Du Toit & Roffey (1987). According to Hughes, Clark & Klenerman (1990), the relationship between the increased pressure and propulsive forces and decreased contact area could be the reason behind the occurrence of ulcers at the first metatarsal region (M1) and big toe (hallux) than the hindfoot, concluding that the hallux is considered the performance ray as its role during walking increases with faster gait speeds (Segal et al. 2004).

Furthermore, the foot proceeds quickly from heel-strike to toe-off at the faster walking speed, leading to a decrease in foot-floor contact duration time continuously, and less time spent weighting the forefoot region (less pressure) (Zhu et al. 1995), therefore resulting in greater forces values (high pressure) under the hallux region during the toe-off portion of gait. This may be the reason why ulcers occur more frequently in the forefoot region. So, suggesting that individuals or patients with a diabetic neuropathic

foot could use different mechanisms or footwear than a normal foot, to adapt their gait to faster walking speeds, thus increasing pressure at the forefoot and avoiding ulcers and foot pain (Segal et al. 2004). Similarly, such an increase in pressure recorded under the forefoot region of normal subjects was demonstrated through studies conducted by Nurse & Nigg (2001) and Eils et al. (2002).

Importantly, the linear relationship of faster speed-high pressure found at the heel and hallux and the quadratic relationship of faster speed-less pressure found at the forefoot in healthy adults can provide useful information regarding footwear and orthosis design (Segal et al. 2004). Understanding how different plantar regions respond and function at different walking speeds may indicate the types of materials used to design the optimal walking shoe and foot orthosis for a specific patient (Segal et al. 2004).

The higher values of peak plantar pressure at the hallux and heel and the lower values of peak plantar pressure at the forefoot are in line with many other investigations (Rosenbaum et al. 1994; Zhu et al. 1995; Kernozek, LaMott & Dancisak 1996; Burnfield et al. 2004). However, Warren, Maher and Higbie (2004) documented that the highest peak pressure values were recorded under the central forefoot at all speeds. These differences between the previously mentioned studies regarding the peak plantar pressure value in specific region may be associated with using and implementing different data processing techniques (Segal et al. 2004). For instance, the peak plantar pressure was calculated based on the average of each sensor reading for a specific foot region (Warren, Maher & Higbie 2004). In contrast, other studies measured the peak plantar pressure at any one sensor with the specific foot region (Rosenbaum et al. 1994; Zhu et al. 1995; Kernozek, LaMott & Dancisak 1996; Burnfield et al. 2004; Segal et

al. 2004). Thus, understanding the concepts behind the effects of dividing the foot into specific regions (masking) and data processing techniques on plantar pressure results may develop a standard plantar pressure analysis for a specific case study (Segal et al. 2004).

2.9 CONCLUSION

The literature review shows that many studies have investigated the effect of multiple types of ankle foot orthoses on the lower limb's kinematics and kinetics for people with different disorders such as cerebral palsy and stroke. It also found that most of the research work regarding the plantar pressure characteristics were focused on older people wearing different types of footwear. However, there is a lack of research investigating AFOs and their effects on gait cycle characteristics for patients with severe DDH who did not receive early treatment or surgery. Therefore, the current work aims to fill this research gap and provide a better understanding of the gait parameters of DDH patients with severe hip dislocation during walking in the sagittal plane under different conditions with and without AFO.

This aim can be achieved by applying a set of objectives. The first objective is investigating the kinematics and kinetics of both lower limbs under four walking conditions: barefoot, custom-made orthosis, Leaf Spring orthosis, and shoes only. The second objective is to study the effects of both AFOs on the plantar pressure distribution registered beneath the feet during the main phases of gait. Finally, the research will investigate the COP trajectory and its relationship with lower limb movement during walking by developing a photogrammetry correlation technique.

CHAPTER 3: METHODOLOGY

3.1 AN OVERVIEW

This chapter will first describe the methods applied to study the kinematics and kinetics of the lower limbs during walking in the sagittal plane with and without orthosis. The setup of the measurement system (Qualisys 2.14, Gothenburg, Sweden) will be illustrated in Section 3.2.2. The gait protocol and implementation of the Qualisys PAF package (Istituti Ortopedici Rizzoli (IOR)), lower body marker set will be explained in Section 3.2.3. Next is the digitizing and modelling process in Section 3.2.4. This section will explain the process of creating a new model for a patient with developmental dysplasia of the hip using Visual 3D Professional (C-Motion Inc., Germantown, MD). The calculation process of the kinematics and kinetics parameters will be illustrated in Section 3.2.6, followed by the statistical procedures that were undertaken to analyse the collected data under the various conditions in Section 3.3. Finally, the second part of this chapter will include the methods applied to study the plantar pressure distribution during walking under three conditions: barefoot, custom-made-orthosis, and Leaf Spring AFO orthosis.

3.2 THE LIMITATIONS OF PREVIOUS METHODS AND JUSTIFICATION FOR USING THE CURRENT METHOD

Over the past few decades, the need for new information about the characteristics of normal and abnormal (pathological) human movement has inspired many scientists and researchers to develop new methods of capturing human movement. Many devices have been utilized to measure joint kinematics and kinetics, force, and pressure data such as accelerometers, goniometers, and image processing

techniques to analyse and evaluate human movement. The most modern and advanced frequently used method are video motion capture systems such as the Vicon motion capture system. There are two motion capture methods: marker-based systems and marker-less motion capture systems. The capture of human movement without markers is technically challenging and not very accurate, so fails to provide an exact interpretation of musculoskeletal systems. Despite the recent and tremendous development in computing vision techniques, the need for more investigation is required to use marker-less human motion capture analysis. Marker-based motion capture systems offer higher accuracy than marker-less motion capture systems, goniometers, and accelerometers. Compared to modern motion marker-based capture systems, old marker-less motion capture systems and accelerometers do not provide precise information for the mechanical and biomechanical properties of the lower limb joints.

Consequently, marker-based motion capture systems can have minimal value for the mechanical dynamics of body movement while walking in comparison to the former less marker-based methods. The new system measures all markers in a global 3D space. Thus, there is no accumulation of errors when deriving the locations of multiple linked segments or body parts. That is why, in this study, marker-based motion capture was preferred compared to the other mentioned methods to develop an accurate musculoskeletal model for individuals with developmental dysplasia of the hip joint. The markers used in this study, from the Qualisys track manager hardware, will be described in the following sections. The system is considered the most developed technique used to build human models and assess the gait cycle of healthy and pathological individuals.

3.3 KINEMATICS AND KINETICS

3.3.1 Subjects and case description

One male adult (the author of this research) (26 years old, 124cm height, 42 kg in weight) was recruited for this study. He has a history of developmental hip dysplasia as shown in Figure 3.1, severe deformity of the spine, severe deformity in the left foot and ankle, and hyper flexed knee in the right limb. The patient uses two types of ankle-foot orthoses (Leaf Spring AFO and a custom ankle orthosis fabricated by the Prosthetics Centre in Brisbane, Australia) every day, as shown in Figure 3.2.



Figure 3.1: X-ray image of the dislocated area of the patient's left hip joint

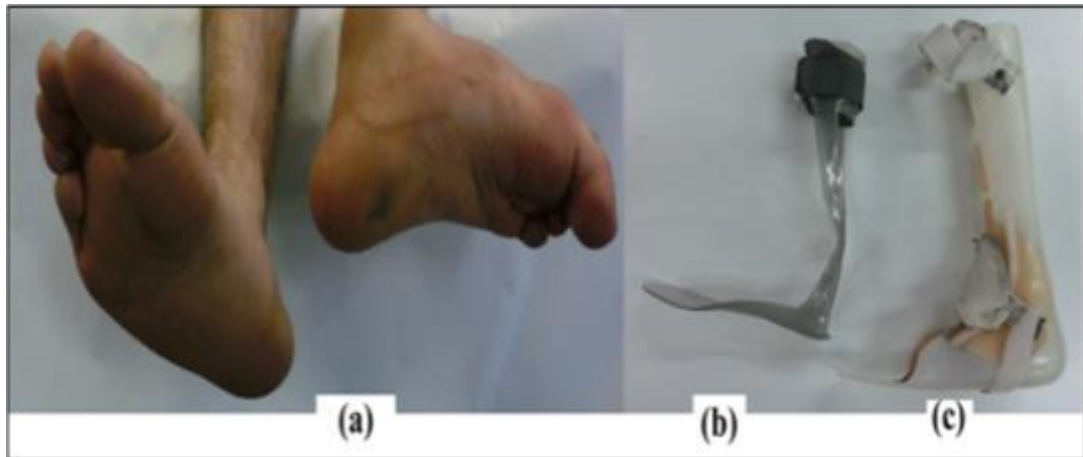


Figure 3.2: (a) Right and left foot shape of the patient with DDH, (b) Leaf AFO, (c) Custom-made AFO

3.3.2 Measurement system

Ten Qualisys Oqus computerised motion analysis system (Qualisys 2.14, Gothenburg, Sweden) infrared motion cameras were utilised for testing at the gait laboratory at the University of Southern Queensland. Three cameras were positioned at the back of the walkway, three cameras at the front of the walkway, and two cameras on each side of the walkway. These cameras are designed to obtain the three-dimensional coordinates of the retro-reflective markers that were positioned on the lower limb of the patient during walking. One force platform (AMTI: Advanced Mechanical Technology Incorporation, Watertown, USA, model BP600400) embedded in the walkway was used to collect the patient's kinetic data during walking under all four conditions: barefoot, with Custom-made orthosis, with Leaf AFO orthosis and with shoes only.

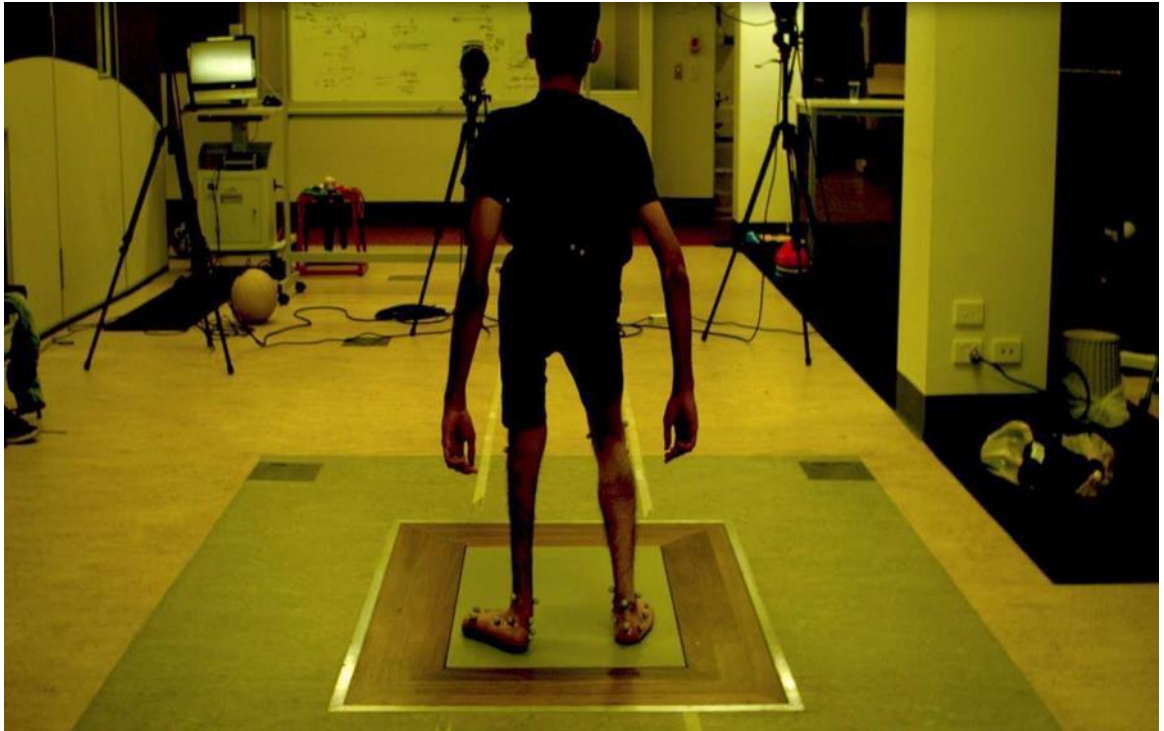


Figure 3.3: Subject standing on the force plate during the static trial

3.3.3 Test protocol and system calibration.

Data were captured during a single visit to the Sport and Exercise Centre Research Lab at the University of Southern Queensland. After consent and a short warm-up, the reflective markers were attached to the subject's pelvis and both lower limbs as shown in Figure 3.3. Four markers were placed at the femur lateral and medial epicondyle, two for each limb [L-FLE, L-FME, R-FLE, R-FME]; two markers were placed at the proximal tip of the head of the fibula with one on each limb [L_FAX, R_FAX]; two other markers were attached to the most anterior border of the tibial tuberosity, one for each limb [L_TTC, R_TTC]; four markers were placed on the lateral and medial prominence of the lateral and medial left and right malleolus respectively [L_FAL, L_TAM, R_FAL, R_TAM], two markers were placed at the lateral side of greater trochanter 1/ from the proximal end [L_FTC, R_FTC]; and the remaining four markers were attached to the anterior superior iliac spine [L_IAS, R_IAS] and to the posterior superior iliac spine [L_IPS, R_IPS]. The placement of the markers was according to

the Ortopedici Rizzoli (IOR) lower body marker set, as shown in Figure 3.4.

The data were captured under four conditions: barefoot, custom-made, Leaf AFO, and shoes only. These markers allowed each segment of the limb (foot, shank, and thigh) and the pelvis to be treated as a 6-degrees-of-freedom rigid segment. A static standing trial was captured with the individual in the anatomical position, which was defined as a normal stance on the force plate. After the static calibration, all the calibration-only markers (L-FME, R-FME, R-TAM, L-TAM) were removed.

Data were collected using 10-Camera Qualisys motion capture system and QTM software. Markers and force plate data were collected at 100Hz and 1000Hz, respectively. At the start, the subject was asked to walk at normal speed across the capture space, with his eyes facing forwards towards the wall in front of him. Three practice trials were given to make sure that, during recording, the subject's starting position was adjusted to increase the likelihood of initial right foot or left foot contact occurring on the force plate. Ten gait trials (five for each limb) on the force plate were recorded for every condition: barefoot, with custom orthosis, with Leaf AFO and shoes only. Additionally, two more trials for each condition were registered as a replacement in case the subject did not entirely strike the force plate. Finally, following data collection, all the IOR lower body markers were removed from the subject's body.

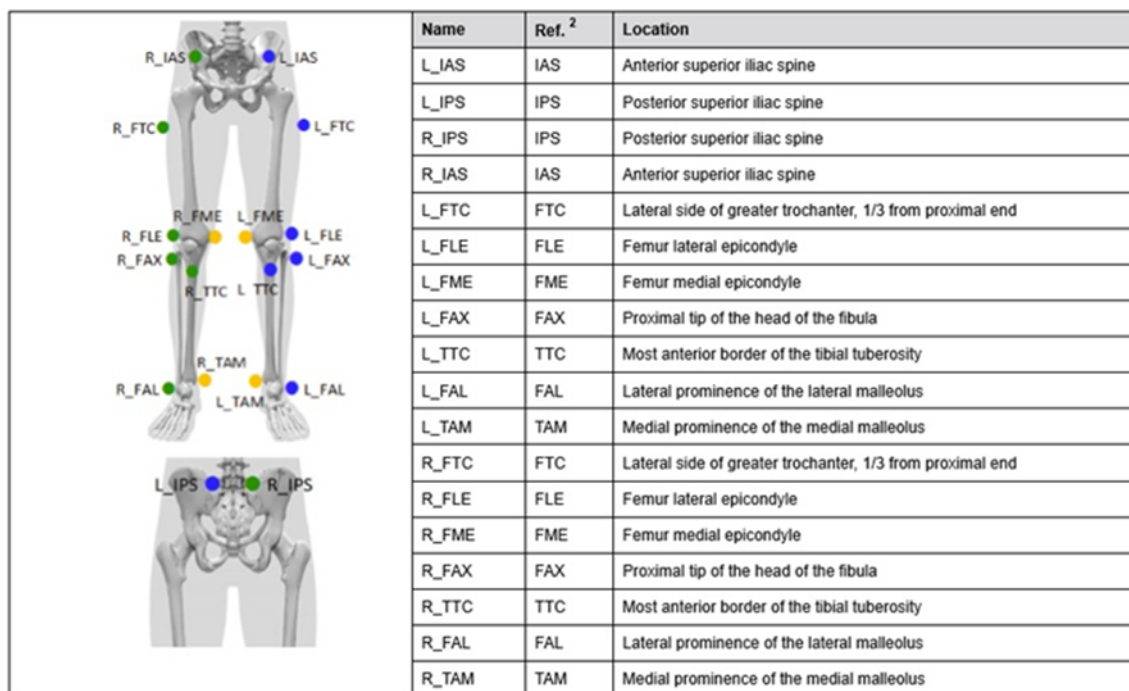


Figure 3.4: Qualisys PAF package lower body marker set (Leardini et al. 2007)

Before the recordings, the camera system was calibrated to produce a calibrated volume using an L-shaped metallic structure that represents the global coordinate system. This L shape had four markers, the long axis of the frame had three markers aligned with the edge of the force plate in the x-direction and the short axis of the frame with two markers aligned with the edge of the force plate in y-direction. Importantly, throughout the calibration process, the alignment of the long axis with the force plate was more critical than the short axis, so height adjustment screws were used to keep both axes horizontal. A dynamic calibration was performed by fixing the L frame to the medial edge of the force plate, and the calibration wand was waved with a fixed distance between the three markers around the capture area to provide a data capture. At least two left and two right dynamic trials were recorded while the patient was walking at the same speed. The participant had to strike the force plate with the whole region of the foot. Between each calibration trials, the participant asked to rest for 5 minutes in order to make sure the alignment

of the L frame axis is correct and similar to that of the previous trial. The camera system calibration was accepted when the residual errors were less than 2 mm to ensure that most of the motion capture system was covered in all the trials. Three axes (in positive and negative directions) then defined the laboratory coordinate system. The X-axis was defined as the anterior-posterior (forward/backward direction), the Y-axis was defined as mediolateral (left/ right), and the Z-axis as proximal-distal (upward/downward) as shown in Figure 3.5.

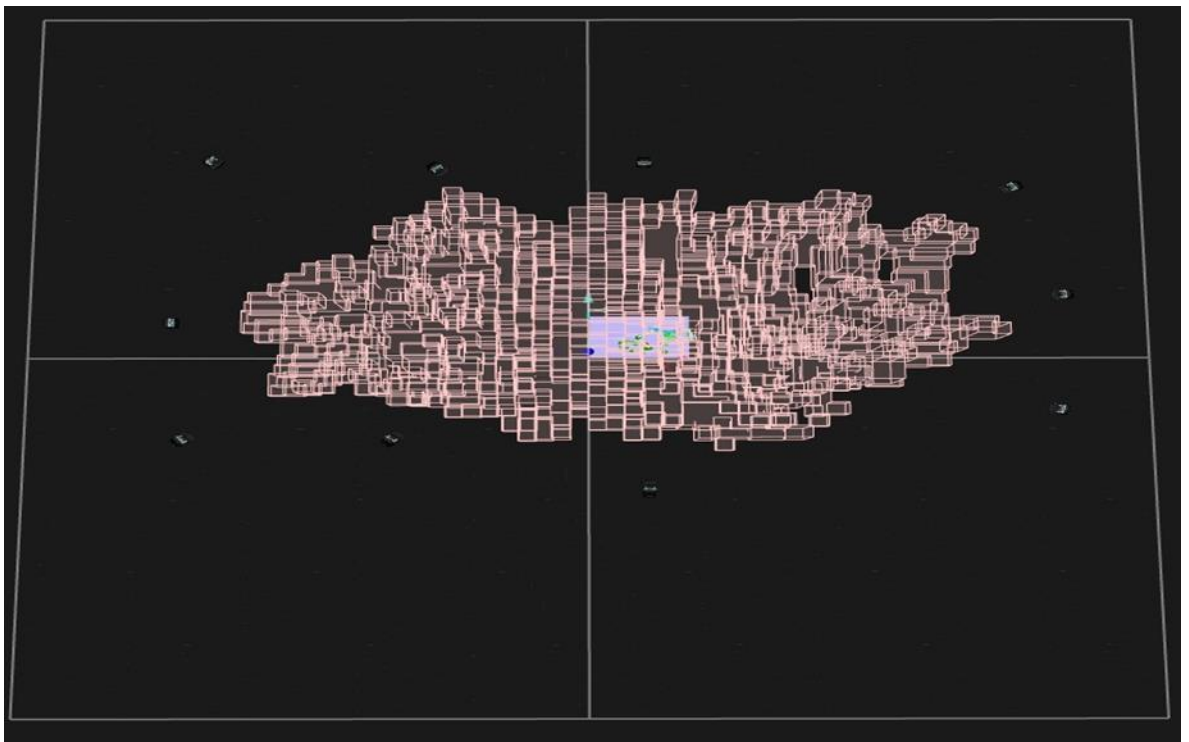
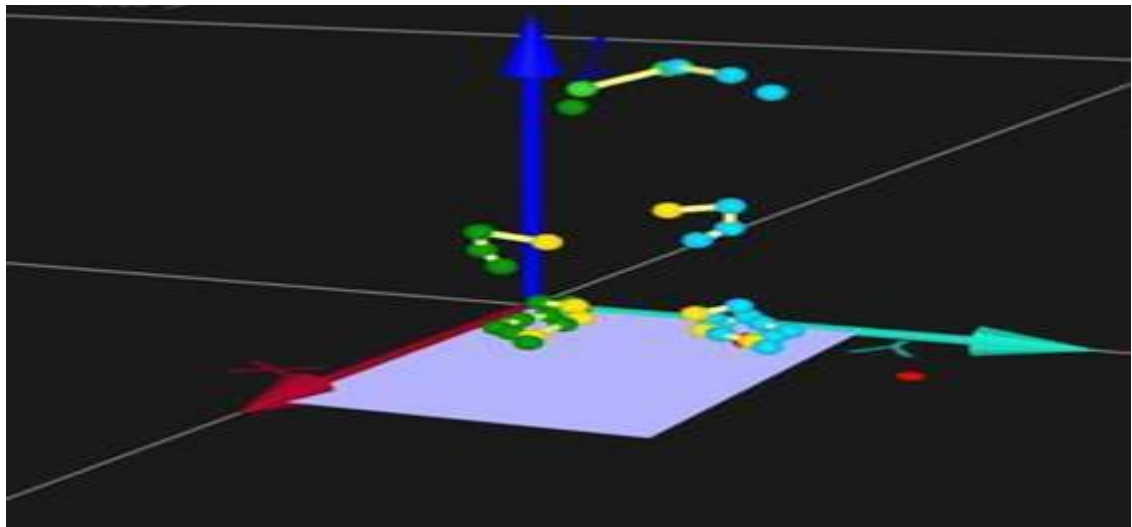


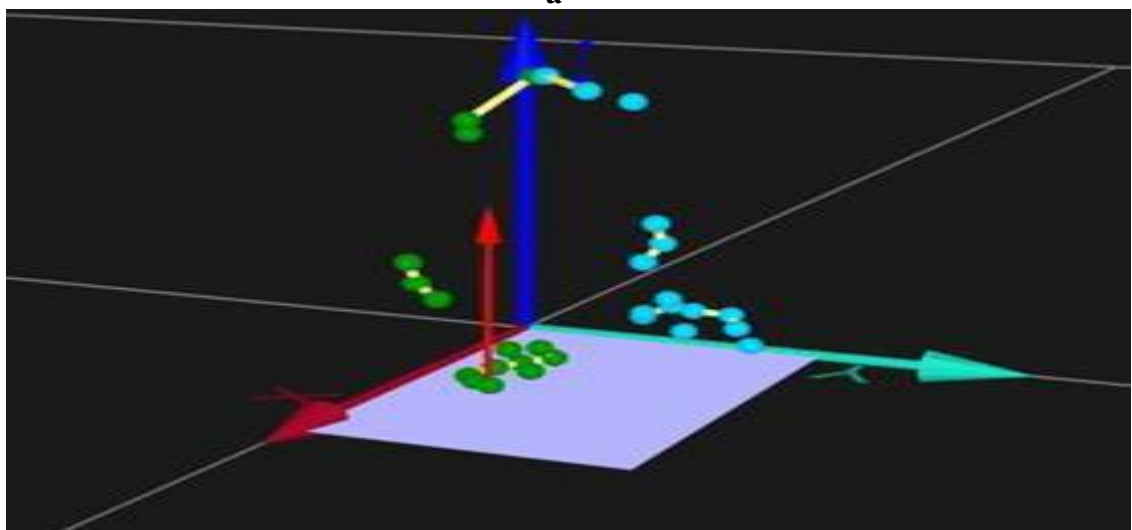
Figure 3.5: Calibrated volume of the space representing the walkway area surrounded by 10 Qualisys cameras

3.3.4 Digitizing and modelling

The 2-d markers position data for each of the 10 cameras were labelled and combined into a 3-D representation using the Qualisys tracking manager software. The automatic identification of trajectories in the Qualisys Track Manager 2.14 software was performed by a module called AIM (The automatic identification of markers). The IOR static lower body marker set with 18 markers attached to the ankle, knee, thigh and spine areas (as illustrated before in the test protocol part of this chapter) was applied to identify the static markers for all the four conditions. After labelling and identifying the static trials for the four conditions, the marker set, including the identifications of 14 markers, was applied to all five trials of each limb of each condition to identify all trajectories for the whole gait cycle of both right and left limbs.



a



b

Figure 3.6: Digitized model for subject stepping onto the force plate during standing (a) and dynamic trial (b). The red arrow shows the direction of the ground reaction force GRF

Then, all data were converted and exported to C3D files to be imported into Visual 3D Professional. The model was built using a six-degree of freedom, that shows a full representation of the coordination and orientation of the joints in space. The model was created to examine the linear movement and angular movements in all planes (three rotations and three translations). This was done by establishing a rigid body frame based on segments that link the hip, knee, and ankle joint. The Coda type pelvic segment was created by defining the calibration targets, the anterior superior iliac spine (R-IAS, L-IAS) and the posterior superior iliac spine (L-IPS, R-

IPS). The right joint centre of the hip unaffected by DDH was computed by the anterior-posterior iliac spine markers positions (ASIS) depending on a regression equation developed by Bell et al. (1990) determined by 14% of the average distance between the left and right ASIS with a position 30% distally and 19% posterior to this point. Due to the dislocation of the left hip affected with severe developmental dysplasia of the hip, a new land mark was created to represent the hip joint centre which was positioned 69% distally and 1% posterior to this point according to an approximate value measured by 3-D X-ray reviewer software. The reference point for the new hip landmark was the original hip determined automatically by the Visual 3D following the same regression equation illustrated above.

The right thigh segment was built by considering that the proximal joint is the right hip, the distal joint is the knee centre which is determined by the lateral and the medial knee markers (R-FME, R-FLE), and the measured value of the proximal radius was 0.0881291mm computed by visual 3D according to the equation $0.5 * \text{DISTANCE}(\text{RIGHT_HIP}, \text{LEFT_HIP})$. The left thigh segment was built differently to that of the right thigh due to the severe dislocation of the hip. The lateral marker L-FTC, and the joint centre (NEW LANDMARK), a radius of 0.0742mm, defined the proximal joint of the thigh. The distal joint of the thigh was defined by the lateral and medial knee markers (L-FME, L-FLE). The medial and lateral malleoli markers identified the ankle joint centre. The patient's height and mass were entered to allow the model to calculate then the segments' centre of mass and segment radius based on the anthropometrical indices published by Dempster (1955) as shown in Figure 3.7.

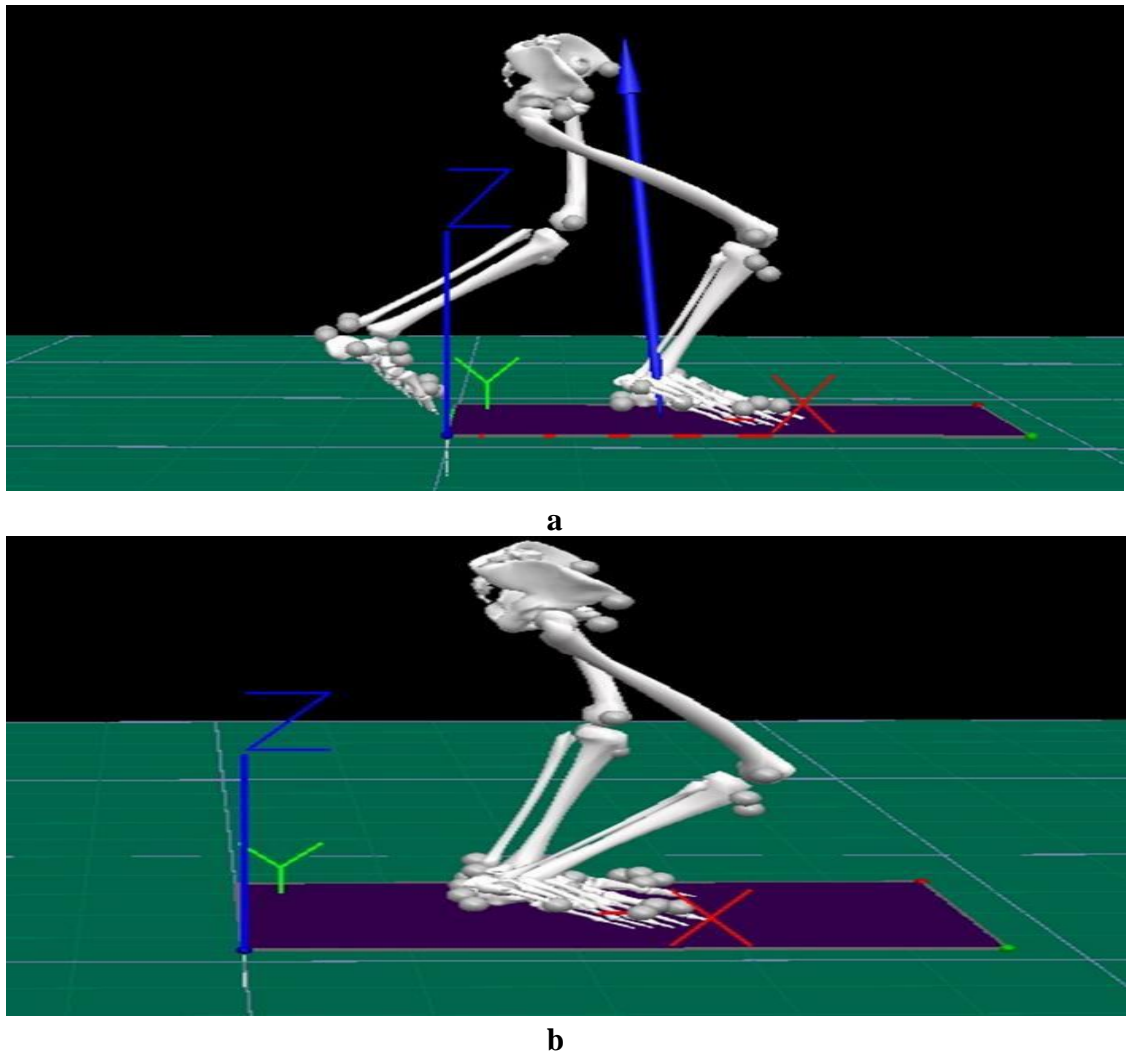


Figure 3.7: Musculoskeletal model generated by the visual 3D modelling system. Example of a patient with DDH stepping onto the force plate with the right foot during a dynamic trial (a), and both feet stepping on the force plate during a standing trial (b)

3.3.5 Calculations

For further analysis, all marker-positions and force plate data were then exported to Visual 3D professional. The data were filtered using a Butterworth zero-lag fourth-order bi-directional low-pass filter with a cut-off value of 6 Hz for walking for the marker-location, and 25 Hz for the force-plate data. A Butterworth filter prevents the high frequency data and accepts the low frequency signals which occur due to the noisy results, resulting from the random movements of markers and soft tissue artifacts. The

anthropometric data calculated from individual body mass and height using Dempster's equations were then combined with the low pass filtered data, and used as an input for the inverse-dynamics calculation method resulting in sagittal joint angular positions and net moment and power of the ankle, knee, and hip joint in the stance phase.

During walking, gait cycle events were identified from (heel strike to terminal swing) to normalise data and allow comparisons between the four main conditions and with the published healthy control data. The gait cycle for each limb starts when any part of the foot strikes the force plate (initial contact) until the same foot touches the ground again in the next step at the end of the swing phase. The inverse-dynamic method due to internal muscle activity examines the external ground reaction force of the body segments and moments on the anatomical joints as shown in Figure 3.8 for the right barefoot condition and Figure 3.9 for the left barefoot condition.

An equilibrium mathematical formula is a key to the inverse dynamic approach starting by calculating the moments and force for every joint from toe to hip (Silva and Ambrósio, 2002). The moment of inertia for each segment was calculated based on the location and magnitude of the mass for each segment, and the subject's anthropometric parameters (Dempster, 1955). The angles between every two segments were calculated according to the relative positions using the Euler rotation sequence equivalent XYZ (ankle plantarflexion-extension, knee flexion-extension, hip flexion-extension, pelvic tilt). For example, the proximal for the ankle is the shank, while the shank is the distal segment therefore, the ankle range of motion during the entire gait cycle in the sagittal plane depends on the orientation of the two segments. The new intention of this research was to test the angle, moments and power values statistically then determine the peak values to identify changes for the four conditions: barefoot, custom-made

orthosis, Leaf AFO and shoes only.

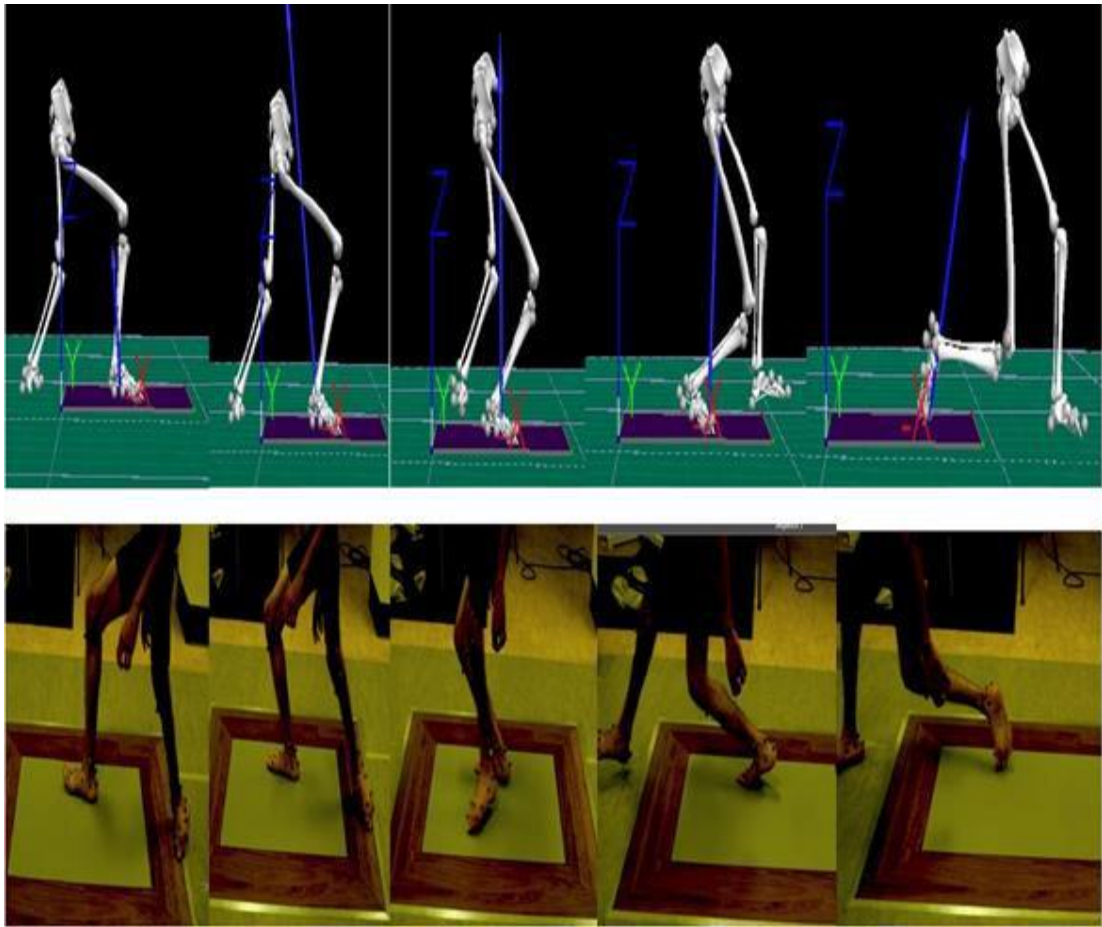


Figure 3.8: Musculoskeletal model generated by the visual 3D modelling system. Example of patient stepping onto the force plate with the right foot during the five sub-phases of the walking stance trials (initial strike, loading response, mid-stance, push-off, and toe-off). The figure shows the same moments for each phase exerted from the video camera

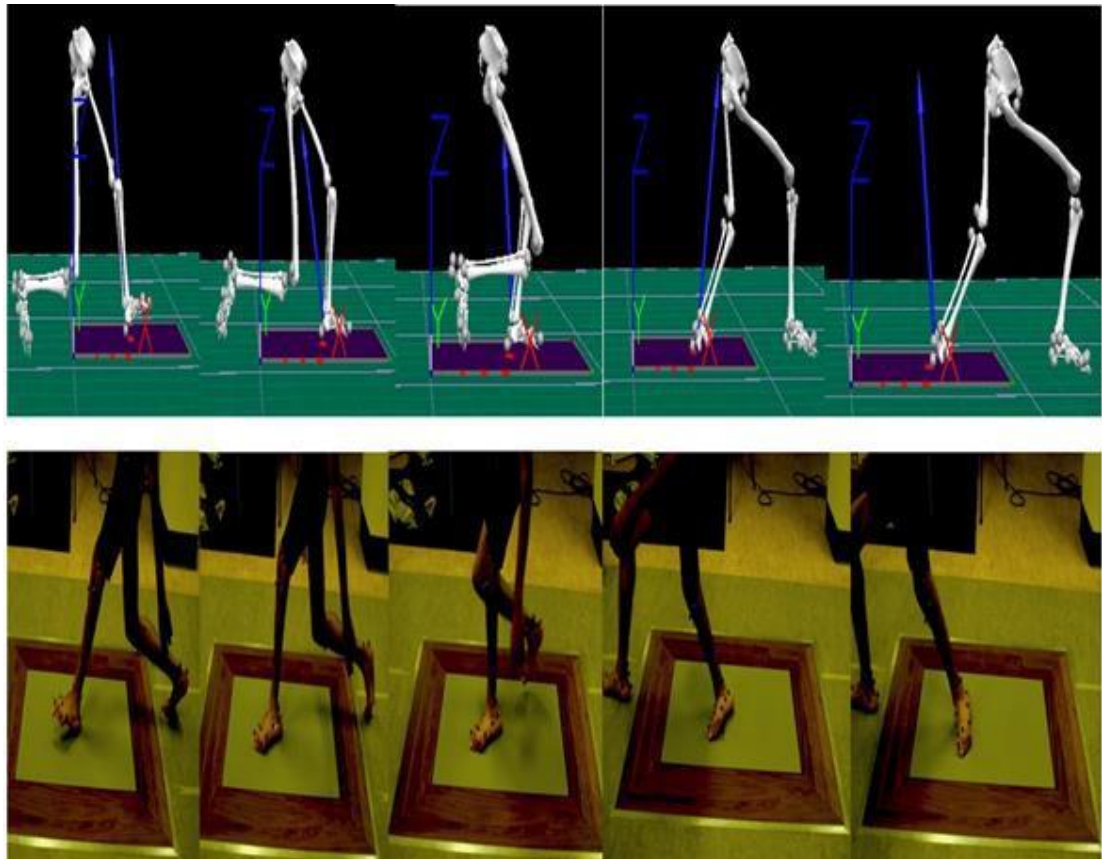


Figure 3.9: Musculoskeletal model generated by the visual 3D modelling system. Example of patient stepping onto the force plate with the left foot affected by DDH during the five sub-phases of the walking stance trials (initial strike, loading response, mid-stance, push-off, and toe-off). The figure shows the same moments for each phase exerted from the video camera

3.3.6 Statistics

The statistical package (SPSS version 20, IBM SPSS) was used to undertake the statistical analysis of the data collected. A repeated measure analysis of variance (ANOVA) was used with the four factors with a post-hoc Bonferroni correction to determine statistical differences (mean differences) between each two factors (conditions). The p value would be significant if it was less than 0.025, according to the analytical regression equations of (Perneger, 1998). All trails of data collected were used for the analysis due to the small sample size (one patient).

3.4 CORRELATION BETWEEN LOWER LIMB MOVEMENTS AND PLANTAR PRESSURE CHARACTERISTICS.

3.4.1 Introduction

Image-based motion capture and photogrammetry image-processing methods have been used widely to create 3D movement models of the lower limb and foot. These models are utilized by doctors, clinicians, podiatrists and physiotherapists to develop reliable treatment strategies for individuals suffering from physical disorders such as drop foot, spinal cord injuries and joint dislocation (Petre 2007). This research studies plantar pressure and 3D limb-foot movement of a left side hip-dislocation and scoliotic patient (wearing different types of ankle-foot orthosis) using close-range photogrammetry techniques, pressure IN sole system and high throughput load cell.

3.4.2 The plantar pressure measurement system

The plantar pressure measurement system is comprised of:

- a-** 3000E F-scan in-shoe sensors sampling at 100 Hz to capture COP excursions in the anterior-posterior (AP) and mediolateral (ML) directions. From these, contact area, direction of sway, distance, and direction travelled by the COP, and variability of distance travelled by the COP will be obtained using F-Scan Research ver. 6.70-03 software
- b-** Small size and 0.5 mm thickness force pressure sensors to measure the load between the ground support and human foot (Noce 2005; Rana 2009). These thin sensors are sufficient to enable non-intrusive measurements and are ideal for measuring the forces and pressure without testing the dynamics of test patients.

Therefore, in this research the Force Resistance Sensors (FRS) were selected due to of their electronic simplicity, inexpensiveness, moderate accuracy (better than $\pm 5\%$ of full use force (780 kPa)) and capability of observing the load of the foot during gait (slow or fast walking and running) (Noce 2005; Rana 2009).

3.4.3 Low-cost photogrammetry measurement system

3.4.3.1 Video Camera Calibration

Camera calibration is a very crucial stage in photogrammetric work as it ensures that the measured imaged coordinates (x, y) have a high level of accuracy. In this study, all six JVC cameras were measured and calibrated by finding all of the radial distortion parameters (K1, K2, K3), the interior orientation parameters (xo, yo, f), and the lens alignment (P1, P2, P3) to obtain an accurate result. The selected cameras were calibrated individually using a self-calibration technique (Remondino & Fraser 2006; Udin & Ahmad 2011) at an object distance of 900 mm. This pointed distance is close in resemblance to the gait characteristics of imaging the plantar pressure and 3D lower limb movements this object distance is similar to the gait specifications for imaging the plantar surface and the 3D. The frames were extracted from the clips using the off-the-shelf camera calibration software Australis®. The PLPC technique (Chong 2011) will be utilized for the determination of the lens parameters during imaging processing sessions. These video clips were processed simultaneously to obtain the parameters for each video camera before and after the session, and that was achieved using camera calibration software. First, the predicted lens parameter was obtained using: 1) the self-calibrated maximum distance, 2) the EXI file FL and 3) the algorithms found in Fraser and Al-Ajlouni (2006). For example, the root mean

square is generated by fitting a linear function between FL and the self-calibrated PD. These values were utilized to process the captured images to determine the 3D distances and angles between the anthropometric marks for the limb and plantar pressure (Chong 2011). Table 3.1 illustrates camera calibration results for six JVC video cameras.

Table 3.1: Video Camera Calibration Results marking the targets

	X	Y	Z	RMS		X	Y	Z	RMS		X	Y	Z	RMS
B2	1110.851	1613.499	101.1233	0.5		1110.852	1613.498	101.1233	0.6		1110.852	1613.498	101.1232	0.7
B3	1211.639	1610.382	50.8539	0.5		1211.639	1610.383	50.8541	0.4		1211.639	1610.383	50.8542	0.3
B4	1311.564	1611.765	50.8314	0.6		1311.565	1611.765	50.8314	0.8		1311.564	1611.765	50.8317	0.6
B5	1410.235	1616.492	-1.0444	0.1		1410.582	1616.711	-0.6236	0		1410.971	1616.434	0.1464	0.2
B6	1512.664	1612.238	99.9711	0.9		1512.664	1612.239	99.9712	1		1512.664	1612.238	99.9714	1.2
B7	2251.64	1604.673	57.4593	0.6		2257.258	1608.147	61.0349	0.5		2254.385	1605.891	62.2643	0.4
B8	2346.43	1601.071	4.4078	0.3		2352.846	1604.834	9.4166	0		2349.629	1602.396	10.6278	0.1
B9	2442.591	1600.86	-47.4032	0.5		2449.543	1604.819	-41.5863	0.6					
C2	1112.019	1512.633	0.6331	0.3		1112.02	1512.633	0.6328	0.6		1112.02	1512.633	0.6328	0.6
C3	1210.776	1510.726	101.4213	0.3		1210.777	1510.726	101.421	0.6		1210.776	1510.726	101.421	0.6
C4	1312.202	1512.19	0.6668	0.2		1312.203	1512.19	0.6679	0.3		1312.203	1512.19	0.6678	0.2
C5	1410.603	1510.786	150.8158	1		1410.603	1510.785	150.8162	1.1		1410.604	1510.787	150.8156	1.2
C6	1513.301	1512.58	50.4376	0.5		1513.3	1512.58	50.4374	0.7		1513.3	1512.58	50.4374	0.4
C7	2247.133	1505.738	-40.3827	0.4		2252.881	1509.481	-35.2148	0.4		2250.44	1507.62	-34.7176	0.2
C8	2346.225	1504.121	-93.1492	0.2		2353.19	1507.869	-87.9956	0.2		2350.27	1506.002	-87.0337	0.3
C9	2443.669	1501.728	0.9295	0.1		2450.56	1505.68	7.4541	0.2		2446.753	1503.926	9.3677	0.2
D1	1011.094	1415.013	1.0127	0.3		1011.094	1415.013	1.0127	0.3		1011.094	1415.013	1.0127	0.4
D2	1110.794	1413.523	101.2991	0.3		1110.794	1413.523	101.2992	0.2		1110.793	1413.523	101.2995	0.5
D3	1211.233	1410.825	51.5147	0.4		1211.233	1410.825	51.5146	0.4		1211.233	1410.825	51.5147	0.5
D4	1311.462	1412.976	51.0912	0.3		1311.462	1412.976	51.0911	0.4		1311.462	1412.975	51.0912	0.4
D5	1410.165	1410.002	100.3083	0.9		1410.165	1410.001	100.3081	1		1410.165	1410.002	100.3079	1.1
D6						1511.292	1411.874	0.0163	0.3		1511.291	1411.874	0.0164	0.5
D7	2246.583	1408.492	-88.4149	0.7		2252.753	1411.398	-82.9503	0.4		2250.208	1409.145	-84.6188	0.7
D8	2346.992	1404.404	5.5041	0.3		2353.599	1407.956	10.5258	0.4		2350.495	1406.537	11.5002	0.3
D9	2444.228	1403.006	-46.7368	0.2		2451.548	1407.007	-40.3061	0.2		2447.931	1405.456	-39.1223	0.2
D10	2537.387	1404.005	-48.014	0.4		2544.698	1408.946	-39.4084	0.3		2540.592	1407.056	-38.98	0.4

3.4.3.2 *Imaging Platform and Synchronising Device*

A new close-range photogrammetric system was developed for video clip capture of a human foot during gait, using multi video cameras (6 HD video cameras) connected to the photogrammetric control frame. The accuracy of the calculated object coordinates of the foot were increased by a plate fixed on the ground attached to the control frame on the walkway, which contains control points. The plate allowed the capture of the video recording of the subject's foot plantar. At the same time, lower limb movements' were measured in synchronization with the plantar pressure in different positions of gait such heel down, mid-stance, and push-off. Therefore, in every single phase of the gait, there were two readings: one for the joints' movements and the second for plantar pressure data. The mounting camera platforms are designed to provide a 100% twelve-images overlap of the plantar

surface. A low-cost electronic synchronizing device was constructed for the multiple camcorder arrangements for two purposes: 1) to provide video-frame synchronization and 2) to minimize error introduced by the disparity of the single video camera.

3.4.4 Data Processing of the correlation technique

3.4.4.1 Data collecting of the plantar pressure characteristics during walking.

After consent, the patient was asked to walk along a 10-meters long walkway for a short warm-up trail. Before the recording of the trial, the participant was given three minutes to practice the procedure, thus minimising walking errors without alteration of step characteristics. The subject had left-side hip dislocation and scoliotic spine with atypical gait characteristics. In the trial, the participant was shown a standard gait procedure from standing position to stepping onto the floor using the 3000E F-scan in-shoe sensors sampling at 100 Hz. After inserting the 3000E F-scan in-shoe sensors inside the patient's shoes, six walking trials were recorded for each condition: barefoot, custom-made orthosis, and Leaf Spring AFO. Ten steps were collected per straight-line walk for each of the six trials under the three mentioned conditions.

Regarding the barefoot trails, the 3000E F-scan in-shoe sensors was fitted inside the socks of the left foot affected by DDH. The patient was wearing the custom-made orthosis and the Leaf Spring AFO in the left foot with sports shoes (flat rocker Adidas type). The test began with the left foot stepping forward first for three trials and was completed with three trials having the right foot stepping forward first. In order to collect high accuracy plantar pressure data, the average of the three middle

steps was taken from the ten steps for each trial under the three conditions. The three best trial recordings were chosen for processing using F-scan research software. The foot was divided into thirteen main regions according to the F-scan research software's automatic classification of the foot. The foot regions were total foot TF, lateral heel LH, medial heel MH, midfoot MF, first metatarsal M1, second metatarsal M2, third metatarsal M3, fourth metatarsal M4, fifth metatarsal M5, Hallux T1, second toe T2, third toe T3, and fourth and fifth toes T4-5 as shown in Figure 3.11.

The F scan software calculates information on the most clinically relevant parameters chosen in this study for each foot under the three previously mentioned walking conditions. First, we examined the total right and left foot parameters during the three main phases of gait (heel strike, mid-stance and push off). These parameters are peak pressure PP (kpa), contact time CT (sec), ground reaction force (N), contact pressure CP (KPA), and contact area CA (cm²). Second, we examined the foot region parameters of peak pressure, pressure-time integral and contact area recorded under each foot. Finally, the centre of pressure trajectory was recorded for each foot to be correlated with knee-joint positions, as shown in the example Figure 3.10 below.

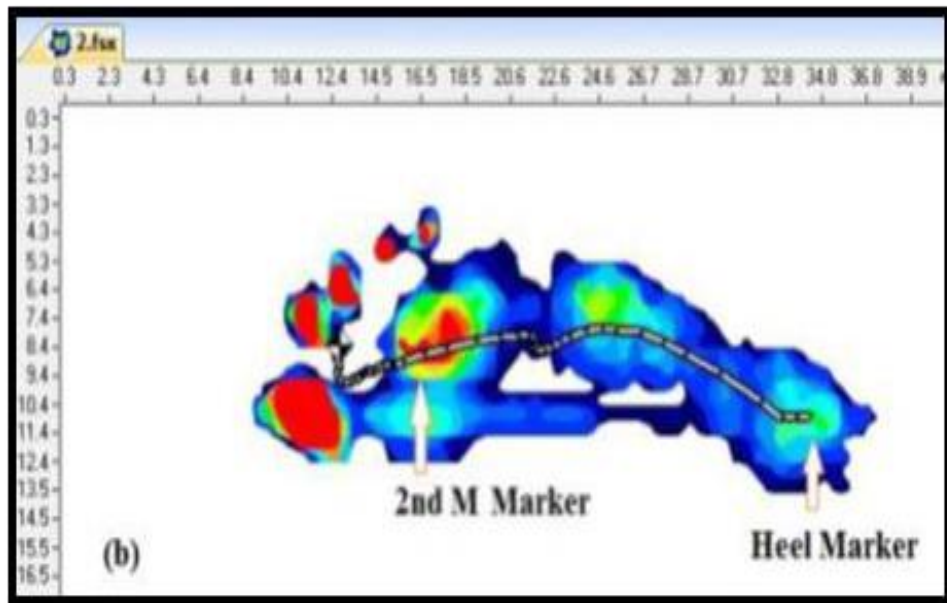


Figure 3.10: COP trajectory and target imprints' location of the right foot

Abbreviation	Description	
TF	Total Object (covers the full foot)	
MH	Medial Heel (covers the medial -or inner side- half of heel)	
LH	Lateral Heel (covers the lateral -or outer side- half of heel)	
MF	Midfoot (covers the middle section of foot)	
M1	Metatarsal 1 (covers the 1 st metatarsal bone, is the one most inside)	
M2	Metatarsal 2 (covers the 2 nd metatarsal bone, is the one next to and outside the 1 st)	
M3	Metatarsal 3 (covers the 3 rd metatarsal bone, is the one next to and outside the 2 nd)	
M4	Metatarsal 4 (covers the 4 th metatarsal bone, is the one next to and outside the 3 rd)	
M5	Metatarsal 5 (covers the 5 th metatarsal bone, is the one next to and outside the 4 th)	
T1	Hallux (covers the big toe, is the 1 st toe or Hallux)	
T2	Second Toe (covers the 2 nd toe, is the one next to and outside the 1 st)	
T3	Third Toe (covers the 3 rd toe, the one next to and outside the 2 nd)	
T45	Fourth and Fifth Toes (covers the 4 th & 5 th toes, are the ones next to and outside the 3 rd)	
WM	Width across the Metatarsal heads or Metatarsus (Yellow Line)	
LF	Length of Foot - Heel to longest toe (Gray Line)	
FA	Foot Axis - Heel through center of Metatarsal 2 (Cyan Line)	

Figure 3.11: Definition of the thirteen main regions according to F-scan software classification

3.4.4.2 Calculation of the 3D coordinates of the gait cycle.

The Virtual DuD converted the video clips taken by the twelve cameras into a set of image frames. Producing an accurate 3D surface model for the foot plantar can be achieved by obtaining less than 1mm base/height ratio. The captured images of each gait movement for both limbs under three conditions (barefoot, custom-made orthosis, Leaf Spring AFO) were processed in Australis® software using the DSM technique. Image-pairs were uploaded and relatively orientated. The imaged coded targets were used to identify the orientation process. It showed that the black/white circular point's targets were more acceptable and digitized by the software. Initially, a depth-range was assigned to expedite the search for a good match in the subsequent images. This setting was particularly crucial for this project as the human skin surface has a smooth texture. The orientation results were considered satisfactory as the total error was less than 1.0 mm. A medium-density rate (medium sample rate value) was applied because the 3D dorsal and plantar surfaces were smooth. Thus, a low density resulted in insufficient details on the 3D model, and a high density resulted in a wavy and rippled model appearance.

In this work, the patient put on different types of ankle-foot orthoses. The previous tests showed that the plate and connected software produced high accuracy images for a foot with and without orthosis.

Table 3.2: Example of 3D coordinates of the lower limb.

1		Right barefoot 0.2				Right over-counter orthoses 0.2				Right custom modeld orthoses 0.2			
2	LABEL	X	Y	Z	RMS	X	Y	Z	RMS	X	Y	Z	RMS
3	M1	1903.905	1779.413	928.2264	0	1854.114	1532.105	-8.9477	0.8	1787.109	1545.372	-30.8399	1.1
4	M2	1816.887	1459.09	142.4563	1	1860.449	1495.875	30.4694	1.2	1792.288	1507.617	9.7232	0.8
5	M3	1811.203	1420.142	174.7502	0.4	1869.503	1445.759	81.4646	1.4	1796.654	1451.475	48.9516	0.1
6	M4	1834.668	1219.003	78.6696	1.1	1871.359	1215.974	0.2176	1	1817.467	1224.92	-6.5986	0.6
7	M5	1853.135	1113.209	8.8955	1	1880.934	1113.897	-46.8574	0.5	1838.717	1117.342	-46.8428	0.6
8	M6	1851.051	1031.947	6.4996	1.2	1872.522	1032.409	-41.7347	1.2	1829.765	1029.665	-37.3543	1.2
9	M7	1837.056	1019.767	31.9678	0.5	1859.285	1014.81	-5.8234	0.9	1804.771	1012.221	-5.2955	1
10	M8	1848.076	1007.266	72.0343	1	1885.706	997.0496	38.7536	0.8	1815.456	1004.732	47.1266	1
11	M9	1819.199	1002.821	58.9242	0.8	1853.075	1002.193	21.7622	1.4	1789.978	999.9547	21.645	0.9
12	M10	1804.545	1007.138	86.9456	1	1842.499	1003.055	67.684	1.4	1767.288	989.6511	56.8945	0.6
13	M11	1785.335	1000.068	14.9241	0.8	1815.494	998.1167	-7.4217	0.9	1763.867	995.4867	-20.5466	1

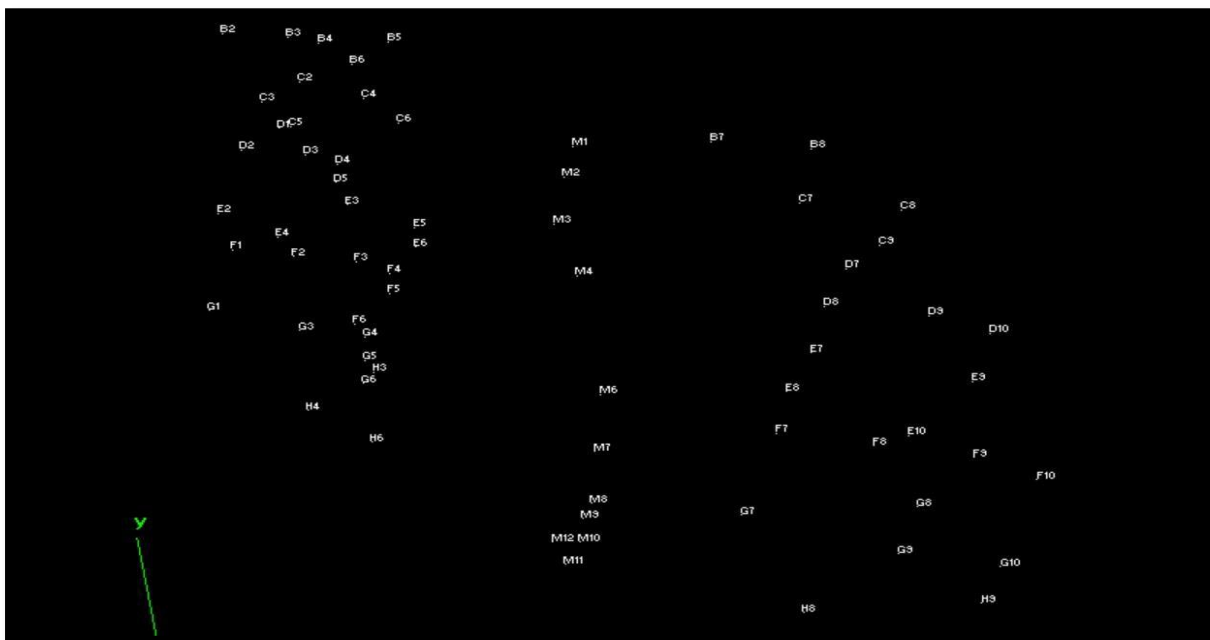


Figure 3.12: Example 3D plot of the lower limb coordinates

3.4.4.3 Correlation of the plantar pressure data and lower limb movements.

The investigation tests involved analysing the correlation of plantar pressure and lower limb movements on both limbs during walking under the three previously mentioned conditions. The experiments were divided into two steps. Step A required recording of the foot movement: two on the mat from three different sides (left, centre and right side) using six video cameras when the plate was on the walkway of the CRPS platform. The results of this test were utilised to generate a 3D surface model of the

subject's foot plantar during a gait, as explained previously. The second step captured the subject's limb movement from three different sides (left, centre, and right) using six video cameras when the plate was placed on the walkway of CRPS platform concurrently. The outcomes of this test were adopted to correlate the movements of the lower limb and plantar pressure data.

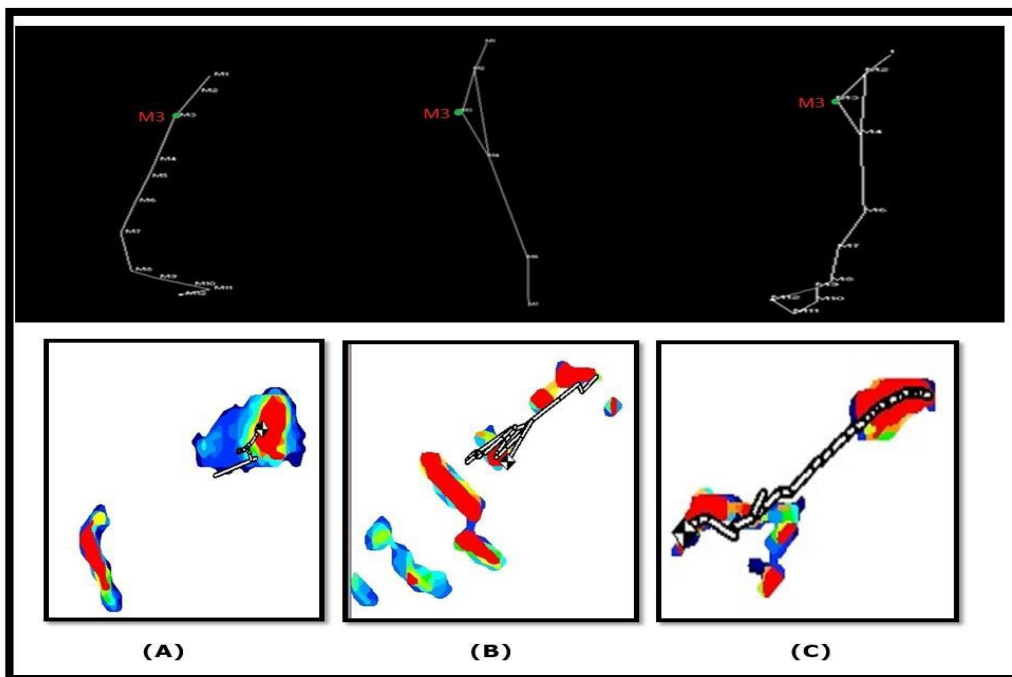


Figure 3-13: Examples of the correlation between the lower limb and plantar centre of pressure.

3.5 CONCLUSION

The marker-based motion capture system has a less and minimal effect on the mechanical dynamics of body movements during walking in comparison with the less marker-based methods as described in Section 3.2. The Qualisys PAF gait model was selected to develop an accurate musculoskeletal model for individuals with developmental dysplasia of the hip, due to its high accuracy and less errors occurring when deriving the location of multiple linked segments or body parts. The system was calibrated, and the data were collected for each condition as illustrated in Section 3.3.3. Then, the kinematics and kinetics data were calculated and filtered using Visual 3D Professional software as explained in Section 3.3.5. The angles, net moments, and the net power for three lower limb joints (ankle, knee, and hip) will be analysed and interpreted in Chapter 4. The correlation approach between the lower limb movements and plantar pressure characteristics was applied to calculate the pressure and forces beneath the foot under different conditions as illustrated in Section 3.4. Thus, the data of peak pressure, contact pressure, pressure-time-integral, and ground reaction forces will be presented and analysed in Chapter 4.

CHAPTER 4: RESULTS

4.1 AN OVERVIEW

The ankle, knee and hip joints kinematics and kinetics results are presented in the first part of this chapter. The ankle joint kinematics and kinetics results under the four conditions are explained in Section 4.2. These results include the dorsi-plantarflexion angles, the dorsi-plantarflexion moments, and ankle power generated during walking in the sagittal plane, followed by the knee and hip joint kinematics and kinetics results, which are presented and summarised in Sections 4.3 and 4.4, respectively. These results will include the knee and hip joint extension-flexion angles, moment and power during walking in the sagittal plane under the four conditions. The second part of this chapter presents the plantar pressure results during the three main phases of gait: heel strike, midstance and push-off phase. In Sections 4.5.1 and 4.5.2, the right and left foot contact area, contact pressure, peak pressure and ground reaction force results for the three conditions are explained along with the entire stance phase of gait. The final part of this chapter presents the results of contact area, peak pressure and pressure-time integral under each of the 14 specified foot regions, as shown in Section 4.6.

4.2 THE KINEMATICS AND KINETICS OF THE LOWER LIMBS

The ankle, knee and hip joint kinematics and kinetics were computed based on the methods explained in Section 3.2. As mentioned in Section 3.2.3, the data for the patient with DDH were captured after a short warm-up and consent at the USQ Sport and Exercise Research Centre Lab. Reflective markers were attached to the pelvis and the lower limbs to treat each segment as 6-degrees of freedom segment. Five gait trials for each limb on the force plate were recorded under each of the four conditions to increase the likelihood of obtaining highly accurate data. The reflective markers were labelled, digitized and identified by using Qualisys tracking manager software. The model was created after converting and exporting all the digitized data from Qualisys to C3D files to be used and modelled by Visual 3D Professional as explained in Section 3.2.4. The model was created by establishing a rigid body frame based on segments that link the hip, knee, and ankle joint.

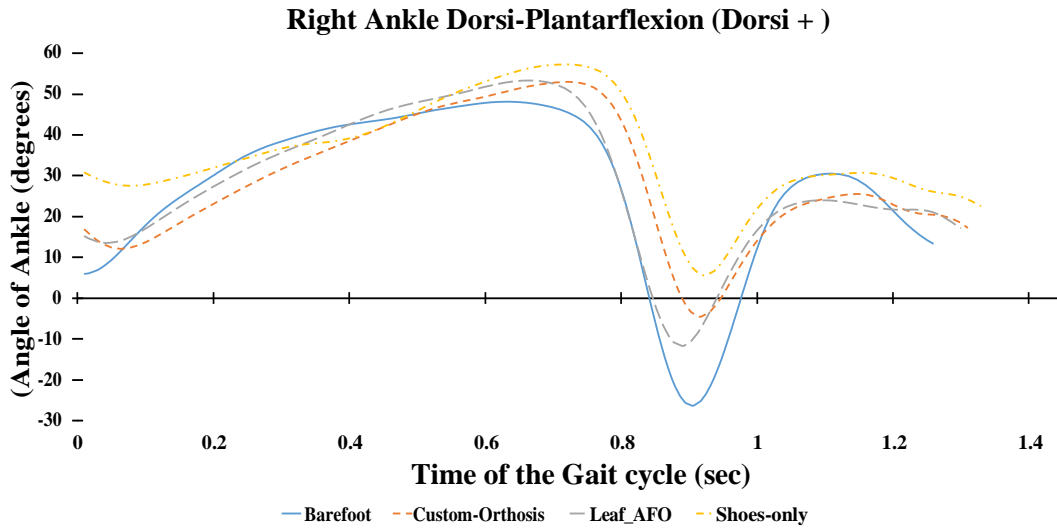
After creating the model, the force plate data were exported to the Visual 3D to calculate subject mass and height, and to identify the gait events for each limb from heel strike to push off as illustrated Section 3.2.5. Ankle plantarflexion-extension, knee flexion-extension, hip flexion-extension angles, moments and power were calculated based on the relative positions between every two segments using the inverse-dynamic approach. The average of these data was calculated, and the mean difference between every two conditions was computed to compare the results as discussed in the following sections.

4.2.1 Ankle joint kinematics and kinetics in the sagittal plane

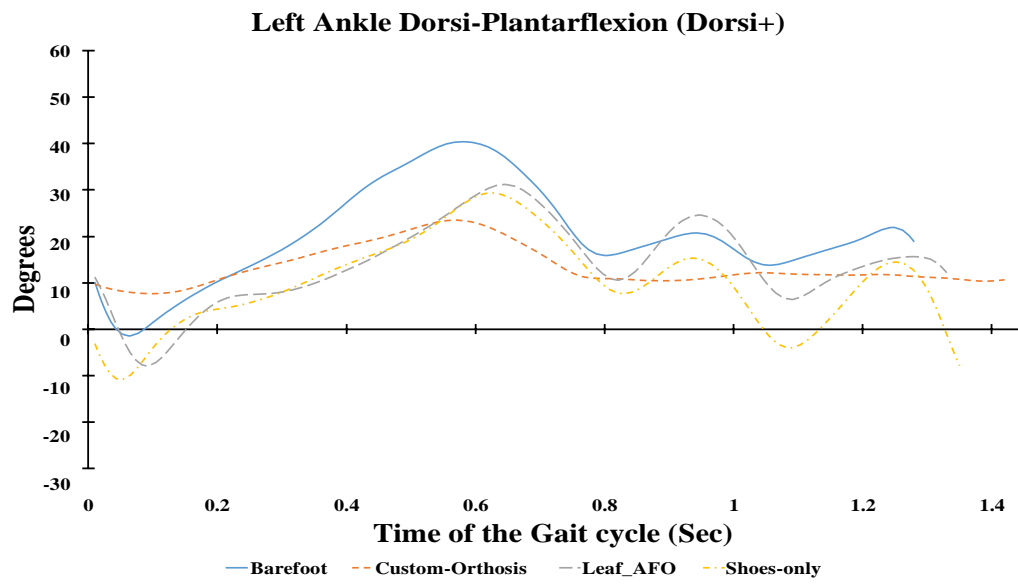
4.2.1.1 Ankle joint Dorsi-plantarflexion angles (ankle kinematics)

During the heel strike phase, the right dorsiflexion ankle was 5.99° for barefoot, 17.06° for custom-made AFO, 15.20° for Leaf Spring AFO, and 30.77° for the shoes only condition. The mean difference between every two conditions was significant during this phase ($p < 0.025$) as shown in Table 4.1. During the late stance phase, the right dorsiflexion angle was 47.71° for barefoot, 49.87° for custom-made AFO, 51.37° for Leaf Spring AFO, and 56.10° for shoes only. The maximum dorsiflexion angle for all conditions occurred between the terminal stance phase and the pre-swing phase, and was not significant ($p < 0.025$) for both orthoses, and the shoes increased the dorsiflexion angle by a mean difference of 2.71° , 4.2° , and 8.9° respectively as shown in Table 4.1 and Figure 4.1 a. The planter flexion angle reached the maximum during the time between the toes-off the ground phase and the initial swing phase. It is worth noting that there was a significant change ($p < 0.025$) as both orthoses and shoe conditions increased the plantar-flexion angle by a mean difference of 21.1° , 14° , and 39° respectively. During the same phase, the left dorsiflexion angles under the four conditions were 10.29° , 9.86° , 11.25° , and -3.18° respectively, as shown in Table 4.2. There was no significant change between barefoot and both orthoses ($p > 0.025$) however, the mean difference between the barefoot and shoes only conditions was significant ($p < 0.025$) showing a value of 13.48° . The ankle-custom made orthosis affected the gait cycle for the left limb rapidly; the maximum dorsiflexion angle occurred as the left foot pushed off the ground, which is less than the maximum-barefoot dorsi-flexion angle by a mean difference of 17.3° . Additionally, the custom-made orthosis had a long-range of

plantar-flexed ankle starting from a position at the initial swing and continuing until the ankle dorsiflexed to the neutral position at the end of the cycle. The results showed that custom, Leaf and shoes decreased the plantar-flexion angle compared to the barefoot by a mean difference of 17.6°, 18.1°, and 10.5° (Table 4.2, Figure 4.1 b).



a



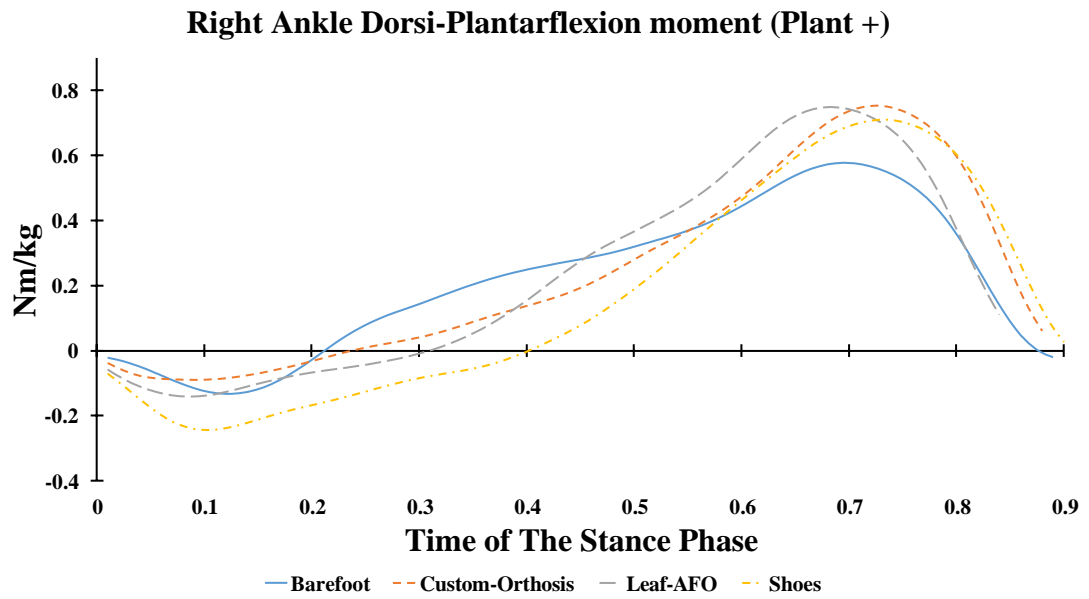
b

Figure 4.1: Ankle joint angles for the right limb (a) and left limb(b) during walking in the sagittal plane

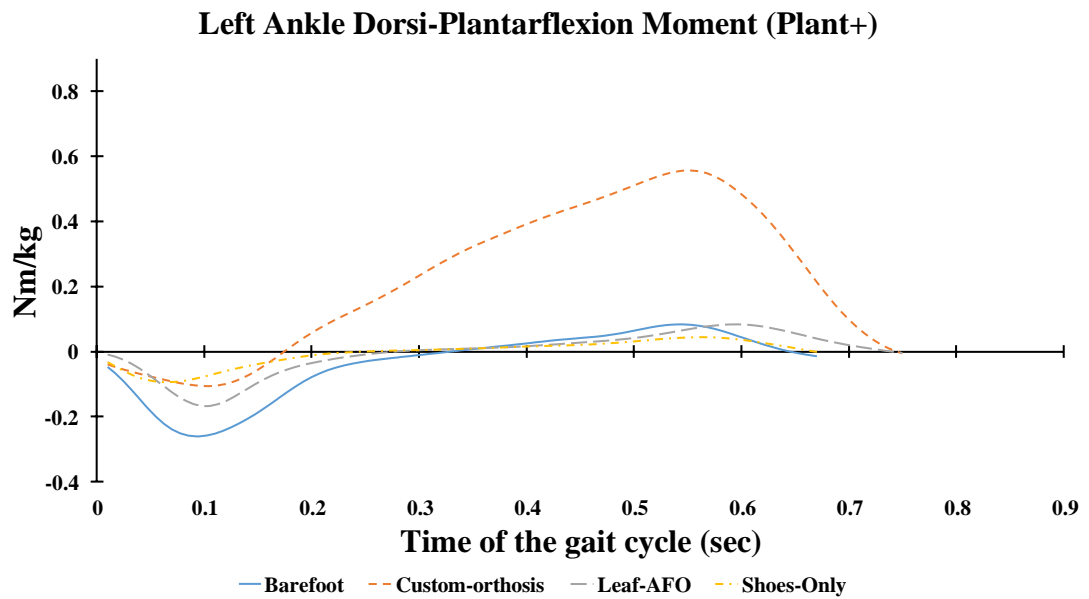
4.2.1.2 Ankle joint moment (ankle joint kinetics)

In terms of moments, the right ankle moment during the heel strike phase was -0.02 Nm/kg for barefoot, -0.04 Nm/kg for custom-made AFO, -0.06 Nm/kg for Leaf Spring AFO, and -0.07 Nm/kg for the shoes only. During the loading response phase, the right ankle moment values for the four conditions were -0.14, -0.04, -0.13, and -0.16 Nm/kg, respectively (Table 4.1, Figure 4.2 a). There was a significant change ($p < 0.025$, mean difference = -0.09 Nm/kg) between the custom-made AFO and barefoot conditions. However, there was no significant change between the Leaf Spring AFO and barefoot conditions ($p > 0.025$, mean difference = 0.008 Nm/kg), as shown in Table 4.1. At the period from the midstance phase until the terminal stance phase (right foot pushes off), the plantar-flexor moment increased until it reached maximum values at the late push off. All the custom, Leaf, and shoe conditions had a higher right ankle plantar-flexor moment than that of barefoot by a mean difference of 0.12, 0.2, and 0.26 Nm/kg), as shown in Table 4.1.

Despite this, the results showed a statistically significant change for the right ankle moments, and there was an asymmetry in the entire stance phase for all four conditions, as seen in Figure 4.2 b. For the left diseased limb and during the period between the midstance phase and push-off phase, the left ankle plantar-flexor moment when wearing the custom-made orthosis, started to increase rapidly until it reached the maximum value of 0.56 Nm/kg as shown in Table 4.2. It showed a significant difference along with the entire stance phase between the custom and barefoot conditions ($p < 0.025$), but the Leaf Spring AFO and shoes did not affect the gait variables compared to the barefoot.



a



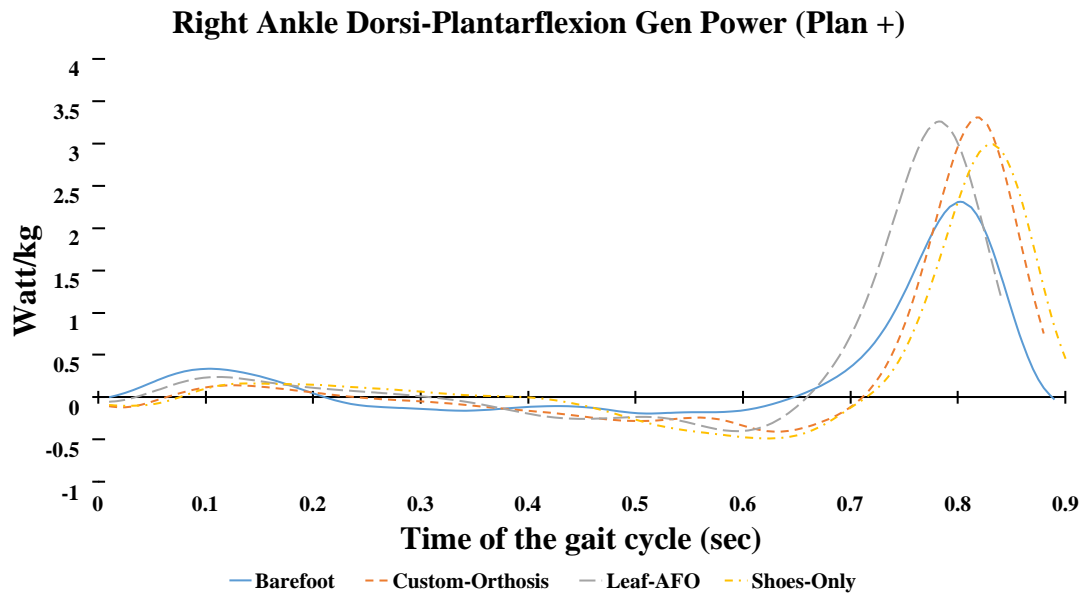
b

Figure 4.2: Ankle joint moments for the right limb (a) and left limb (b) during walking in the sagittal plane

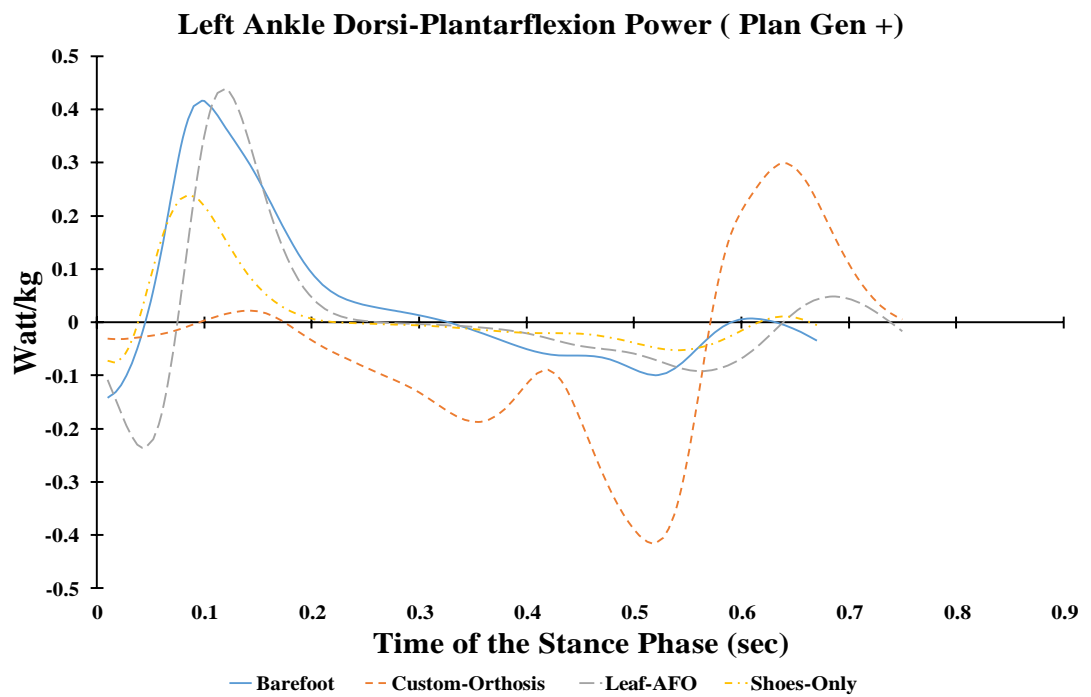
4.2.1.3 Ankle plantar-dorsiflexion power (ankle kinetics)

Finally, in terms of power generated during walking in the sagittal plane, the custom-made AFO, Leaf Spring AFO, and shoes generated a higher maximum plantar-flexion power than the barefoot at the late stance by a mean difference of 1, 0.9, and 0.8 Watt/kg respectively as shown in Table 4.1. However, there was no significant difference between the custom and Leaf in terms of power generated by the right limb during the late stance before the toes left the ground, and the mean difference was 0.08 Watt/kg ($p>0.025$) as seen in Figure 4.3a and Table 4.1.

Additionally, the power graph for the right limb showed consistency and symmetry in values during the period from the initial strike to the late portion of the midstance phase (60%) of the stance. The left limb has a unique pattern gait due to the severe hip dislocation, and this influences the gait parameters especially in the kinetics part. The custom drastically and significantly decreased the power generated by the affected limb during the loading response phase compared to the barefoot by a mean difference of 0.376 Watt/kg ($p<0.025$). However, the Leaf Spring AFO decreased the maximum dorsiflexion power generated during load-bearing by the main difference -0.06 Watt/kg which is considered statistically non-significant ($p>0.025$) compared to the other conditions. Additionally, during the late stance phase, there was no significant change witnessed among all the four conditions. The mean differences and standard deviations within each condition and among all conditions during the whole phases of the gait from heel strike to toe off are shown in Tables 4.1 and 4.2.



a



b

Figure 4-3: Ankle joint power for the right limb (a) and left limb (b) during walking in the sagittal plane

Table 4.1: Ankle kinematics and kinetics for the right limb during walking in the sagittal plane under four conditions: barefoot, custom-made AFO, Leaf Spring AFO, and shoes only. Note, the bold numbers showing the mean difference between conditions is significant, and the P-value is less than 0.025. B vs C refers to the mean difference between barefoot and custom-made AFO

Sagittal Plane		Right Ankle								Mean Difference between conditions					
Phase	Barefoot		Custom		(Leaf-AFO)		Shoes)		B vs C	B vs L	B vs S	LC vs	C vs S	L vs S	
	M	SD	M	SD	M	SD	M	SD	M	M	M	M	M	M	
Angles (degrees)	Heel Strike	5.99	± 0.09	17.06	± 0.43	15.20	0.37	30.77	0.75	-11.07	-9.21	-24.79	1.87	-13.71	-15.58
	Loading Response	21.15	± 0.30	22.38	± 0.57	18.02	0.44	32.37	0.79	-1.23	3.13	-11.22	4.36	-9.99	-14.36
	Midstance	40.00	± 0.57	38.21	± 0.97	43.91	1.07	42.66	1.04	1.79	-3.91	-2.66	-5.70	-4.45	1.25
	Late stance	47.17	± 0.68	49.87	± 1.27	51.37	1.26	56.10	1.37	-2.71	-4.20	-8.94	-1.50	-6.23	-4.73
	Toe off	-25.17	± 0.36	3.64	± 0.09	3.41	0.08	6.48	0.16	-28.82	-28.58	-31.66	0.24	-2.84	-3.08
	Initial Swing	-25.12	± 0.36	-3.53	± 0.09	-11.03	0.27	14.23	0.35	-21.58	-14.09	-39.35	7.49	-17.77	-25.26
	Mid Swing	28.13	± 0.40	23.96	± 0.61	21.80	0.53	28.17	0.69	4.17	6.33	-0.04	2.16	-4.21	-6.37
Terminal Swing	13.47	± 0.19	17.36	± 0.44	17.09	0.42	22.45	0.55	-3.89	-3.62	-8.98	0.27	-5.09	-5.37	
Moment (Nm/Kg)	Heel Strike	-0.02	± 0.00	-0.04	± 0.00	-0.06	0.00	-0.07	0.00	0.02	0.04	0.05	0.02	0.03	0.01
	Loading Response	-0.14	± 0.00	-0.04	± 0.00	-0.13	0.00	-0.16	0.00	-0.09	0.00	0.02	0.09	0.12	0.03
	Midstance	0.17	± 0.00	0.13	± 0.00	0.20	0.00	0.10	0.00	0.04	-0.03	0.07	-0.07	0.03	0.11
	Late Stance	0.36	± 0.01	0.48	± 0.01	0.56	0.01	0.62	0.02	-0.12	-0.20	-0.26	-0.08	-0.14	-0.06
	Toe off	-0.02	± 0.00	0.06	± 0.00	0.11	0.00	0.00	0.00	-0.08	-0.13	-0.02	-0.05	0.06	0.11
Power (Watt/Kg)	Heel Strike	0.00	± 0.00	-0.11	± 0.00	-0.05	0.00	-0.10	0.00	0.11	0.05	0.09	-0.06	-0.01	0.04
	Loading Response	0.33	± 0.00	0.07	± 0.00	0.24	0.01	0.14	0.00	0.26	0.08	0.19	-0.17	-0.07	0.10
	Midstance	-0.16	± 0.00	-0.15	0.00	-0.23	0.01	-0.13	0.00	0.00	0.08	-0.03	0.08	-0.03	-0.11
	Late stance	2.3	± 0.00	3.3	0.01	3.2	0.01	2.9	0.01	-1	-0.9	-0.6	0.08	0.04	0.03
	Toe off	0.1	± 0.00	0.76	0.02	1.20	0.03	0.20	0.00	-0.79	-1.23	-0.23	-0.44	0.56	1.00

Table 4.2: Ankle kinematics and kinetics for the left limb during walking in the sagittal plane under four conditions; barefoot, custom-made AFO, and Leaf Spring-AFO, and shoes only. Note, the bold numbers showing the mean difference between conditions is significant and the P value is less than 0.025 B vs C refers to the mean difference between barefoot and custom-made AFO

<i>Sagittal Plane</i>		<i>Left Ankle the effected side (Mean, SD)</i>								<i>Mean Difference between conditions</i>					
<i>Phase</i>		<i>Barefoot</i>		<i>Custom</i>		<i>Leaf-AFO)</i>		<i>Shoes)</i>		<i>B vs C</i>	<i>B vs L</i>	<i>B vs S</i>	<i>C vs L</i>	<i>C vs S</i>	<i>L vs S</i>
		<i>M</i>	<i>SD</i>	<i>M</i>	<i>SD</i>	<i>M</i>	<i>SD</i>	<i>M</i>	<i>SD</i>	<i>M</i>	<i>M</i>	<i>M</i>	<i>M</i>	<i>M</i>	<i>M</i>
Angles (degrees)	Heel Strike	10.2963	0.15	9.8639	0.2503	11.2336	0.2749	-3.1858	0.0780	0.4324	-0.9373	13.4821	-1.3697	13.0497	14.4194
	Loading Response	3.5938	0.052	7.7953	0.1978	-5.1754	0.1266	-2.4730	0.0605	-4.2015	8.7692	6.0668	12.9707	10.2683	-2.7024
	Midstance	13.0527	0.1875	13.9216	0.3533	10.3767	0.2539	10.2752	0.2514	-0.8689	2.6760	2.7775	3.5450	3.6464	0.1015
	Push off	40.9008	0.5874	23.5718	0.5981	27.0344	0.6615	29.2499	0.7158	17.3291	13.8665	11.6509	-3.4626	-5.6781	-2.2155
	Toe off	34.5960	0.4969	12.2710	0.3114	19.5352	0.4780	26.8301	0.6565	22.3250	15.0608	7.7658	-7.2642	-14.5592	-7.2950
	Initial Swing	28.7544	0.4130	11.0563	0.2805	10.5722	0.2587	18.2153	0.4457	17.6981	18.1822	10.5391	0.4841	-7.1590	-7.6431
	Mid Swing	15.5806	0.2238	11.9470	0.3031	7.3078	0.1788	-2.3111	0.0566	3.6336	8.2728	17.8917	4.6392	14.2581	9.6189
	Terminal Swing	20.8084	0.2988	10.7910	0.2738	12.1776	0.2980	-7.9278	0.1940	10.0174	8.6309	28.7362	-1.3865	18.7188	20.1053
Moment (Nm/Kg)	Heel Strike	-0.0479	0.0007	-0.0407	0.0010	-0.0084	0.0002	-0.0319	0.0008	-0.0072	-0.0394	-0.0160	-0.0322	-0.0088	0.0235
	Loading Response	-0.2446	0.0035	-0.1078	0.0027	-0.1517	0.0037	-0.0673	0.0016	-0.1369	-0.0929	-0.1773	0.0440	-0.0404	-0.0844
	Midstance	-0.0361	0.0005	0.1959	0.0050	0.0112	0.0003	0.0086	0.0002	-0.2320	-0.0473	-0.0446	0.1847	0.1874	0.0027
	Push off	0.0752	0.0011	0.5618	0.0143	0.0204	0.0005	0.0217	0.0005	-0.4866	0.0548	0.0535	0.5414	0.5401	-0.0013
	Toe off	-0.0145	0.0002	-0.0063	0.0002	-0.0041	0.0001	-0.0008	0.0000	-0.0082	-0.0104	-0.0137	-0.0022	-0.0055	-0.0033
Power (Watt/Kg)	Heel Strike	-0.1443	0.0021	-0.0313	0.0008	-0.1084	0.0027	-0.0718	0.0018	-0.1131	-0.0360	-0.0725	0.0771	0.0405	-0.0366
	Loading Response	0.3706	0.0053	0.0031	0.0001	0.4391	0.0107	0.1887	0.0046	0.3675	-0.0685	0.1819	-0.4360	-0.1856	0.2504
	Midstance	0.0379	0.0005	-0.1124	0.0029	-0.0103	0.0003	-0.0107	0.0003	0.1503	0.0481	0.0486	-0.1022	-0.1017	0.0004
	Late stance	-0.0283	0.0004	-0.2595	0.0066	0.0441	0.0011	0.0096	0.0002	0.2312	-0.0725	-0.0379	-0.3036	-0.2691	0.0346
	Toe off	-0.0351	0.0005	0.0051	0.0001	-0.0171	0.0004	-0.0050	0.0001	-0.0402	-0.0180	-0.0301	0.0222	0.0101	-0.0121

4.2.2 Knee joint kinematics and kinetics in the sagittal plane under four conditions

4.2.2.1 Knee joint flexion-extension angle (knee kinematics)

During the heel strike phase, the right knee flexion angle was 72.53° for barefoot condition, 0.96° for custom-made AFO, 60.77° for Leaf Spring AFO, and 61.45° for shoes only condition as shown in Table 4.3 and Figure 4.4 a. Moreover, the left knee flexion angle values under the four conditions were 28.35, 30.84, 27.40, and 26.03, respectively (Table 4.4, Figure 4.4 b). During the late stance phase of gait, the right knee flexion angle was 98.77° for barefoot, 102.09° for custom-made AFO, 94.64° for Leaf Spring AFO, and 98.02° for shoes only condition as shown in Table 4.3. The left knee flexion angle values under four conditions were 33.4° , 54.4° , 50.65° , and 37.27° .

As previously mentioned in the case description, the right knee is hyper-flexed severely due to the dislocated left hip and the limited movement that the patient had during his early age. In the sagittal plane movement, the custom made AFO, Leaf Spring AFO and shoes have had an enormous impact on the gait cycle compared to the barefoot condition and showed a significant ($p < 0.025$) decrease in the right knee-flexion angle at the initial strike by a mean difference of 17.46° , 11.76° , and 11.08° respectively as shown in Table 4.3. Furthermore, during the mid-swing phase, the custom-made and Leaf Spring orthoses decreased the flexion angle by a mean difference of 13.43° and 23.81° , respectively, in comparison with the barefoot condition. However, there was no significant change ($p > 0.025$) regarding the maximum flexion angle for the right knee at the late stance (right foot toe off) except that the condition of the shoes increased the angle by a mean difference of 11.39° as

shown in Table 4.3. The kinematics analysis of the left diseased limb revealed that the most significance change was during the late stance phase of gait correlated with decreasing values of the left knee flexion angle from the period, where the left toes left the ground to the initial swing portion as shown in Table 4.4.

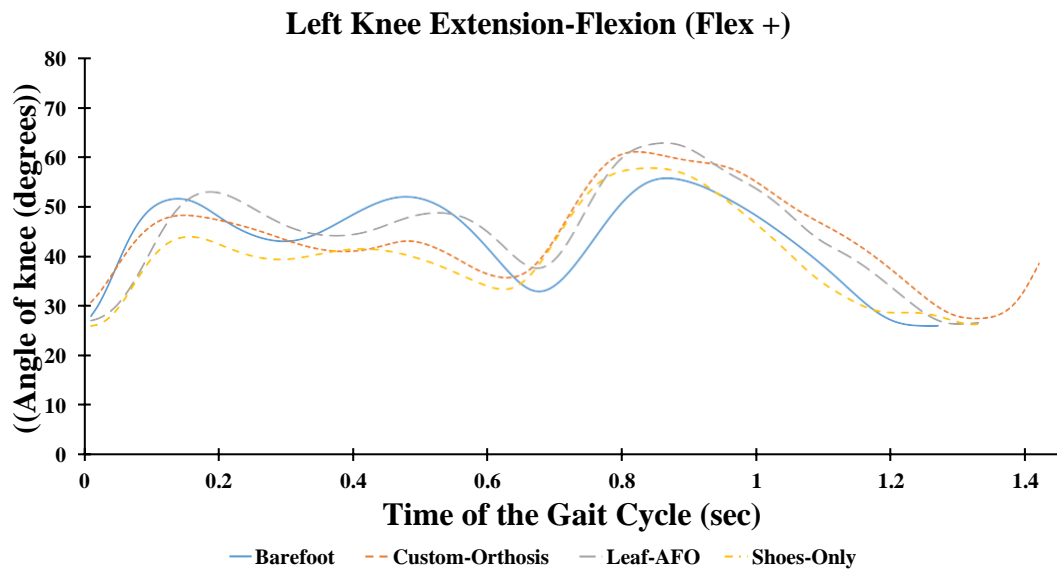
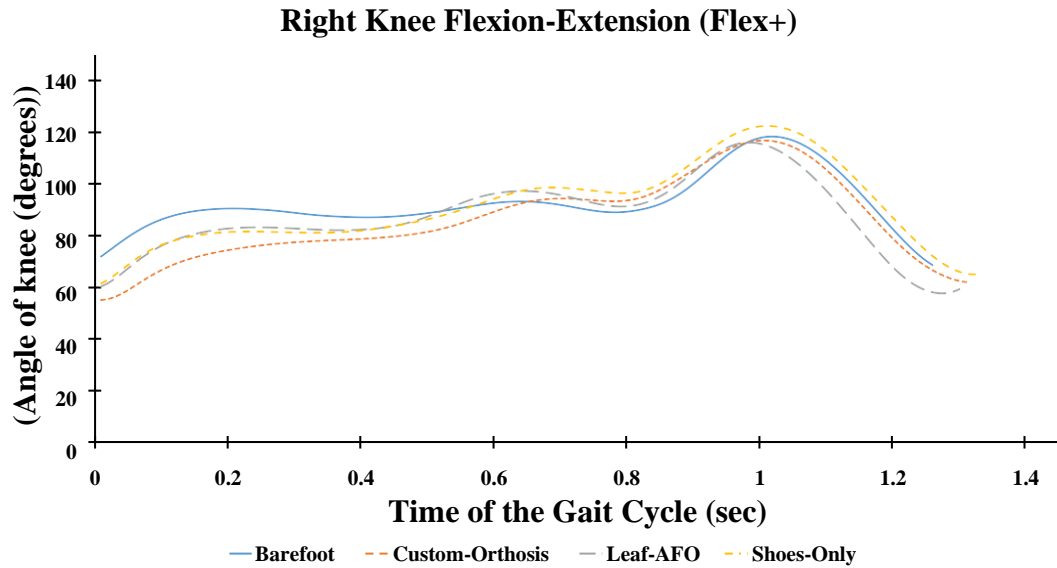
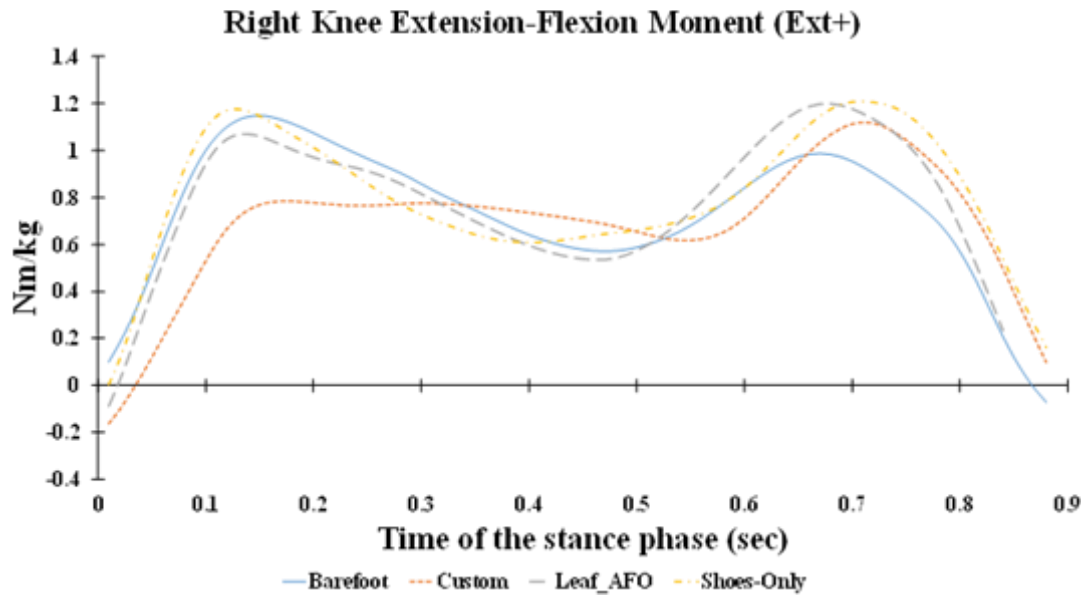


Figure 4.4: Knee joint angles for the right limb (a) and left limb (b) during walking in the sagittal plane.

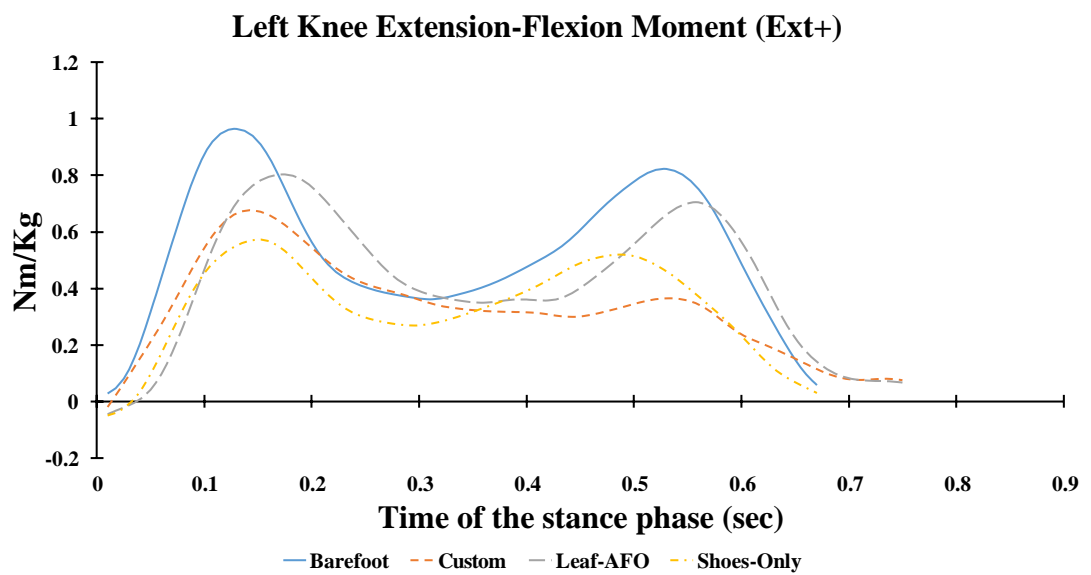
4.2.2.2 Knee joint flexion-extension moments and power (knee kinetics)

During the heel strike phase, the right knee flexion moment was 0.02Nm/kg for barefoot condition, -0.16 Nm/kg for custom-made AFO, -0.09 Nm/kg for Leaf Spring AFO and 0.009 Nm/kg for shoes only condition as shown in Table 4.3 and Figure 4.5 a. Moreover, the left knee flexion moments values under the four conditions were 0.03 Nm/kg, -0.02 Nm/kg, -0.05 Nm/kg, and -0.05 Nm/kg respectively (Table 4.4, Figure 4.5 b). During the loading response phase of gait, the right knee flexion moment was 1.07Nm/kg for barefoot, 0.78 Nm/kg for custom-made AFO, 1.02 Nm/kg for Leaf Spring AFO, and 0.98 Nm/kg for shoes only condition as shown in Table 4.3 and Figure 4.5a. The left knee flexion moment values under the four conditions were 0.97 Nm/kg, 0.54 Nm/kg, 0.65 Nm/kg, and 0.50 Nm/kg (Table 4.4, Figure 4.5b).

The knee kinetics data showed similar results to the ankle kinetics in terms of the custom orthosis influence on overall gait cycle. This fabricated orthosis decreased both the right and left extensor moments significantly ($p < 0.025$) during the load-bearing phase in comparison with barefoot by a mean difference of 0.29 Nm/kg, and 0.43 Nm/Kg respectively for both limbs. In addition, during that loading response phase, the custom had a higher generated knee flexion power in both limbs than those of barefoot, Leaf, and shoes, as shown in Figure 4.6 (a,b). The Leaf Spring AFO and shoe conditions showed similar right knee extensor moment data along the whole gait cycle in comparison with the barefoot condition except for the moment when the right foot pushed off the ground, as both Leaf and shoes had a higher extensor moment than barefoot showing a mean difference of 0.3, 0.4 Nm/kg respectively.

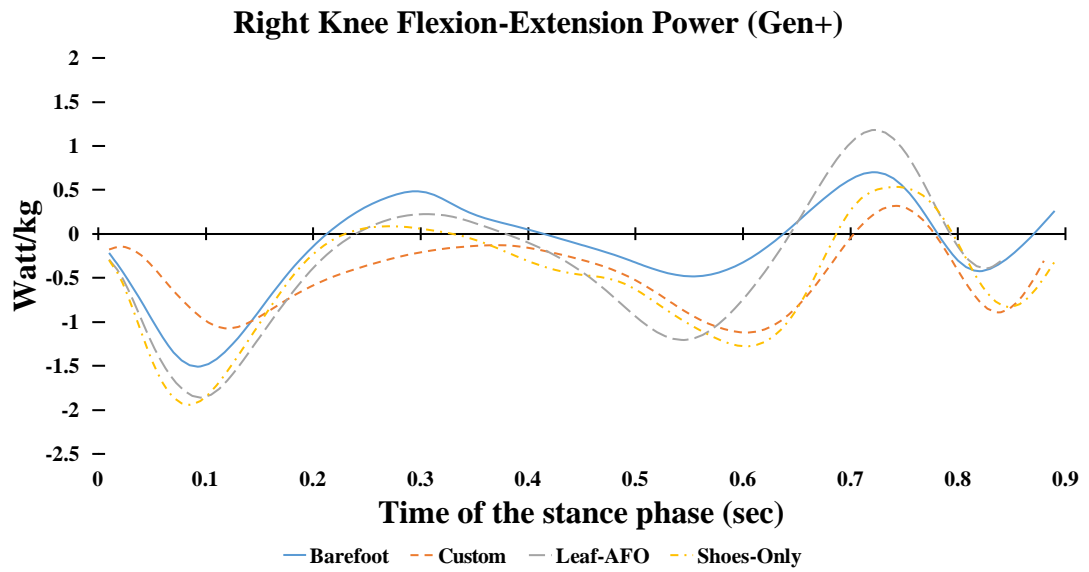


a

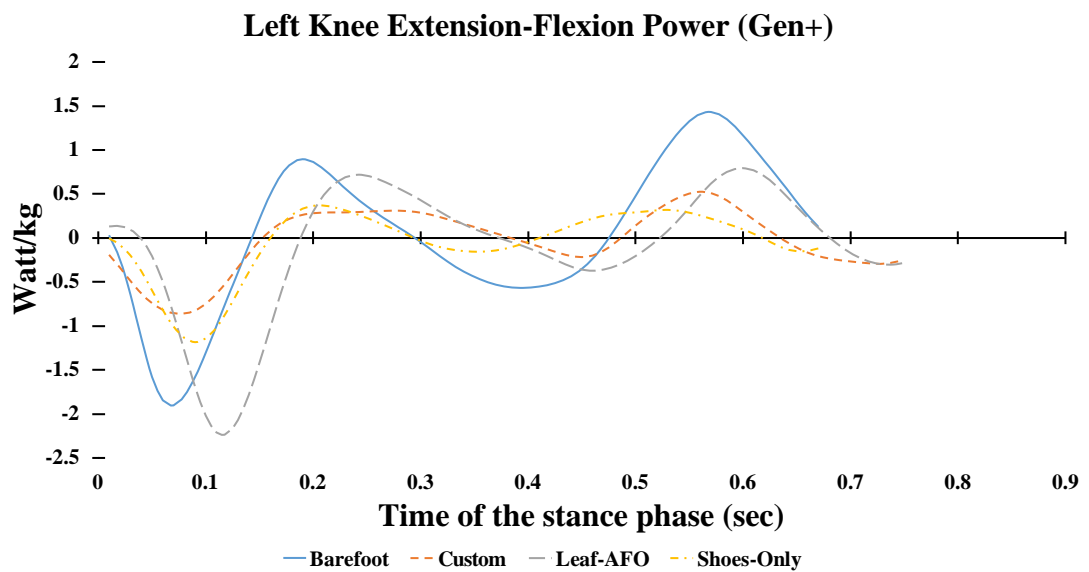


b

Figure 4.5: Knee joint flexion-extension moments for the right limb (a) and left limb (b) during walking in the sagittal plane



a



b

Figure 4.6: Knee joint Flexion-Extension power generation and absorption for the right limb (a) and left limb(b) during walking in the sagittal plane

Table 4.3: Knee kinematics and kinetics for the left limb during walking in the sagittal plane under four conditions: barefoot, custom-made AFO, Leaf SpringAFO, and shoes only. Note, the bold numbers showing the mean difference between conditions is significant, and the P-value is less than 0.025. B vs. C refers to the mean difference between barefoot and custom-made AFO

<i>Sagittal Plane</i>		<i>Right Knee (Mean, SD)</i>								<i>Mean Difference between conditions</i>					
		<i>Barefoot</i>		<i>Custom</i>		<i>(Leaf-AFO)</i>		<i>Shoes)</i>		<i>B vs C</i>	<i>B vs L</i>	<i>B vs S</i>	<i>C vs L</i>	<i>C vs S</i>	<i>L vs S</i>
<i>Phase</i>		<i>M</i>	<i>SD</i>	<i>M</i>	<i>SD</i>	<i>M</i>	<i>SD</i>	<i>M</i>	<i>SD</i>	<i>M</i>	<i>M</i>	<i>M</i>	<i>M</i>	<i>M</i>	<i>M</i>
		<i>Angles (degrees)</i>	<i>Heel Strike</i>	72.53	0.96	55.07	0.95	60.77	0.74	61.45	1.20	17.46	11.76	11.08	-5.70
<i>Loading Response</i>	88.59		1.17	73.83	1.27	77.77	0.95	81.42	1.59	14.76	10.82	7.17	-3.94	-7.59	-3.65
<i>Midstance</i>	89.04		1.18	78.54	1.35	83.30	1.02	84.10	1.65	10.51	5.74	4.95	-4.77	-5.56	-0.79
<i>Push off</i>	90.99		1.20	89.13	1.54	96.40	1.18	98.02	1.92	1.86	-5.41	-7.03	-7.27	-8.89	-1.62
<i>Toe off</i>	98.77		1.31	102.09	1.76	94.64	1.16	110.16	2.15	-3.32	4.13	-11.39	7.45	-8.07	-15.52
<i>Initial Swing</i>	105.18		1.39	110.10	1.90	105.37	1.29	119.99	2.35	-4.92	-0.19	-14.81	4.73	-9.89	-14.62
<i>Mid Swing</i>	94.84		1.25	81.41	1.40	71.02	0.87	81.68	1.60	13.43	23.81	13.15	10.38	-0.27	-10.66
<i>Terminal Swing</i>	69.22		0.92	61.98	1.07	59.74	0.73	65.11	1.27	7.24	9.47	4.10	2.24	-3.13	-5.37
<i>Moment (Nm/Kg)</i>	<i>Heel Strike</i>	0.02	0.00	-0.16	0.00	-0.09	0.00	0.00	0.009	0.19	0.11	0.02	-0.07	-0.17	-0.09
	<i>Loading Response</i>	1.07	0.01	0.78	0.01	1.02	0.01	0.98	0.02	0.29	0.05	0.09	-0.24	-0.20	0.04
	<i>Midstance</i>	0.84	0.01	0.74	0.01	0.57	0.01	0.64	0.01	0.10	0.27	0.20	0.17	0.10	-0.07
	<i>Push off</i>	0.64	0.01	0.71	0.01	0.93	0.01	1.11	0.02	-0.07	-0.30	-0.47	-0.22	-0.40	-0.18
	<i>Toe off</i>	-0.07	0.00	0.10	0.00	0.24	0.00	-0.05	0.00	-0.17	-0.31	-0.02	-0.14	0.15	0.29
<i>Power (Watt/Kg)</i>	<i>Heel Strike</i>	-0.22	0.00	-0.18	0.00	-0.29	0.00	-0.30	0.01	-0.04	0.08	0.08	0.12	0.12	0.00
	<i>Loading Response</i>	-1.33	0.02	-0.65	0.01	-1.81	0.02	-0.13	0.00	-0.68	0.48	-1.20	1.16	-0.52	-1.67
	<i>Midstance</i>	0.41	0.01	-0.14	0.00	-0.21	0.00	-0.48	0.01	0.55	0.62	0.88	0.07	0.34	0.27
	<i>Push off</i>	-0.47	0.01	-1.12	0.02	-0.89	0.01	-0.65	0.01	0.65	0.41	0.17	-0.24	-0.48	-0.24
	<i>Toe off</i>	0.27	0.00	-0.31	0.01	-0.31	0.00	0.06	0.00	0.57	0.58	0.20	0.009	-0.37	-0.37

Table 4.4: Knee kinematics and kinetics for the left limb during walking in the sagittal plane under four conditions; barefoot, custom-made AFO, Leaf Spring AFO, and shoes only Note, the bold numbers showing the mean difference between conditions is significant, and the P-value is less than 0.025. B vs. C refers to the mean difference between barefoot and custom-made AFO

Sagittal Plane		Left Knee the effected side (Mean, SD)								Mean Difference between conditions					
<i>Phase</i>		<i>Barefoot</i>		<i>Custom</i>		<i>(Leaf-AFO)</i>		<i>Shoes)</i>		<i>B vs C</i>	<i>B vs L</i>	<i>B vs S</i>	<i>C vs L</i>	<i>C vs S</i>	<i>L vs S</i>
		M	SD	M	SD	M	SD	M	SD	M	M	M	M	M	M
<i>Angles (degrees)</i>	<i>Heel Strike</i>	28.35	0.38	30.84	0.53	27.40	0.34	26.03	0.51	-2.48	0.96	2.32	3.44	4.80	1.36
	<i>Loading Response</i>	51.63	0.68	46.16	0.80	46.49	0.57	41.06	0.80	5.46	5.14	10.56	-0.33	5.10	5.43
	<i>Midstance</i>	45.32	0.60	44.24	0.76	44.66	0.55	40.19	0.79	1.08	0.66	5.12	-0.42	4.05	4.46
	<i>Push off</i>	46.36	0.61	39.88	0.69	39.78	0.49	33.44	0.65	6.47	6.57	12.91	0.10	6.44	6.34
	<i>Toe off</i>	33.44	0.44	54.40	0.94	50.65	0.62	37.27	0.73	-20.96	-17.21	-3.83	3.75	17.13	13.38
	<i>Initial Swing</i>	35.68	0.47	60.84	1.05	62.14	0.76	51.16	1.00	-25.16	-26.46	-15.48	-1.31	9.68	10.99
	<i>Mid Swing</i>	46.79	0.62	44.87	0.77	42.43	0.52	39.11	0.77	1.92	4.35	7.67	2.43	5.76	3.32
	<i>Terminal Swing</i>	26.39	0.35	38.58	0.66	26.94	0.33	26.38	0.52	-12.19	-0.55	0.01	11.64	12.20	0.56
<i>Moment (Nm/Kg)</i>	<i>Heel Strike</i>	0.03	0.00	-0.02	0.00	-0.05	0.00	-0.05	0.00	0.05	0.07	0.08	0.03	0.03	0.00
	<i>Loading Response</i>	0.97	0.01	0.54	0.01	0.65	0.01	0.50	0.01	0.43	0.32	0.47	-0.10	0.04	0.15
	<i>Midstance</i>	0.42	0.01	0.38	0.01	0.35	0.00	0.30	0.01	0.04	0.07	0.12	0.03	0.08	0.05
	<i>Push off</i>	0.71	0.01	0.36	0.01	0.08	0.00	0.12	0.00	0.35	0.62	0.59	0.27	0.24	-0.03
	<i>Toe off</i>	0.06	0.00	0.07	0.00	0.07	0.00	0.03	0.00	-0.02	-0.01	0.03	0.01	0.05	0.04
<i>Power (Watt/Kg)</i>	<i>Heel Strike</i>	0.03	0.00	-0.19	0.00	0.13	0.00	0.00	0.00	0.23	-0.10	0.03	-0.33	-0.19	0.13
	<i>Loading Response</i>	-0.69	0.01	-0.75	0.01	-2.25	0.03	-1.02	0.02	0.06	1.55	0.32	1.49	0.26	-1.23
	<i>Midstance</i>	0.46	0.01	0.31	0.01	0.05	0.00	-0.15	0.00	0.15	0.40	0.61	0.25	0.45	0.20
	<i>Push off</i>	1.45	0.02	0.50	0.01	-0.17	0.00	-0.07	0.00	0.95	1.62	1.52	0.67	0.57	-0.10
	<i>Toe off</i>	0.13	0.00	-0.25	0.00	-0.29	0.00	-0.12	0.00	0.38	0.42	0.25	0.04	-0.13	-0.17

4.3 HIP JOINT KINEMATICS AND KINETICS IN THE SAGITTAL PLANE UNDER FOUR CONDITIONS

4.3.1.1 *Hip joint flexion-extension angles (hip joint kinematics)*

Importantly, one of the main targets of this research was to study the effects of the orthosis aided devices on the hip parameters, particularly the power generated by the unaffected right hip during walking in the sagittal plane, as well the maximum extension and flexion moments in the loading response and late stance phases of gait. Due to the severe hip dislocation on the left side, we found creating the model to calculate the hip moments and power a substantial challenge. We assumed that the proximal end of the thigh is connected to a virtual joint, as mentioned in the digitizing and modelling section of Chapter 3.

As shown in Table 4.5, the highest hip flexion-extension hip angles were in decreasing order along with the entire stance phase, starting with 97.90° during heel strike phase, 92.66° during loading response, 76.39° during midstance, 50.89° during the push-off phase, and 32.28° during toe-off phase. There was no significant change ($p > 0.025$) in the right hip flexion angle at initial strike. The left flexion angle increased significantly ($p < 0.025$) by a mean difference of 15.87°, 15.07° and 15.23° while using the custom, Leaf, and shoes respectively at initial contact phase. Furthermore, during the loading response phase, the affected left limb had higher values of hip flexion angle when using the orthoses and shoes and, significantly, the mean difference values with barefoot were 11.95°, 16.02°, and 16.27° as shown in the Figure 4.7 b and Table 4.6. Also, the maximum right and left extension hip angles at the late stance increased rapidly with the use of the custom-made orthosis during the period from the push off the ground to the initial swing phase of gait, as shown

in Figure 4.7 a, b.

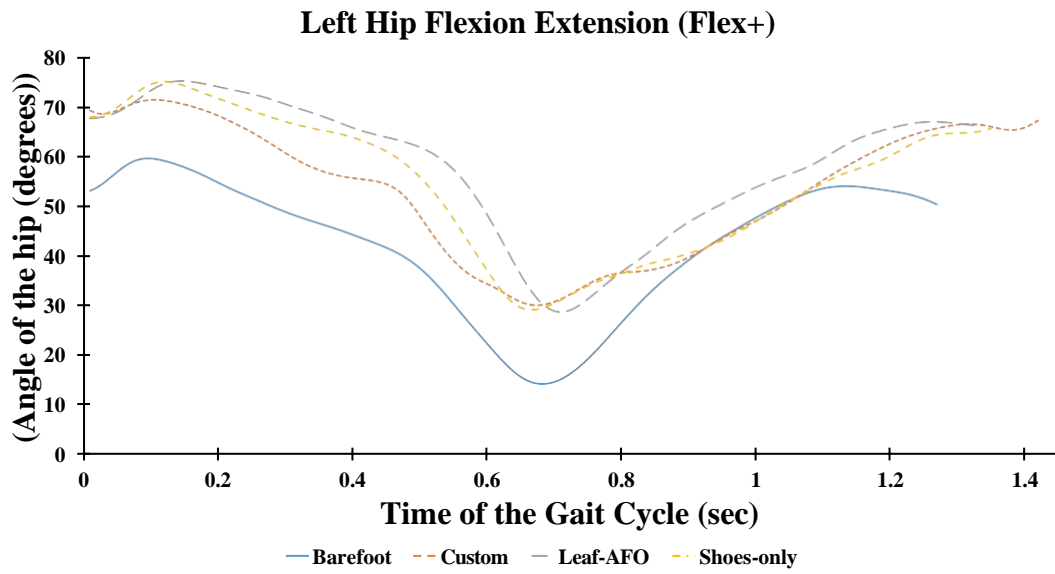
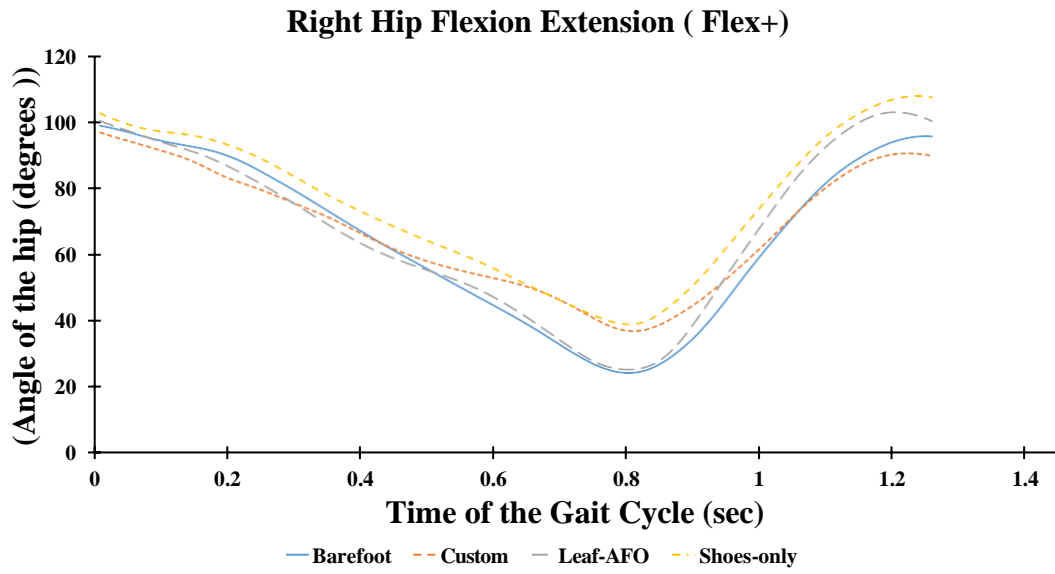
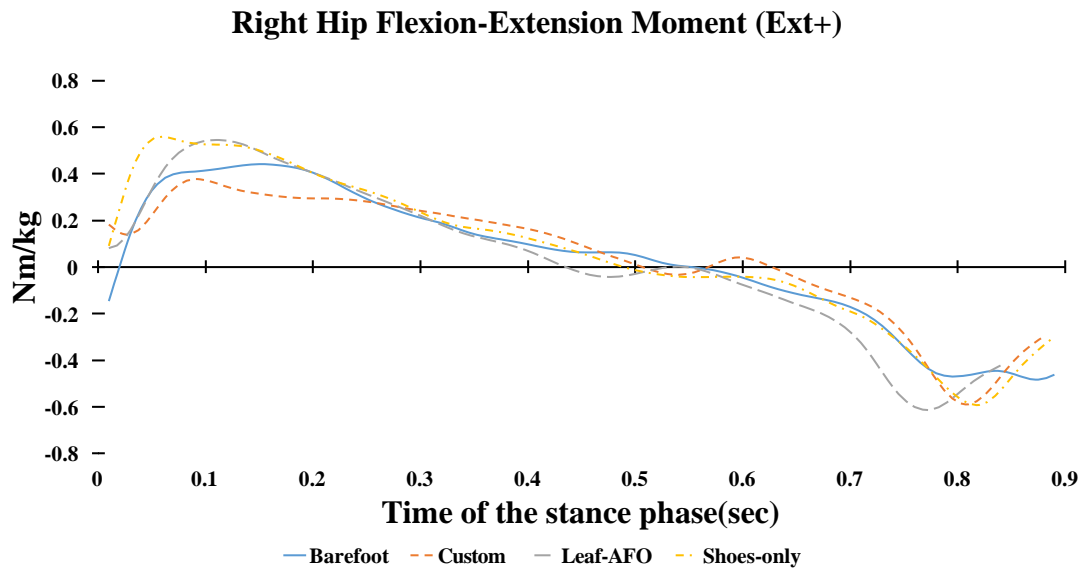


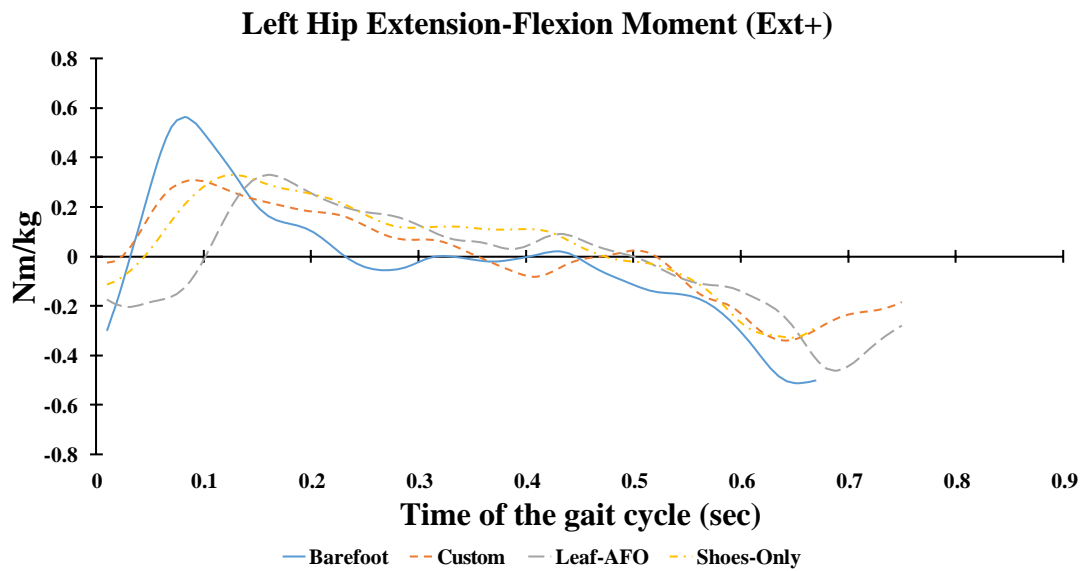
Figure 4-7: Hip joint angles for the right limb (a) and left limb (b) during walking in the sagittal plane

4.3.1.2 Hip joint moments and power (hip joint kinematics and kinetics)

For hip flexion/extension moments and power, the custom-made orthosis decreased the right and left maximum hip flexor moments during the loading response phase by a mean difference of 0.13 Nm/kg, and 0.07 Nm/kg ($p < 0.025$) respectively as shown in Table 4.5 and Figure 4.8 a. The custom-made orthosis had a higher moment during the late stance of the gait cycle than that of the barefoot. The data showed significant change ($p < 0.025$) by a mean difference of 0.1604 Nm/kg. However, the Leaf Spring AFO did not much change the flexion moment during the late stance phase (right toes leaving the ground). Moreover, when the left foot left the ground during the period between the metatarsals pushing off until the big toe left the ground, the left hip moment increased drastically and showed significant change ($p < 0.025$) in comparison to barefoot by a mean difference of 0.31 Nm/kg as presented in Table 4.6. In terms of power generated by the unaffected right hip during walking in the sagittal plane, the right hip under the custom-made orthosis and the Leaf Spring AFO during the initial contact portion of the stance phase generated more extension power in comparison to the barefoot and shoes conditions as shown in Figure 4.9a. Additionally, during the late stance phase of gait especially, at the moment the right foot pushed off the ground, both orthoses decreased the extensor power generation required to push the body forward in comparison to that of barefoot by a mean difference of 0.244, and 0.54 Watt/kg as shown in Table 4.5.



a



b

Figure 4.8: Hip joint Flexion-Extension moments for the right limb (a) and left limb(b) during walking in the sagittal plane

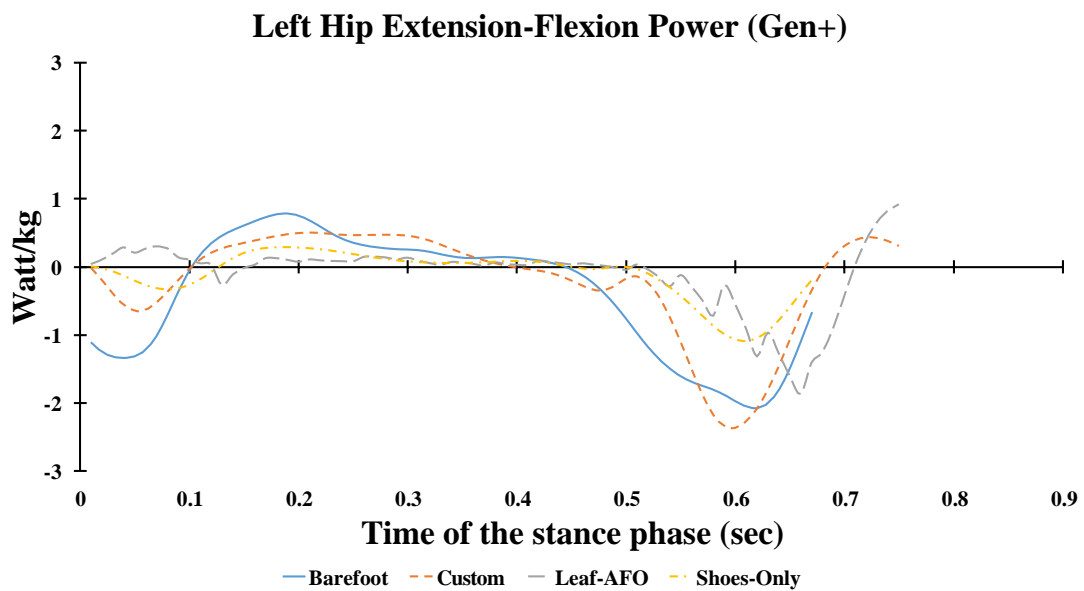
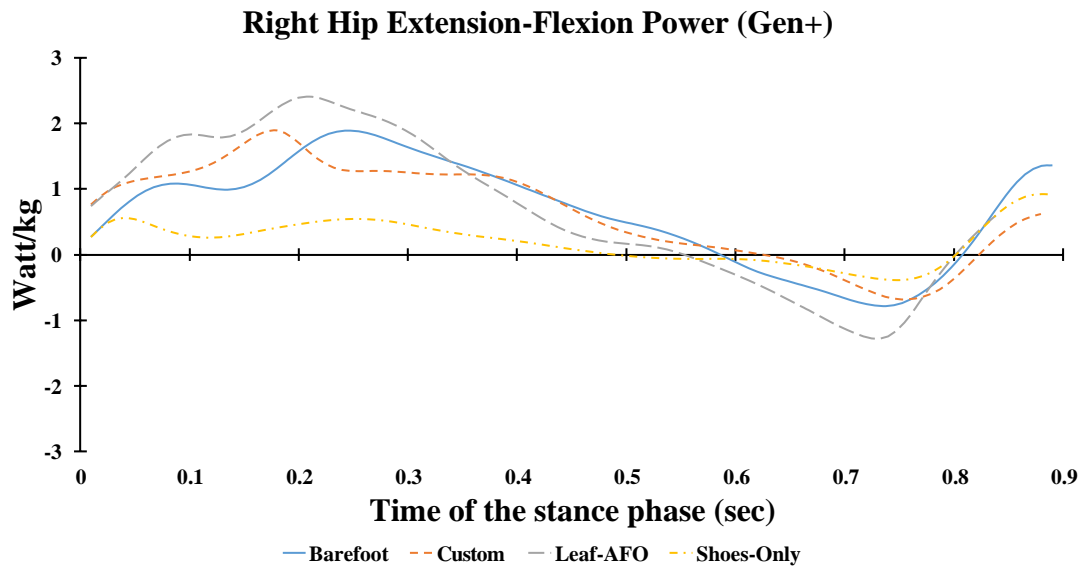


Figure 4.9: Hip joint Flexion-Extension power generation and absorption for the right limb (a) and left limb (b) during walking in the sagittal plane

Table 4.5: Hip joint kinematics and kinetics for the right limb during walking in the sagittal plane under four conditions: barefoot, custom-made orthosis, Leaf Spring AFO, and shoes only. Note, the bold numbers showing the mean difference between conditions is significant, and the P-value is less than 0.025. B vs. C refers to the mean difference between barefoot and custom-AFO.

<i>Sagittal Plane</i>		<i>Right Hip (Mean, SD)</i>								<i>Mean Difference between conditions</i>					
		<i>Barefoot</i>		<i>Custom</i>		<i>Leaf-AFO)</i>		<i>Shoes)</i>		<i>B vs C</i>	<i>B vs L</i>	<i>B vs S</i>	<i>C vs L</i>	<i>C vs S</i>	<i>L vs S</i>
	<i>Phase</i>	M	SD	M	SD	M	SD	M	SD	M	M	M	M	M	M
	<i>Angles (degrees)</i>	<i>Heel Strike</i>	97.9078	1.5493	95.8254	1.4910	100.3020	1.6271	102.5475	1.9317	2.0824	-2.3942	-4.6397	-4.4766	-6.7221
<i>Loading Response</i>		92.6605	1.4663	83.2695	1.2956	93.4268	1.5156	92.4680	1.7418	9.3910	-0.7663	0.1926	-10.1573	-9.1985	0.9589
<i>Midstance</i>		76.3993	1.2090	66.8722	1.0405	61.5352	0.9983	67.7079	1.2754	9.5271	14.8641	8.6914	5.3370	-0.8357	-6.1727
<i>Push off</i>		50.8911	0.8053	52.3749	0.8149	48.3537	0.7844	50.1240	0.9442	-1.4838	2.5374	0.7671	4.0213	2.2509	-1.7703
<i>Toe off</i>		32.2815	0.5108	41.5031	0.6458	26.7823	0.4345	52.5483	0.9899	-9.2215	5.4992	-20.2668	14.7207	-11.0452	-25.7660
<i>Initial Swing</i>		38.2709	0.6056	48.5091	0.7548	38.5219	0.6249	66.5764	1.2541	-10.2382	-0.2510	-28.3055	9.9871	-18.0673	-28.0544
<i>Mid Swing</i>		89.2798	1.4128	88.8237	1.3820	102.6899	1.6659	107.4974	2.0250	0.4561	-13.4101	-18.2176	-13.8662	-18.6737	-4.8075
<i>Terminal Swing</i>		94.7073	1.4987	85.6353	1.3324	96.6342	1.5676	102.2063	1.9253	9.0720	-1.9269	-7.4990	-10.9989	-16.5710	-5.5721
<i>Moment (Nm/Kg)</i>	<i>Heel Strike</i>	-0.1446	0.0023	0.1788	0.0028	0.0810	0.0013	0.0903	0.0017	-0.3234	-0.2256	-0.2349	0.0978	0.0885	-0.0093
	<i>Loading Response</i>	0.4225	0.0067	0.2908	0.0045	0.5453	0.0088	0.3836	0.0072	0.1317	-0.1228	0.0389	-0.2545	-0.0928	0.1617
	<i>Midstance</i>	0.1859	0.0029	0.1690	0.0026	0.0297	0.0005	0.0432	0.0008	0.0169	0.1562	0.1427	0.1394	0.1258	-0.0136
	<i>Push off</i>	0.0058	0.0001	0.0391	0.0006	-0.0598	0.0010	-0.1063	0.0020	-0.0333	0.0656	0.1121	0.0989	0.1454	0.0465
	<i>Toe off</i>	-0.4568	0.0072	-0.2964	0.0046	-0.4233	0.0069	-0.2259	0.0043	-0.1604	-0.0335	-0.2309	0.1269	-0.0705	-0.1974
<i>Power (Watt/Kg)</i>	<i>Heel Strike</i>	0.2658	0.0042	0.7523	0.0117	0.7378	0.0120	0.2681	0.0051	-0.4866	-0.4720	-0.0023	0.0146	0.4843	0.4697
	<i>Loading Response</i>	0.9938	0.0157	1.8101	0.0282	1.7841	0.0289	0.4885	0.0092	-0.8162	-0.7903	0.5053	0.0259	1.3216	1.2956
	<i>Midstance</i>	1.5009	0.0238	1.1456	0.0178	0.5784	0.0094	0.0605	0.0011	0.3553	0.9225	1.4404	0.5673	1.0852	0.5179
	<i>Push off</i>	0.3095	0.0049	0.0646	0.0010	-0.2371	0.0038	-0.1671	0.0031	0.2449	0.5466	0.4766	0.3017	0.2317	-0.0700
	<i>Toe off</i>	1.3423	0.0212	0.6102	0.0095	0.6158	0.0100	0.8599	0.0162	0.7321	0.7265	0.4824	-0.0056	-0.2497	-0.2441

Table 4.6: Hip joint kinematics and kinetics for the left limb during walking in the sagittal plane under four conditions: barefoot, custom-made orthosis, Leaf Spring AFO, and shoes only . Note, the bold numbers showing the mean difference between conditions is significant and the P value is less than 0.025. B vs C refers to the mean difference between barefoot and custom-made AFO

<i>Sagittal Plane</i>		<i>Left Hip the effected side (Mean, SD)</i>								<i>Mean Difference between conditions</i>					
	<i>Phase</i>	<i>Barefoot</i>		<i>Custom</i>		<i>Leaf-AFO)</i>		<i>Shoes)</i>		<i>B vs C</i>	<i>B vs L</i>	<i>B vs S</i>	<i>C vs L</i>	<i>C vs S</i>	<i>L vs S</i>
		M	SD	M	SD	M	SD	M	SD	M	M	M	M	M	M
<i>Angles (degrees)</i>	<i>Heel Strike</i>	52.6123	0.8325	68.4903	1.0657	67.6859	1.0980	67.8440	1.2780	-15.8780	-15.0736	-15.2317	0.8044	0.6463	-0.1581
	<i>Loading Response</i>	58.6255	0.9277	70.5838	1.0982	74.6510	1.2110	74.8977	1.4109	-11.9583	-16.0255	-16.2722	-4.0672	-4.3139	-0.2467
	<i>Midstance</i>	51.8137	0.8199	61.7813	0.9613	67.9035	1.1016	65.6839	1.2373	-9.9675	-16.0898	-13.8702	-6.1223	-3.9026	2.2196
	<i>Push off</i>	26.9159	0.4259	38.7184	0.6024	28.8630	0.4682	31.7504	0.5981	-11.8024	-1.9470	-4.8344	9.8554	6.9680	-2.8874
	<i>Toe off</i>	14.2820	0.2260	33.8613	0.5269	31.1830	0.5059	29.1182	0.5485	-19.5793	-16.9010	-14.8363	2.6783	4.7430	2.0648
	<i>Initial Swing</i>	14.9617	0.2368	36.2655	0.5643	38.5719	0.6257	33.2314	0.6260	-21.3038	-23.6102	-18.2697	-2.3064	3.0341	5.3405
	<i>Mid Swing</i>	48.6629	0.7701	56.2185	0.8747	60.3577	0.9791	51.7224	0.9743	-7.5556	-11.6947	-3.0594	-4.1392	4.4961	8.6353
	<i>Terminal Swing</i>	49.9234	0.7900	66.4932	1.0346	66.2534	1.0748	65.6119	1.2359	-16.5699	-16.3301	-15.6886	0.2398	0.8813	0.6415
<i>Moment (Nm/Kg)</i>	<i>Heel Strike</i>	-0.2991	0.0047	-0.0257	0.0004	-0.1742	0.0028	-0.1146	0.0022	-0.2734	-0.1249	-0.1845	0.1485	0.0889	-0.0596
	<i>Loading Response</i>	0.3790	0.0060	0.3001	0.0047	0.1549	0.0025	0.3110	0.0059	0.0789	0.2241	0.0680	0.1452	-0.0109	-0.1561
	<i>Midstance</i>	-0.0249	0.0004	0.0707	0.0011	0.0554	0.0009	0.1191	0.0022	-0.0956	-0.0802	-0.1440	0.0154	-0.0484	-0.0637
	<i>Push off</i>	-0.1906	0.0030	-0.1100	0.0017	-0.4452	0.0072	-0.3200	0.0060	-0.0806	0.2546	0.1295	0.3352	0.2101	-0.1251
	<i>Toe off</i>	-0.4970	0.0079	-0.1832	0.0028	-0.2796	0.0045	-0.2866	0.0054	-0.3138	-0.2174	-0.2104	0.0965	0.1034	0.0070
<i>Power (Watt/Kg)</i>	<i>Heel Strike</i>	-1.0915	0.0173	-0.0062	0.0001	0.0417	0.0007	0.0108	0.0002	-1.0853	-1.1332	-1.1024	-0.0479	-0.0171	0.0309
	<i>Loading Response</i>	0.3454	0.0055	-0.0239	0.0004	-0.2701	0.0044	-0.1822	0.0034	0.3693	0.6155	0.5276	0.2462	0.1583	-0.0879
	<i>Midstance</i>	0.4116	0.0065	0.4729	0.0074	0.0469	0.0008	0.0594	0.0011	-0.0613	0.3648	0.3523	0.4260	0.4135	-0.0125
	<i>Push off</i>	-1.7258	0.0273	-1.0818	0.0168	-0.4275	0.0069	-0.9398	0.0177	-0.6441	-1.2983	-0.7861	-0.6542	-0.1420	0.5123
	<i>Toe off</i>	-0.6530	0.0103	0.3091	0.0048	0.9208	0.0149	-0.1859	0.0035	-0.9621	-1.5738	-0.4671	-0.6117	0.4950	1.1067

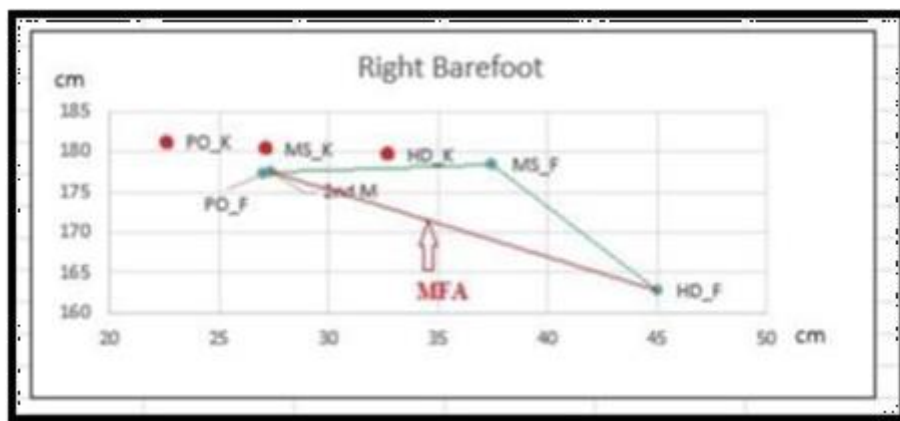
4.4 PLANTAR PRESSURE DISTRIBUTION

4.4.1 Right foot characteristics during the three main phases of the gait.

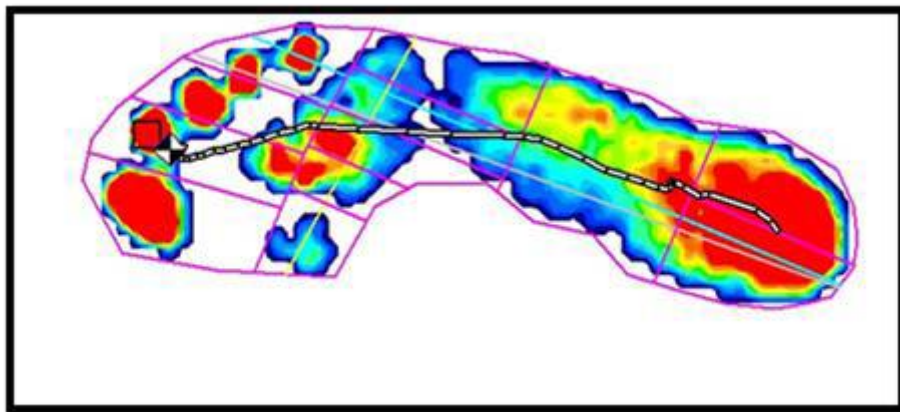
As mentioned previously in the kinematics and kinetics analysis section, the right knee was excessively flexed during the heel strike phase of gait while the patient was barefoot. The alignment of the force vector for the right limb appeared posterior to the knee axis, and the magnitude of this ground reaction force was 199.2 ± 0.94 N. During this phase, the COP was located centrally in the middle of 24.26 ± 1.10 cm² heel area. The contact pressure and the peak pressure magnitude were (83.5 ± 0.95 , 126 ± 2 kPa), respectively. During the mid-stance phase of gait, the right knee was vertically aligned with the body and posteriorly aligned to the knee axis; the ground reaction force magnitude was 239.1 ± 1.54 N.

Throughout the mid-stance phase, the right foot contact area magnitude was 36.88 ± 0.553 cm² and included the mid-foot region with a small part of the medial heel region. The COP trace located centrally along the entire mid-stance phase with the magnitude of 67.8 ± 1.101 kPa contact pressure and 134 ± 2.94 kPa of peak pressure. The knee joint location advanced drastically ahead of the ground reaction force vector at the initiation of the right foot push off the ground; the GRF magnitude was at its second peak 444.567 ± 2.08 N. The peak pressure reached the maximum at this phase, concentrating at a point on the big toe and second toe regions with a magnitude of 568.99 ± 1.001 kPa, the contact area of 30.97 ± 0.60 cm² had 153.34 ± 1.12 kPa, contact pressure included the big toe, second toe, third and fourth toes regions and part of the first three metatarsal regions as shown in Table 4.10.

Figure 4.10 shows a plot of the relative position of the significant COP excursions (HD, MS and PO) location and the corresponding kneecap position for the right barefoot trial. The point label “_F” and “_K” indicated the foot and KC position, respectively. Figure 4.10 shows that the MS_F was further away from the MFA. However, the KC was aligned with MFA closer to the right foot. Also, worth noting is that the KC trajectory started at a point ahead of the midfoot (MS_F).



a



b

Figure 4.10: Correlation between the COP (b) trajectory and lower limb movement (a) during barefoot walking

Table 4.7: Correlation between the COP trajectory and lower limb movement during barefoot walking

Right barefoot				
Parameters	Heel strike	Mid stance	Push –of	2 nd metatarsal
(X, Y)				
Knee cap position (mm)	32.7,179.5	27.1,180.2	22.6,181.1	-
Cop position (mm)	45,162.8	37.5,178.5	27,177.3	27.4,177.4
Knee offset (mm)	-	-	-	9.8,149.7

Wearing the custom-made AFO on the left limb affected with DDH increased the right foot’s ground reaction force significantly by a mean difference of 167.65 N at the initial contact portion of the gait, and the alignment of the GRF vector still appeared posterior to the knee axis. The custom–made orthosis allowed more contact area than that of the barefoot condition, and the patient initially stepped on the ground with a heel area of $29.16 \pm 0.71 \text{ cm}^2$, which maximized the contact pressure significantly by a mean difference of 44.286 kPa in comparison to that of barefoot. Moreover, the custom-made AFO increased peak pressure substantially by a mean difference of 72 kPa compared to barefoot condition. The PP magnitude of 198 kPa was noted as the first peak was reached by the foot during the whole stance phase of gait.

Additionally, the custom-made orthosis shifted the right foot centre of pressure laterally along the entire midstance portion of the gait spending 0.1 sec more than that of barefoot from the end of heel-strike to the midstance phase. At the initiation of the midstance portion, the contact area was less than that of barefoot by a mean difference of 15.46 cm^2 including the mid-foot region only. However, the contact pressure

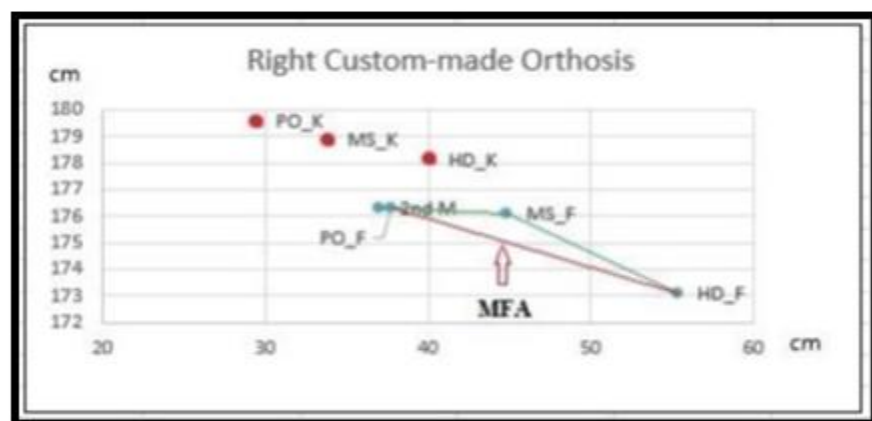
increased significantly by a mean difference of 66.18 kPa, as well as the peak pressure, which reached its second peak magnitude of 280.76 ± 3.73 kPa. It is worth noting that the ground reaction force had a similar finding to that of the barefoot condition during the MD phase. It increased by a mean difference of 55.5 N. While the right foot pushed off the ground, the custom-made orthosis kept the COP trace laterally along with the entire phase over the fourth metatarsal region.

Peak pressure and contact pressure reached their third and final peak magnitude of 283 ± 3.109 kPa and 134 ± 4.06 kPa respectively, and PP concentrated at a point between the third metatarsal and second toe, which was significantly less than that of the barefoot by a mean difference of 285.99 kPa. The custom-made orthosis also reduced the contact area by a mean difference of 7.47 cm², including the upper part of the metatarsal regions and the lesser toes regions. The ground reaction force vector aligned vertically to the body more closely posteriorly to the knee axis, and GRF had a closer value to that of barefoot reaching its second peak, as shown in Table 4.10.

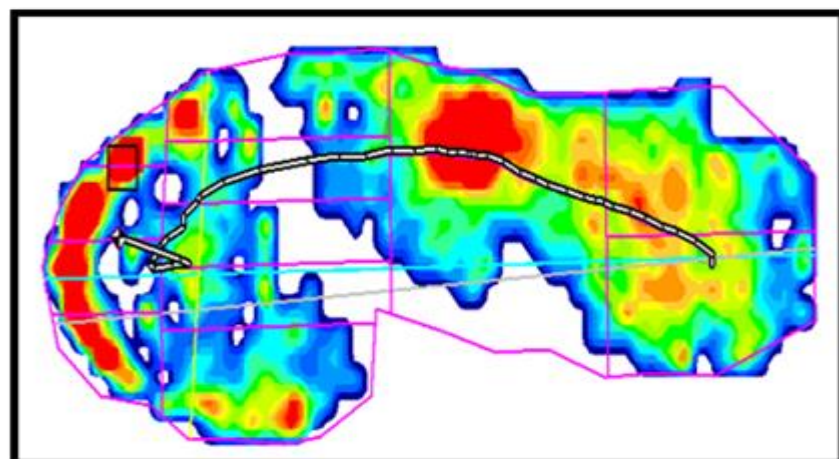
Figure 4.11 shows a plot of the relative position of the significant COP excursion locations and the corresponding KC position for the custom-made orthosis trial. The wearing of the custom-made AFO improved the gait of the left limb by allowing the KC trajectory within the footprint on the ground, thus giving more body support. The orthosis also enhanced the right foot gait by shifting the COP at MS_F closer to the KC trajectory. The knee offset was computed after correlating the measurements for both COP and KC trajectory, as shown in Table 4.8 below.

Table 4.8: Correlation between the centre of pressure trajectory and lower limb movements during custom-made-orthosis trial

Right Custom made AFO				
Parameters	Heel strike	Mid stance	Push -of	2 nd metatarsal
(X, Y)				
Knee cap position (mm)	40,178.1	33.8,178.9	29.4,179.6	-
Cop position (mm)	55.3,173.1	44.8,176.1	37.7,176.3	37,176.3
Knee offset (mm)	-	-	-	9.3,145.7



a



b

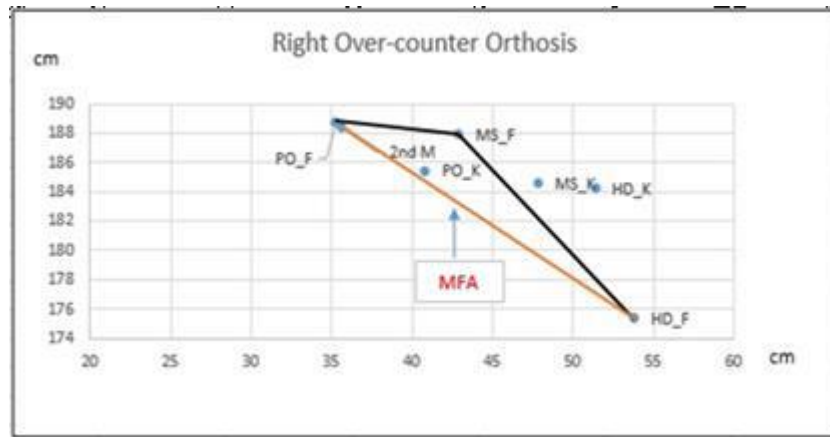
Figure 4.11: Correlation between the centre of pressure trajectory (b) and lower limb movements (a) during custom-made orthosis trial

The Leaf Spring AFO had an impact on the right foot's COP and pressure distribution along with the whole stance phase of the gait cycle. At the initiation of the right foot striking the ground, the Leaf Spring AFO shifted the alignment of the ground reaction force vector anteriorly close to the knee joint axis, and the magnitude of the GRF decreased significantly by a mean difference of 128.8 N in comparison to the barefoot GRF value. It is worth noting that the GRF values of both orthoses had a similar approximate value and did not change significantly. Statistically, the peak pressure and contact pressure of the right foot while wearing the Leaf Spring AFO during the heel strike phase increased to 140 ± 1.57 kPa and 92 ± 0.65 kPa, and neither value was significantly changed. However, the results revealed a significant change in the contact area between barefoot and Leaf Spring AFO conditions. The orthosis increased the heel contact area to 35.89 ± 0.38 cm² by a mean difference of 11.63 cm² (Table 4.10, Figure 4.13).

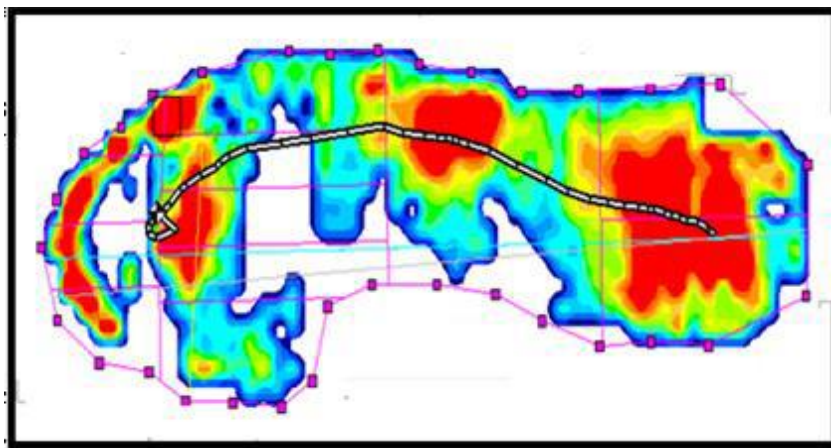
The results pointed out increases in the contact pressure and peak pressure during the mid-stance phase of gait by a mean difference of 48.2 kPa and 124 kPa, respectively. The COP trace moved laterally along the entire midstance phase over the mid-foot region area of 29.56 ± 1.26 cm², and the time spent to finish the phase was more than that of the barefoot by 0.1 sec. Noticeably, the peak pressure started increasing gradually until reaching its maximum value of 371 ± 2.08 kPa at the moment right foot pushed off the ground concentrated on the significant and second toes regions, which was less than that of the barefoot by a mean difference of 197.99 kPa. Also, the GRF had its second peak value 371 ± 2.08 N during this phase, less than its barefoot magnitude by a mean difference of 197.99 N, as shown in Table 4.10.

Table 4.9: Correlation between the plantar centre of pressure trajectory and lower limb movements during walking while the patient is wearing the Leaf Spring AFO

Right Leaf AFO spring Orthosis				
Parameters	Heel strike	Mid stance	Push –of	2 nd metatarsal
(X, Y)				
Knee cap position (mm)	50.06,184	40.05,179.4	25.15,179.25	-
Cop position (mm)	58.69,163.9	49.69,175.3	42.69,175.58	42.58,176.78
Knee offset (mm)	-	-	-	22.3,144.28



a



b

Figure 4.12: Correlation between the plantar centre of pressure trajectory (b) and lower limb movements (a) during walking while the patient is wearing the Leaf-AFO-Spring orthosis.

Figure 4.12 showed a plot of the relative position of the major COP excursions (HD, MS, and PO) location and the corresponding kneecap position for the right foot while the patient was wearing the Leaf Spring AFO on the left foot. Wearing the Leaf Spring AFO also improved the gait of the right foot by decreasing the rotation in the foot throughout, shifting the COP trajectory close to the KC trajectory, thus giving more body support as well. However, the knee trajectory at the heel strike started at a point before the MS-RF. It is worth noting that both AFOs shifted the COP trajectory more laterally along the entire gait cycle for the right foot unaffected by DDH. There are many reasons behind the shifting of COP towards the lateral surface of the foot, and these will be discussed in the next chapter.

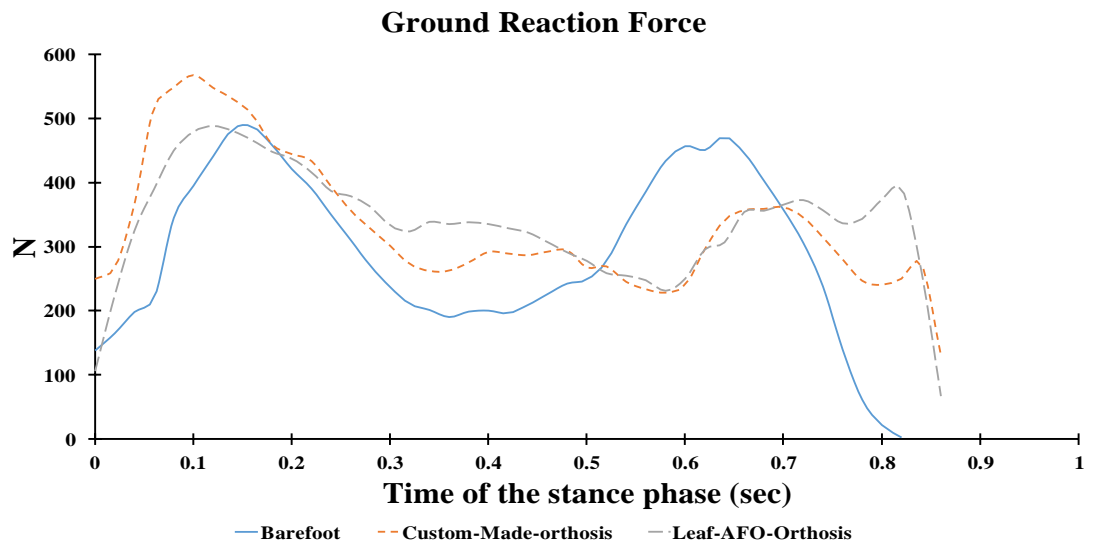


Figure 4-13: Ground reaction force along with the entire stance phase for DDH patient right foot under the three conditions; barefoot, custom-made, and Leaf Spring AFO

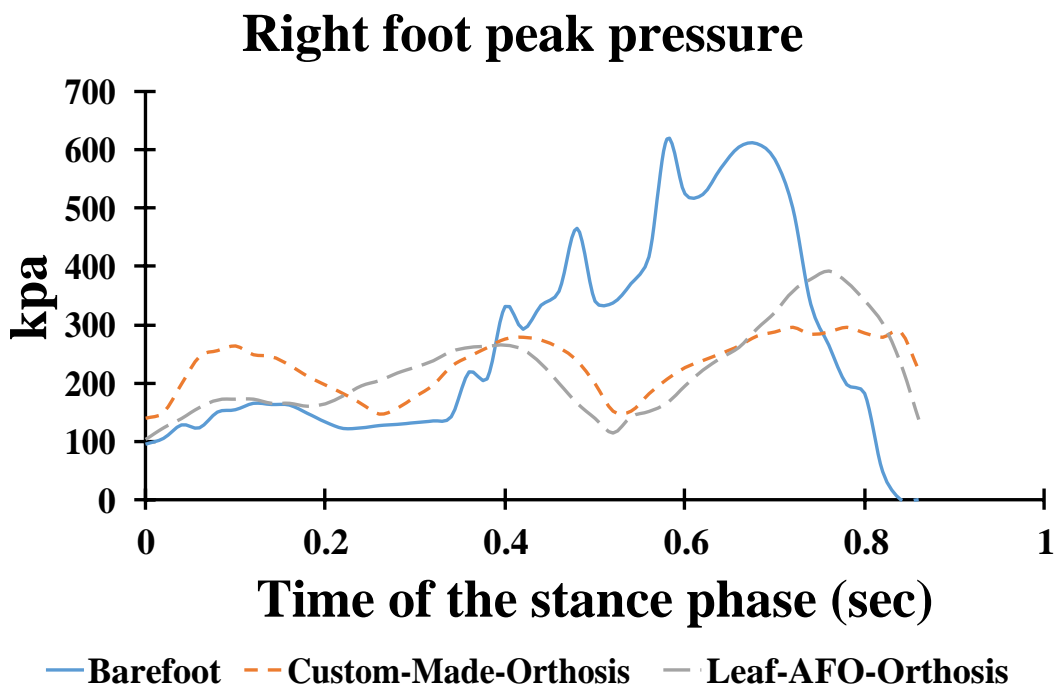


Figure 4.14: Peak pressure readings registered under the total foot during the whole stance phase of the gait under three conditions; barefoot, custom-made, and Leaf Spring AFO

Table 4.10: Right foot characteristics during the main three phases of the gait; heel strike, midstance, and push off under three conditions of barefoot, custom-Made-Orthosis and Leaf-AFO Orthosis

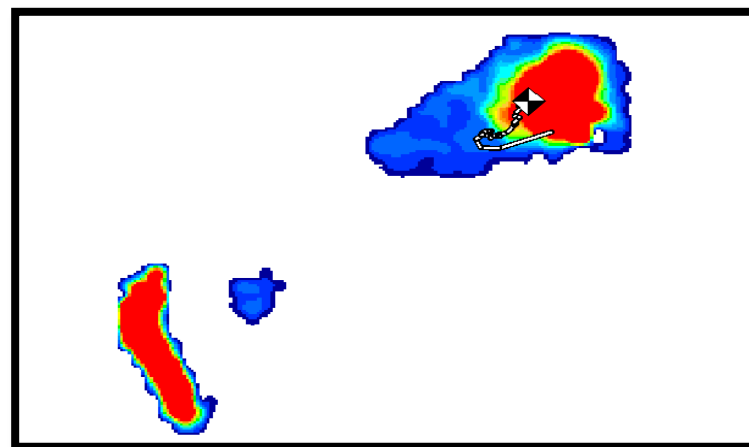
Right foot Parameters		Barefoot	Custom	Leaf-Afo	B Vs C	B Vs L	C Vs L
		M SD	M SD	M SD	M	M	M
Heel	Contact Area (m ²)	24.26±1.10	29.16±0.71	35.89±0.38	4.9	11.63	6.73
	Contact Pressure(kpa)	83.5±0.95	127.786±1.24	92±0.65	44.286	8.5	35.786
	Contact Time (sec)	0.04±0.02	0.04±0.12	0.042±0.002	0.006	0.002	0.004
	Ground Reaction Force(Newton)	199.2±0.94	366.85±3.13	328±2.30	167.65	128.8	38.85
	Peak Pressure (kpa)	126±2	198±6.46	140±1.57	72	14	58
Midstance	Contact Area (cm ²)	36.88±0.553	21.42±0.76	29.56±1.26	15.46	7.32	8.14
	Contact Pressure(kpa)	67.8±1.101	133.98±1.76	116±2.21	66.18	48.2	17.98
	Contact Time (sec)	0.32±1.3	0.4±0.02	0.42±0.02	0.08	0.1	0.02
	Ground reaction Force(Newton)	239.1±1.54	294.6±1.66	328.37±1.73	55.5	89.27	33.77
	Peak Pressure (kpa)	134±2.94	280.76±3.73	258±1.52	146.76	124	22.76
Push off	Contact Area (cm ²)	30.97±0.60	23.5±0.71	28.39±1.89	7.47	2.58	4.89
	Contact Pressure(kpa)	153.34±1.12	134±4.06	121±2.51	19.34	32.34	13
	Contact Time (sec)	0.65±0.01	0.66±0.02	0.74±0.02	0.01	0.09	0.08
	Ground Reaction Force(Newton)	472.4±1.14	314.67±2.54	342.99±1.50	157.73	129.41	28.32
	Peak Pressure (kpa)	568.99±1.001	283±3.109	371±2.08	285.99	197.99	88

4.4.2 Left foot characteristics

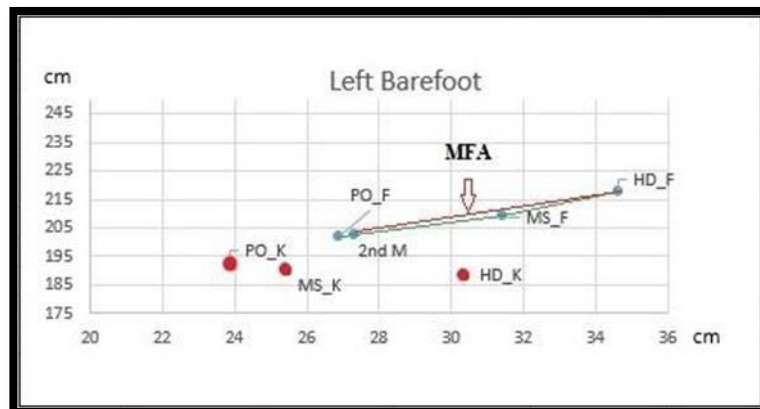
The ground reaction force vector appeared in the same line with the knee joint axis at the heel strike, and the GRF magnitude was 198.1 ± 2.35 N. The peak pressure was concentrated at the middle of 16.99 ± 0.57 cm² heel area with a value of 483 ± 2.78 kPa. Moreover, during the mid-stance phase, the knee joint axis advanced of GRF vector, the GRF value was 205.54 ± 1.40 N. Noticeably, due to the drop foot, the patient had to put more pressure on the heel area, so the contact pressure and peak pressure values were 128 ± 1.31 kPa and 356 ± 4.04 kPa respectively as shown in the table below. When the left foot pushed off the ground, the GRF vector was located posteriorly behind the whole body, and the force reached its second peak magnitude of 444.567 ± 2.08 N. The patient had a larger contact area of 34.78 ± 0.99 cm including the heel region and approximately half of the mid-foot region. The peak pressure was at its peak value of 563 ± 3.00 kPa, as shown in Table 4.14.

The results of the left foot affected with severe DDH and severe drop showed different outcomes and revealed many changes in plantar pressure distribution magnitudes and COP trace while wearing the custom-made orthosis and Leaf Spring AFO. The COP trace of the left foot affected with DDH while the patient was barefoot, started occurring at a point on the edge of the heel area during the initial strike phase, and then the trace was depicted at a point at the centre of the heel region. Eventually, during the time the left foot pushed off the ground, the trace was shown at a point on the lateral part of the heel (lateral heel region). Figure 4.15 shows a plot of the relative position of the major COP excursions (HD, MS and PO) location and the corresponding kneecap position for the barefoot trial. The point label “_F” and “_K” indicate the foot and KC position respectively. The correlation of the COP trajectory and a point on the

knee joint KC trajectory showed that the KC trajectory was further away from the centre of pressure during the whole stance phase however, the MFA was close to MSF. The correlation method showed that the computed knee offset reading was higher than that of the right foot (25.4 in x-direction, 199.8 in Y-direction) as shown in Table 4.11, thus indicating a bigger distance travelled by the knee to complete a single sub-phase of gait as seen as in Figure 4.15 (below) between the HD-K and MS-K.



a



b

Figure 4.15: Correlation between the COP trajectory (a) and lower limb movement (b) during barefoot walking for a patient with severe developmental dysplasia of the hip joint.

Table 4.11: Correlation between the COP trajectory and the lower limb movement during barefoot walking for a patient with severe developmental dysplasia of the hip joint.

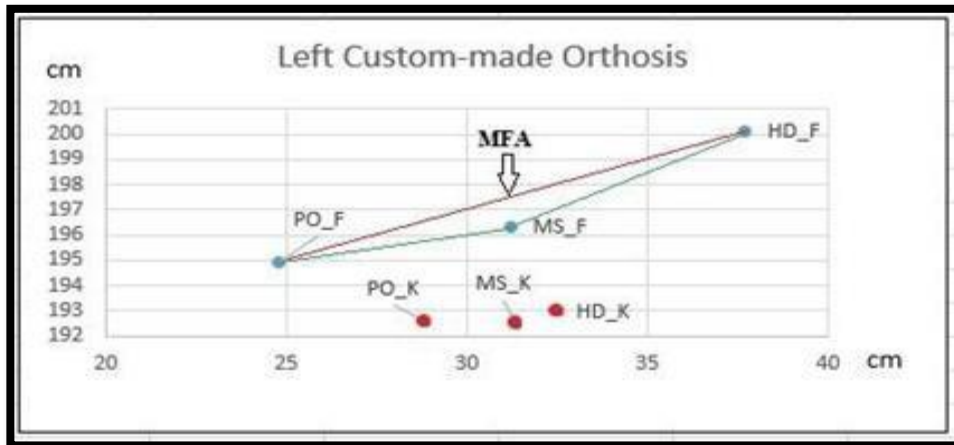
Left barefoot				
Parameters	Heel strike	Mid stance	Push –of	2 nd metatarsal
(X,Y)				
Knee cap position (mm)	59.16,200.88	42.2,203	26.8,203.58	-
Cop position (mm)	63.2,204.3	53.4,203.5	45.2,202.3	45.1,207.9
Knee offset (mm)	-	-	-	25.4,199.8

Wearing the custom-made orthosis on the left foot affected with DDH changed the COP trajectory along the entire stance phase. The COP began occurring at a point on the medial heel during the initial strike phase, and the trace continued medially over the mid-foot region until the end of the mid-stance phase. At the initiation of the push off phase, the custom- made orthosis shifted the COP trace further medially towards the fourth metatarsal region. When the left foot struck the ground, the custom-made AFO increased the contact heel area by a mean difference of 8.11 cm². In contrast, the contact pressure and the peak pressure were significantly decreased by the custom-made AFO. The results revealed decreases in both magnitudes in comparison to the barefoot condition by a mean difference of 31.02 kPa and 255 kPa, respectively. Figure 4.16 shows a plot of the relative position of the significant COP excursions (HD, MS, and PO) location and the corresponding kneecap position for the left side affected with DDH while the patient is wearing the custom-made AFO. Integrating the COP and KC

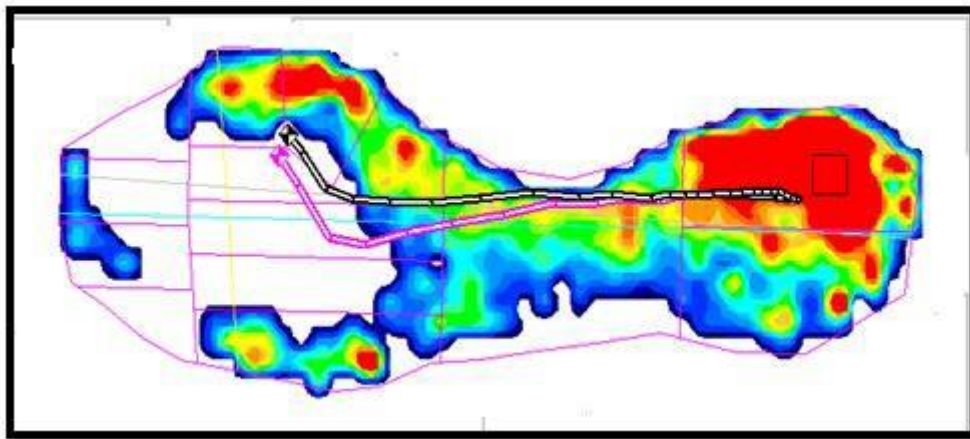
trajectory (x, y) components showed that the custom-made AFO decreased the knee-offset excursion in the x-direction to 9.3 cm, as shown in Table 4.12, thus bringing the KC trajectory at HD-k (heel-down) as close as possible to MS-K. Therefore, the distance travelled by the knee to complete a single sub-phase was less than that of the barefoot. It is worth noting that the MS-F to MFA distance was close to that of the healthy individual shown by the studies of Abbas and Chong (2018).

Table 4.12: Correlation between the COP trajectory and lower limb movement for the left foot under custom-made-AFO condition walking for a patient with severe developmental dysplasia of the hip joint.

Left custom-made-orthosis				
Parameters	Heel strike	Mid stance	Push –of	2 nd metatarsal
(X,Y)				
Knee cap position (mm)	32.4,193	31.3,192.6	28.8,192.6	-
Cop position (mm)	37.7,200.1	31.2,196.3	24.8,194.9	25.8,201.3
Knee offset (mm)	-	-	-	9.3,184



a



b

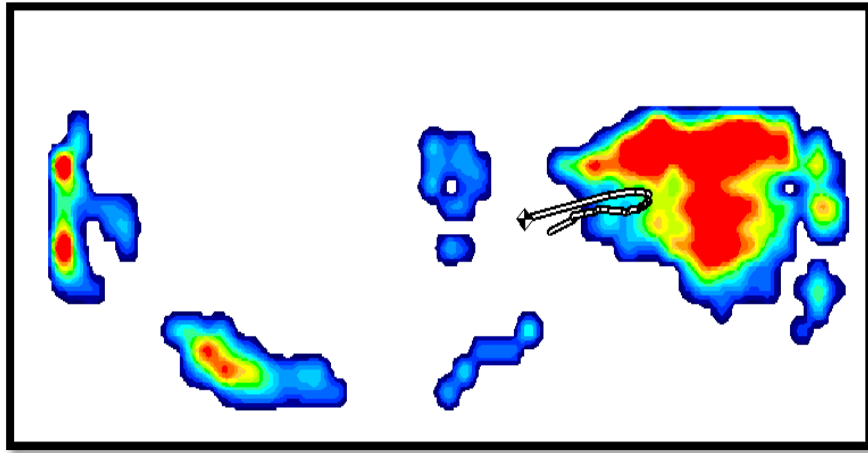
Figure 4.16: Integrating the COP (b) and KC trajectory (a) during walking while the patient is putting on the custom-made orthosis on the left foot.

Furthermore, the vector of 214.5 ± 2.02 N ground reaction force still appeared in the same line with the knee joint axis. The magnitude of this force during the heel down phase was statistically higher than that of the barefoot by a mean difference of 16.4 N. It is worth noting that at the initiation of the left foot single limb support phase (mid-stance), the custom-made AFO maximized the contact area to 37.16 ± 1.39 cm² including the heel and most of the mid-foot. However, the contact pressure and peak pressure values had no change compared to the barefoot case, and PP was at its peak during this phase at a point on the medial heel. A significant difference in the magnitude of the GRF was witnessed from the results during this phase reaching its second peak of 452.8 ± 2.15 N. The results showed a significant reduction in the peak

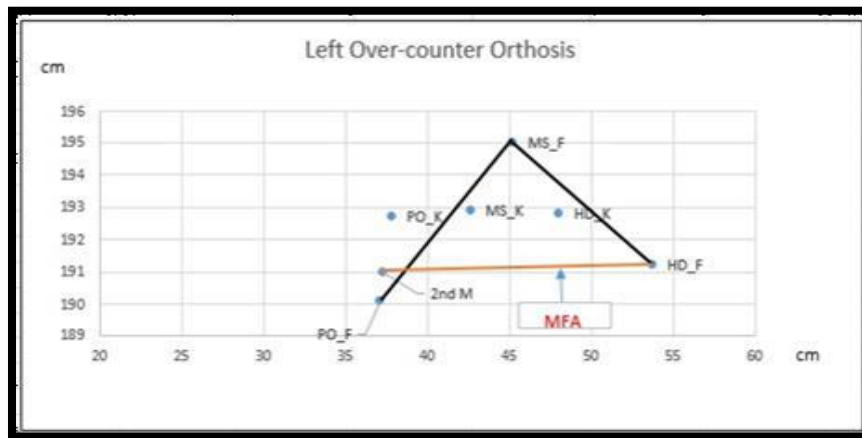
pressure amount by a mean difference during the push off phase, and the pressure was concentrated on the medial part of the metatarsal region particularly on the fifth metatarsal.

Finally, the results showed a significant reduction in the peak pressure amount by a mean difference during the push-off phase, and pressure was concentrated on the medial part of the metatarsal region, particularly on the fifth metatarsal. The GRF vector was aligned posteriorly close to the knee joint axis, and the GRF magnitude needed for foot clearance while wearing the custom-made AFO during this phase was lower than that required by the patient. At the same time, barefoot by mean difference was 247.26 N. The patient stepped off the ground using an area of $33.87 \pm 0.75 \text{ cm}^2$, which included most of the five metatarsals regions and a small part of the mid-foot region.

When the patient was wearing the Leaf Spring AFO, The COP trajectory began at a point ahead on the edge of the mid-foot region area, then started moving backward towards the heel area until the end of the mid-stance phase. Eventually, the COP moved forward again, completing the stance phase on the medial part of the mid-foot region. The GRF vector, in accordance with the knee joint position, was located in the same line parallel to the shank and anterior to the pelvis during the heel strike phase. Then the GRF vector shifted posteriorly to the knee joint axis at the single limb support (mid-stance phase). Later during the initiation of the left foot moment stepping off the ground, the knee axis was positioned anteriorly to the GRF vector. Figure 4.17 shows a plot of the relative position of the major COP excursions (HD, MS and PO) location and the corresponding kneecap position for the left side affected with DDH while the patient was wearing the Leaf Spring AFO on the left foot.



a



b

Figure 4.17: Integrating the COP (b) and KC trajectory (a) during walking while the patient is wearing the Leaf Spring AFO on the left foot

Table 4.13: Correlation between the COP trajectory and lower limb movement for the left foot under Leaf Spring AFO condition walking

Left foot with Leaf-AFO spring				
Parameters	Heel strike	Mid stance	Push –of	2 nd metatarsal
(X,Y)				
Knee cap position (mm)	59.16,200.88	42.2,203	26.8,203.58	-
Cop position (mm)	63.2,204.3	53.4,203.5	45.2,202.3	45.1,207.9
Knee offset (mm)	-	-	--	25.4,199.8

The contact area was significantly different between the Leaf Spring AFO and the other two conditions, showing a mean difference of 19.66 and 11.55 cm². The area included the heel and the upper part of the fifth metatarsal region when the left foot stepped on the ground. Importantly, The Leaf Spring AFO reduced contact pressure by a mean difference of 20.32 kPa in comparison with the barefoot condition. The peak pressure was also significantly reduced by a mean difference of 223 kpa. However, the results pointed out an increase in the GRF magnitude by a mean difference of 169.22N. During the mid-stance phase, the contact area and the GRF had higher values than that of the barefoot, as shown in the table below. The Leaf Spring AFO reduced the peak pressure value to 253±3.05 kPa concentrated at a point on the medial heel region. The data show that there was no significant change during the time the left foot pushed off the ground except that peak pressure was at its second peak of 302±2 kPa at a point on

the surface of the medial heel (MH) region as shown in Figures 4.18 and 4.19 below and Table 4.14.

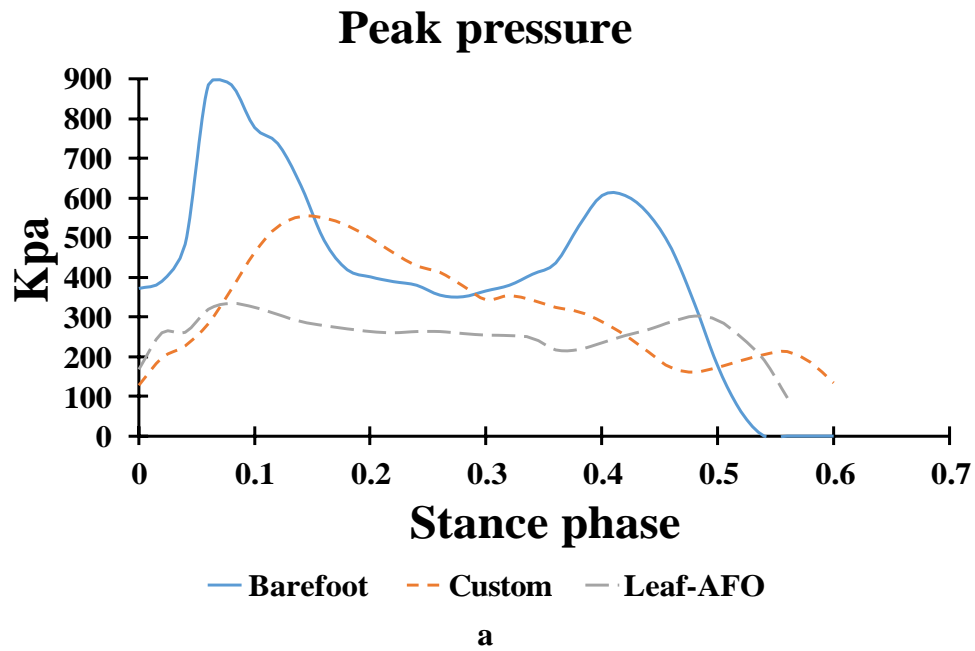


Figure 4.18 Shows the peak pressure readings registered under the total left foot during the whole stance phase of the gait under three conditions; barefoot, custom-made, and Leaf-AFO-orthosis.

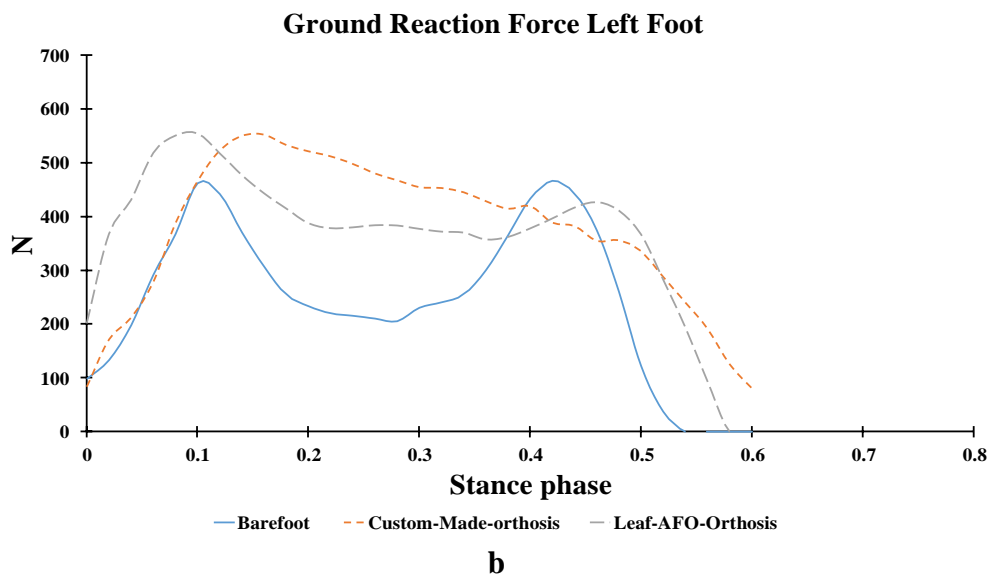


Figure 4.18: Peak pressure readings registered under the total left foot during the whole stance phase of the gait under three conditions: barefoot, custom-made orthosis, and Leaf Spring AFO

Table 4.14: Left foot characteristics during the main three phases of gait: heel strike, midstance, and push off under three conditions of barefoot, custom-made orthosis and Leaf Spring AFO

Left foot Parameters		Barefoot	Custom	Leaf-Afo	B Vs C	B Vs L	C Vs L
		M SD	M SD	M SD	M	M	M
Heel	Contact Area (m ²)	16.99±0.57	25.1±1.1	36.65±0.97	8.11	19.66	11.55
	Contact Pressure(kpa)	120.32±1.53	89.3±1.05	100±2.06	31.02	20.32	10.7
	Contact Time (sec)	0.04±2.12	0.04±0.02	0.02±0.01	0	0.02	0.02
	Force (Newton)	198.1±2.35	214.5±2.02	367.32±6.70	16.4	169.22	152.82
	Peak Pressure (kpa)	483±2.78	228±2	260±3.05	255	223	32
Midstance	Contact Area (m ²)	16.23±0.92	37.16±1.39	33.29±1.25	20.93	17.06	3.87
	Contact Pressure(kpa)	128±1.31	122±2.52	112±3.41	6	16	10
	Contact Time (sec)	0.27±0.01	0.32±0.02	0.32±0.01	0.05	0.05	0
	Force (Newton)	205.54±1.40	452.8±2.15	371.6±2.91	247.26	166.06	81.2
	Peak Pressure (kpa)	356±4.04	355±2	253±3.05	1	103	102
Push off	Contact Area (m ²)	34.78±0.99	33.87±0.75	35.3±1.15	20.93	0.52	1.43
	Contact Pressure(kpa)	130.56±2.02	87±2.08	117±2.51	6	13.56	30
	Contact Time (sec)	0.48±0.03	0.52±0.02	0.64±0.03	0.05	0.16	0.12
	Force (Newton)	444.567±2.08	289.43±1.39	410.73±3.00	247.26	33.837	121.3
	Peak Pressure (kpa)	563±3.00	191±3.23	302±2	1	261	111

4.5 FOOT REGIONS CHARACTERISTICS

4.5.1 Contact area

For the left foot affected with developmental dysplasia of the hip, the results revealed significant changes in the contact areas for the thirteen regions selected in this study when wearing both the custom-made AFO and the Leaf Spring AFO. The lateral heel region (LH) had the most significant contact area with the insoles while the patient was barefoot $16.05 \pm 0.40 \text{ cm}^2$. This value was followed by the midfoot (MF) region $13.46 \pm 0.34 \text{ cm}^2$, medial heel (MH) $12.94 \pm 0.32 \text{ cm}^2$ and then the fourth-fifth toes region (T45) $4.92 \pm 0.12 \text{ cm}^2$. No contact area was recorded for the metatarsal regions except for the metatarsal three (M3) $2.59 \pm 0.06 \text{ cm}^2$. The contact area gradually reduced from the big toe to the third toe regions. The results recorded readings in the metatarsal regions when the patient had the custom-made AFO on the left foot. The maximum value was seen in the M1 region followed by M5. However, the Leaf Spring AFO did not change the contact area values for the metatarsal regions except for a little contact area in the M4 region.

Furthermore, the custom-made orthosis increased the contact area in the mid-foot region significantly by a mean difference of 8.8 cm^2 . In contrast, the Leaf Spring AFO reduced the contact area by a mean difference of 7.56 cm^2 . The hallux had a smaller contact area while wearing the AFOs in comparison to that of the barefoot condition. Regarding the total foot contact area, the barefoot condition had the bigger value significantly higher than the other two conditions as shown in Table 4.15 and Figure 4.20.

Table 4.15: Mean, standard deviation (S.D.) and mean differences between each two conditions of contact area (CA) for the 13 regions of the left foot with DDH

CA	Left Foot						Mean difference between conditions		
Regions	Custom		Leaf		Barefoot		B vs C	B vs L	L VS C
	M	SD	M	SD	M	SD	M	M	M
TF	44.43	1.38	39.06	0.25	56.45	1.42	12.02	17.39	-5.37
MH	15.11	0.43	14.50	0.03	12.94	0.32	-2.17	-1.56	-0.61
LH	14.34	1.22	8.89	0.16	16.05	0.40	1.71	7.16	-5.45
MF	22.26	0.24	5.90	0.14	13.46	0.34	-8.80	7.56	-16.3633
M1	10.50	0.95	0.00	0.00	0.00	0.00	-10.50	0.00	-10.5
M2	3.66	0.23	0.00	0.00	0.00	0.00	-3.66	0.00	-3.65667
M3	2.07	0.52	0.00	0.00	2.59	0.06	0.52	2.59	-2.07333
M4	1.91	0.61	0.63	0.00	0.26	0.01	-1.65	-0.37	-1.27667
M5	5.95	1.79	5.35	0.12	0.00	0.00	-5.95	-5.35	-0.6
T1	0.33	0.21	1.60	0.12	3.62	0.09	3.29	2.02	1.266667
T2	0.96	0.07	2.48	0.03	1.82	0.05	0.85	-0.66	1.513333
T3	1.22	0.08	1.13	0.17	1.82	0.05	0.60	0.69	-0.09333
T45	0.07	0.05	0.22	0.14	4.92	0.12	4.85	4.69	0.156667

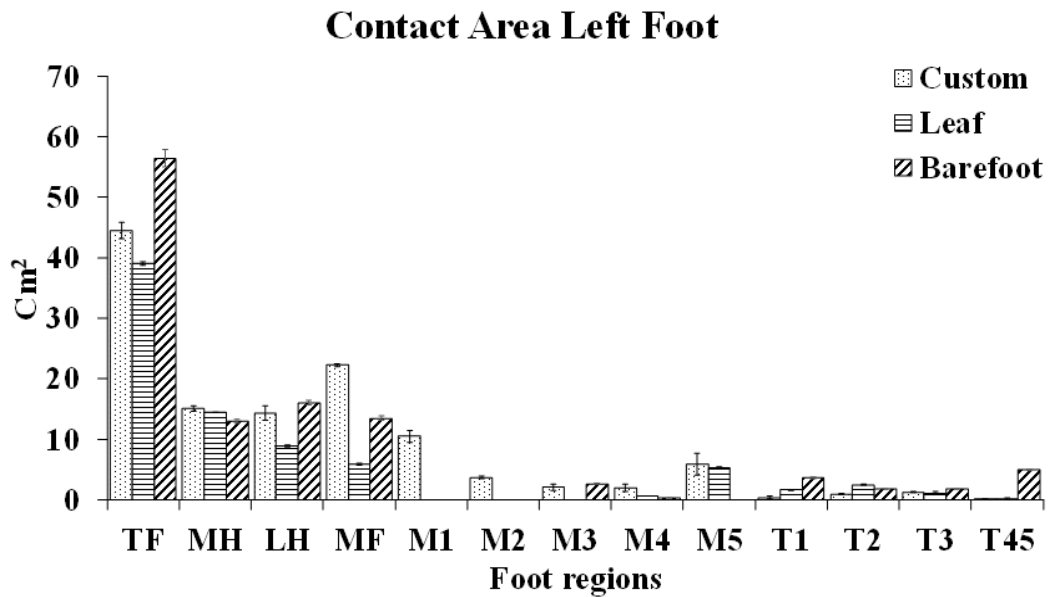


Figure 4.20: Mean, standard deviation (S.D.) and mean differences between each two conditions of contact area (CA) for the 13 regions of the left foot with DDH

The right foot (unaffected with DDH) had different readings in comparison with the left foot for the contact area values across the 13 regions. The highest contact area values for the rearfoot and midfoot region were, in decreasing order starting with the midfoot region, $27.36 \pm 2.66 \text{ cm}^2$, lateral heel (LH) $13.89 \pm 0.22 \text{ cm}^2$ and medial heel (MH) $11.98 \pm 1.02 \text{ cm}^2$. Furthermore, the metatarsal regions were in increasing order, with the lowest value recorded in the first metatarsal (M1) $3.12 \pm 0.69 \text{ cm}^2$, and the highest value in the fifth metatarsal region (M5) $8.00 \pm 2.38 \text{ cm}^2$. Additionally, the big toe (hallux) had the highest reading of $5.97 \pm 1.89 \text{ cm}^2$, and then the other three lesser toes regions were in decreasing order. The custom-made and Leaf Spring AFOs increased the contact area values significantly in both the lateral and medial heel regions of the right foot as shown in Table 4.16 and Figure 4.21. However, the midfoot region had a smaller reading than the barefoot while wearing the custom-made AFO by a mean difference of 4.19 cm^2 .

The first metatarsal region had the highest mark in both AFO conditions, recording readings of $6.21 \pm 2.85 \text{ cm}^2$ and $10.26 \pm 2.80 \text{ cm}^2$. This was followed by the fifth metatarsal (M5) region, fourth (M4), third (M3), then second metatarsal region (M2), as seen in the table. Noticeably, the increase in the heel contact areas while wearing the AFOs was accompanied by a significant decrease in the hallux reading.

Table 4.16: Mean, standard deviation (S.D.) and mean differences between each two conditions of contact area (CA) for the 13 regions of the right foot

CA Regions	Right Foot (Mean and SD)						Mean difference Between conditions		
	Custom	Leaf	Barefoot	B vs C	B vs L	C vs L			
TF	42.18	1.45	48.34	0.13	55.46	3.16	13.28	7.13	6.16
MH	15.90	0.53	17.70	0.72	11.98	1.02	-3.92	-5.72	1.79
LH	16.15	0.50	16.42	1.09	13.89	0.22	-2.25	-2.52	0.27
MF	23.17	0.43	28.47	0.13	27.36	2.66	4.19	-1.11	5.30
M1	6.21	2.85	10.26	2.80	3.12	0.69	-3.10	-7.15	4.05
M2	3.30	0.78	3.48	0.60	4.85	0.97	1.56	1.37	0.19
M3	3.79	0.23	4.64	0.15	6.49	0.66	2.70	1.84	0.86
M4	3.79	0.87	5.50	0.20	7.71	2.62	3.92	2.21	1.71
M5	5.60	1.96	7.92	1.03	8.00	2.38	2.40	0.08	2.33
T1	2.41	0.04	3.56	0.25	5.97	1.89	3.56	2.40	1.15
T2	2.05	0.20	3.16	0.32	3.81	1.26	1.76	0.65	1.11
T3	1.70	0.34	3.30	0.29	3.86	0.99	2.16	0.56	1.60
T45	1.16	0.05	1.39	0.08	3.33	0.21	2.18	1.94	0.24

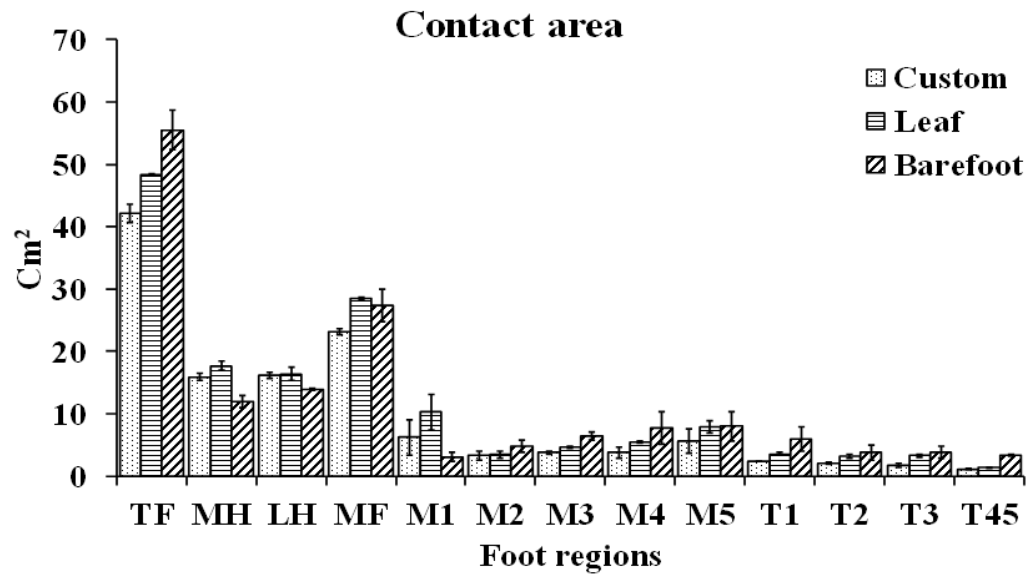


Figure 4.21: Mean, standard deviation (S.D.) and mean differences between each two conditions of contact area (CA) for the 13 regions of the right foot

4.5.2 PEAK PRESSURE

The highest mean pressure for the left foot affected by DDH was found under the lateral heel region 778.59 ± 19.53 kPa and medial heel region 728.42 ± 18.27 kPa, followed by the pressure under the big toe 620.06 ± 15.55 kPa, the second toe 557.85 ± 13.99 kPa, and then the small toes (T45) 523.74 ± 13.14 kPa. The mean PP values are presented in Table 4.17. Standard deviation ranges for each region under the three conditions are shown in Figure 4.22.

The custom-made AFO and Leaf Spring AFO reduced peak pressure significantly under the medial and lateral heel region by a mean difference of 291.75 kPa, and 430.09 kPa) and 460.92 kPa , and 453.92kPa respectively. In contrast, higher PP values were recorded under the mid-foot area while wearing the AFOs. The results of the custom-made AFO condition showed the highest reading under the first metatarsal (M1) 200.33 ± 26.03 kPa, followed by the fifth metatarsal (M5) 163.33 ± 37.65 kPa, and

then the second Metatarsal (M2) 133.33 ± 5.69 kPa.

The average results of the three-recorded steps revealed that both AFOs had an impact on the toes region peak pressure values, pointing out a significant reduction under all the four toe regions, as shown in Table 4.17. Finally, the highest total foot peak pressure was recorded during the barefoot condition 819.72 ± 20.56 kPa at a point on the heel area, followed by the custom-made AFO 436.67 ± 51.08 kPa, and then the Leaf Spring AFO 328.00 ± 13.86 kPa.

Table 4.17 Mean, standard deviation (S.D.) and mean differences between each two conditions of peak pressure (PP) for the 13 regions of the left foot with DDH

PP Regions	Left Foot						mean the difference between conditions		
	Custom		Leaf		Barefoot		B vs C	B vs L	C vs L
	M	SD	M	SD	M	SD	M	M	M
TF	436.67	51.08	328.00	13.86	819.72	20.56	383.06	491.72	-294.33
MH	436.67	51.08	298.33	8.08	728.42	18.27	291.75	430.09	-170.33
LH	317.67	76.00	324.67	19.63	778.59	19.53	460.92	453.92	-385.00
MF	178.67	4.73	139.33	16.74	43.14	1.08	-135.52	-96.19	86.00
M1	200.33	26.03	0.00	0.00	0.00	0.00	-200.33	0.00	200.33
M2	133.33	5.69	0.00	0.00	0.00	0.00	-133.33	0.00	133.33
M3	61.33	7.02	0.00	0.00	35.12	0.88	-26.22	35.12	47.00
M4	57.00	8.19	82.33	4.04	21.07	0.53	-35.93	-61.26	-164.67
M5	163.33	37.65	158.00	1.73	0.00	0.00	-163.33	-158.00	-61.00
T1	102.33	8.96	145.67	9.81	620.06	15.55	517.73	474.39	-30.33
T2	79.33	5.51	161.33	4.62	557.85	13.99	478.52	396.52	-108.00
T3	64.00	5.57	91.67	0.58	470.56	11.80	406.56	378.90	-97.67
T45	16.67	8.74	57.00	1.73	523.74	13.14	507.07	466.74	-120.67

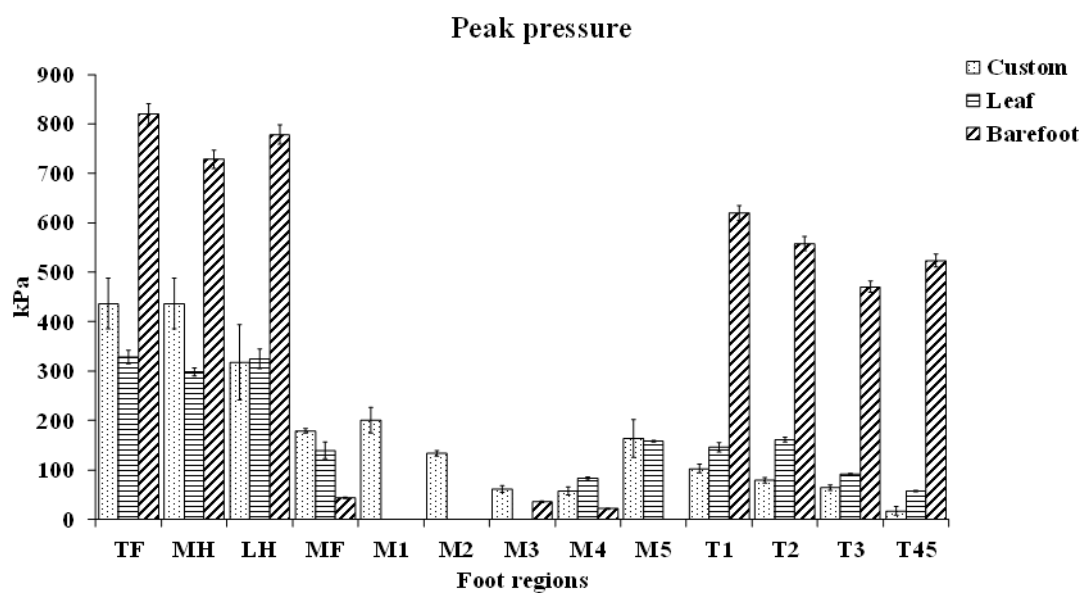


Figure 4.22: Mean, standard deviation (S.D.) and mean differences between each two conditions peak pressure (PP) for the 13 regions of the left foot with DDH

The results of the normal right foot revealed that the highest mean pressure was recorded under the second toe 636.33 ± 75.05 kPa and first toe regions 588.00 ± 83.88 kPa, followed by the pressure under the fourth and fifth toes 461.67 ± 98.64 kPa, lateral heel (LH) 381.67 ± 103.45 kPa, and then the medial heel region (MH) 350.00 ± 74.99 kPa. The mean PP values are provided in Table 4.18. Standard deviation ranges for each region under the three conditions are presented in Figure 4.23 and Table 4.18.

The custom-made AFO had a massive impact on the toe regions' readings; more than the effect recorded by the Leaf Spring AFO, decreasing the mean peak pressure significantly under all four regions (T1, T2, T3, and T45) as shown in the table and figure. Also, both AFOs reduced the mean PP under the medial and lateral heel regions by a mean difference of 104 kPa, and 113.33 kPa, and 173.67 kPa and 191 kPa respectively as shown in Table 4.18. In contrast, the results revealed an increase in the mean PP under the mid-foot region from both the custom-made and Leaf Spring AFOs by mean a difference of 133.33 kPa and 43.33 kPa.

Additionally, the highest PP reading for the metatarsal regions was recorded under the fifth metatarsal (M5) while wearing the custom-made AFO and Leaf Spring AFO, showing a reading of 238.33 ± 90.39 kPa and 262.67 ± 70.44 kPa respectively. Finally, the highest total right foot peak pressure was recorded during the barefoot condition 653.67 ± 45.21 kPa, followed by the custom-made AFO 355.67 ± 43.10 kPa, and then the Leaf Spring AFO 372.67 ± 31.75 kPa.

Table 4.18: Mean, standard deviation (S.D.) and mean differences between each two conditions of peak pressure (PP) for the 13 regions of the right foot

PP Regions	Right Foot						Mean difference Between conditions		
	Custom	Leaf	Barefoot		B vs C	B vs L	B vs Insole		
TF	355.67	43.10	372.67	31.75	653.67	45.21	298.00	281.00	17.00
MH	246.00	9.64	176.33	23.09	350.00	74.99	104.00	173.67	-69.67
LH	268.33	13.58	190.67	30.60	381.67	103.45	113.33	191.00	-77.67
MF	355.67	43.10	265.67	1.15	222.33	51.94	-133.33	-43.33	-90.00
M1	176.33	97.37	151.33	34.06	101.67	47.50	-74.67	-49.67	-25.00
M2	184.00	41.07	113.00	3.46	234.33	80.28	50.33	121.33	-71.00
M3	188.00	31.19	106.00	0.00	260.67	91.68	72.67	154.67	-82.00
M4	144.00	14.00	134.00	25.98	115.33	39.80	-28.67	-18.67	-10.00
M5	238.33	90.39	262.67	70.44	176.00	79.57	-62.33	-86.67	24.33
T1	246.67	28.92	242.67	2.89	588.00	83.88	341.33	345.33	-4.00
T2	176.00	25.24	233.33	9.24	636.33	75.05	460.33	403.00	57.33
T3	184.33	50.14	340.00	3.46	325.00	63.91	140.67	-15.00	155.67
T45	187.00	5.29	356.00	53.69	461.67	98.64	274.67	105.67	169.00

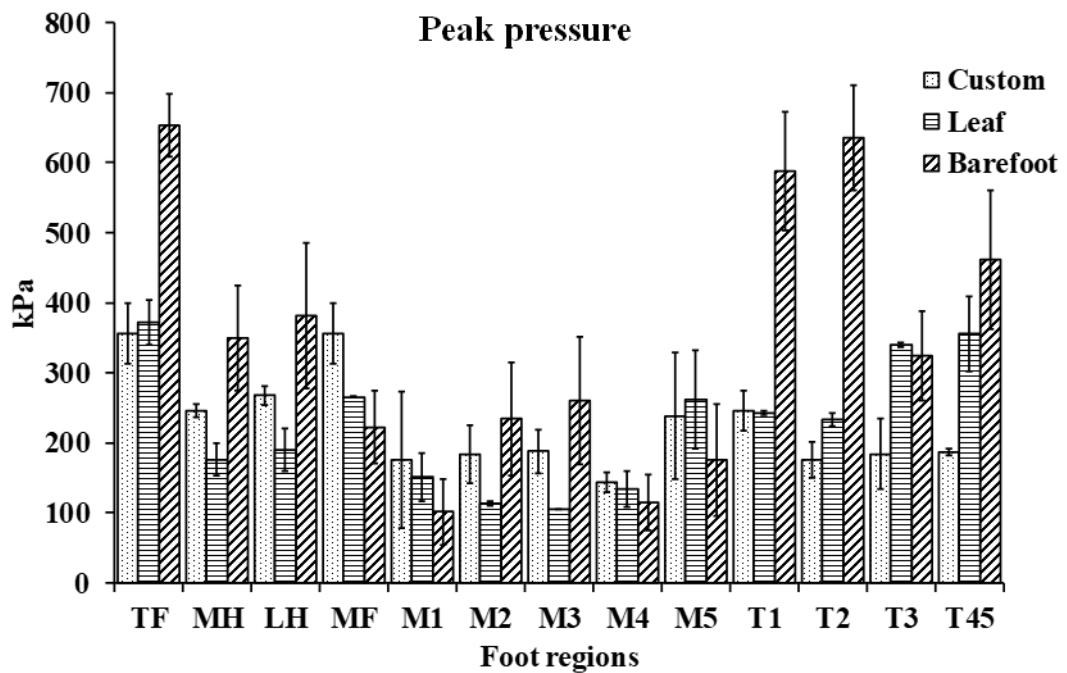


Figure 4.23: Mean, standard deviation (S.D.) and mean differences between each two-conditions peak pressure (PP) for the 13 regions of the right foot

4.5.3 Pressure time integral (PTI)

The highest-pressure time integral values for the left barefoot condition were, in decreasing order, in the regions of the lateral heel (LH) 115.92 ± 2.91 kPa.sec, medial heel (MH) 101.66 ± 2.55 kPa.sec, first toe (T1) 73.79 ± 1.85 kPa.sec, fourth and fifth toes (T45) 49.90 ± 1.25 kPa.sec and second toe (T2) 42.94 ± 1.08 kPa.sec. The mean of these values was in the range of 0.43 kPa.sec (M3) – 115.92 kPa.sec (LH), as shown in Table 4.19 below. The standard deviation scales for each region under the three conditions are presented in Figure 4.24.

The custom-made and Leaf Spring AFOs reduced the medial and lateral heel values significantly recording medial heel values of 83.87 ± 0.80 kPa.sec and 80.87 ± 1.33 kPa.sec and lateral heel values of 41.67 ± 1.80 kPa.sec and 59.33 ± 0.29 kPa.sec, respectively. However, there was a massive increase in the mid-foot region reading by

a mean difference of 19.19 kPa.sec and 23.59 kPa.sec resulted from the wearing of both orthoses, respectively. The solid custom-made AFO showed readings in the left foot metatarsal regions in decreasing order, first metatarsal (M1) 19.70±2.69 kPa.sec, second metatarsal (M2) 15.27 ±2.48 kPa.sec, and then fifth metatarsal (M5) 14.63±3.15 kPa.sec.

Finally, the total foot pressure-time integral reduced by the AFOs to 65.50±3.08 kPa.sec and 61.97±0.29 kPa.sec, respectively. Furthermore, the highest PTI was recorded under the big toe and the second toe regions when the patient wearing the AFO, while the lowest value was found under the fourth and fifth toe (T45) 0.63±0.50 kPa.sec and 9.23±1.62 kPa.sec respectively

Table 4.19: Mean, standard deviation (S.D.) and mean differences between each two conditions of the pressure-time integral (PTI) for the 13 regions of the left foot

PTI Regions	Left Foot (Mean and SD)						mean difference between conditions		
	Custom		Leaf		Barefoot		B vs C	B vs L	B vs L
	M	SD	M	SD	M	SD	M	M	M
TF	65.50	3.08	61.97	0.29	106.15	2.66	40.65	44.19	16.55
MH	83.87	0.80	80.87	1.33	101.66	2.55	17.79	20.79	-5.01
LH	41.67	1.80	59.33	0.29	115.92	2.91	74.25	56.58	35.75
MF	35.10	2.26	39.50	2.25	15.91	0.40	-19.19	-23.59	-7.75
M1	19.70	2.69	0.00	0.00	0.00	0.00	-19.70	0.00	0.00
M2	15.27	2.48	0.00	0.00	0.00	0.00	-15.27	0.00	0.00
M3	7.97	1.34	0.00	0.00	4.28	0.11	-3.68	4.28	3.08
M4	8.33	3.21	26.07	1.15	0.43	0.01	-7.90	-25.64	-52.84
M5	14.63	3.15	38.00	0.35	0.00	0.00	-14.63	-38.00	-52.93
T1	39.97	2.04	49.27	0.81	73.79	1.85	33.82	24.52	34.42
T2	25.20	0.98	50.10	0.35	42.94	1.08	17.74	-7.16	4.98
T3	25.17	3.97	30.03	0.92	38.23	0.96	13.06	8.19	1.23
T45	0.63	0.50	9.23	1.62	49.90	1.25	49.26	40.66	12.33

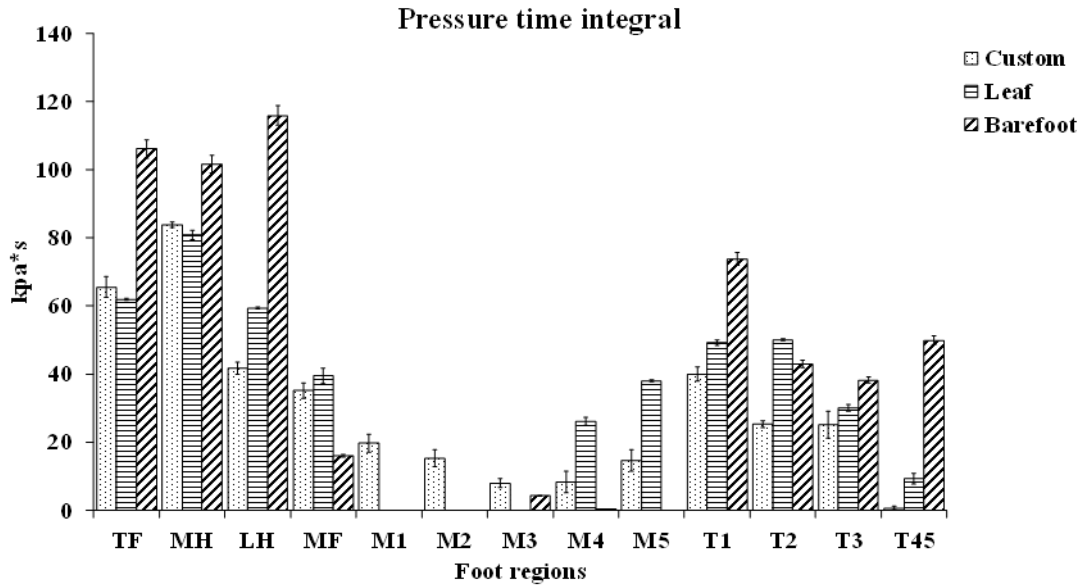


Figure 4.24: Mean, standard deviation (S.D.) and mean differences between each two conditions of pressure time integral for the 13 regions of the left foot

The right barefoot mean pressure-time integral values were consistent under the three regions of lateral heel (LH) 34.40 ± 7.92 kPa.sec, medial heel (MH) 33.67 ± 8.85 kPa.sec, and the mid-foot region 33.33 ± 4.08 kPa.sec. Furthermore, the results of the five metatarsal regions showed close values of approximately 40 kPa.sec PTI except for the first metatarsal, which had the lowest value of 19.83 ± 14.55 kPa.sec. The highest PTI reading was under the (T45) 85.87 ± 9.96 kPa.sec, followed by the reading under the second toe (T2) 76.23 ± 10.28 kPa.sec, then the PTI under the hallux (T1) 62.83 ± 13.89 kPa.sec.

The custom-made AFO significantly increased the PTI reading under the regions of MH, LH and MD by a mean difference 5.3, 12.5, and 47.7 kpa.sec. However, the Leaf Spring AFO reduced the magnitudes under the MH and LH regions by a mean difference of 5.27 kPa.sec, and 3.13 kPa.sec. It is worth noting that the total foot PTI increased significantly while the patient was walking with the custom-made AFO, and the results revealed an increase in the PTI readings by a mean difference of 23.13

kPa.sec. The average results of the three-recorded steps are presented in Table 4.20 below, and the standard deviation ranges for each region under the three conditions are shown in Figure 4.25

Table 4.20: Mean, standard deviation (S.D.) and mean differences between each two conditions of the pressure time integral (PTI) for the 13 regions of the right foot

PTI Regions	Right Foot (Mean and SD)						Mean difference Between conditions		
	Custom	Leaf	Barefoot	B vs C	B vs L	B vs Insole			
TF	117.20	8.75	88.70	4.33	94.07	9.27	-23.13	5.37	-2.70
MH	38.97	4.93	28.40	3.38	33.67	8.85	-5.30	5.27	-9.17
LH	46.90	2.25	31.27	3.06	34.40	7.92	-12.50	3.13	-9.00
MF	81.07	8.25	62.13	0.58	33.33	4.08	-47.73	-28.80	-25.83
M1	30.20	9.72	19.73	0.81	19.83	14.55	-10.37	0.10	-10.87
M2	35.10	5.40	22.90	1.91	42.80	12.84	7.70	19.90	12.03
M3	42.10	3.64	27.13	1.44	42.47	8.51	0.37	15.33	9.33
M4	71.10	18.96	41.73	5.60	35.43	11.14	-35.67	-6.30	-8.90
M5	92.90	25.55	72.63	7.16	42.67	16.71	-50.23	-29.97	-23.17
T1	49.87	4.77	50.00	5.20	62.83	13.89	12.97	12.83	9.93
T2	39.30	5.47	50.93	1.50	76.23	10.28	36.93	25.30	30.37
T3	60.17	34.42	77.70	6.75	51.83	7.89	-8.33	-25.87	6.93
T45	88.07	33.85	88.60	0.17	85.87	9.96	-2.20	-2.73	23.63

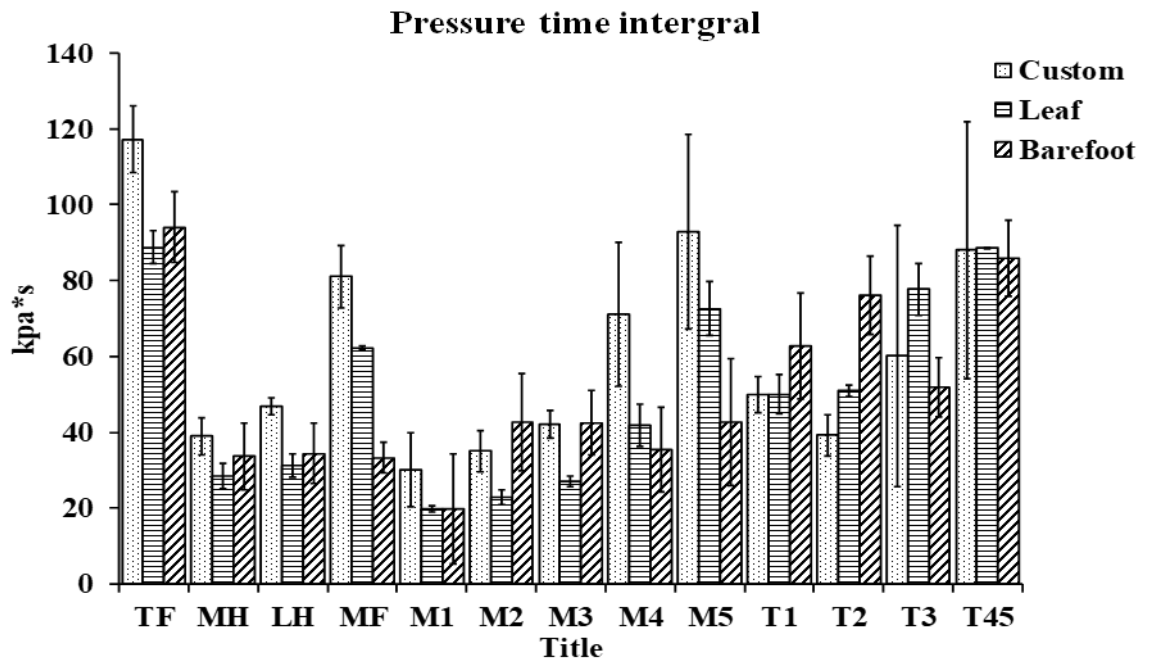


Figure 4.25: Mean, standard deviation (S.D.) and mean differences between each two conditions of pressure time integral (PTI) for the 13 regions of the right foot

CHAPTER 5 DISCUSSIONS

5.1 AN OVERVIEW

This study investigated the following main points:

- 1- The ankle joint kinematics and kinetics including dorsi- plantarflexion angles, the dorsi-plantarflexion moments, and ankle power generated during walking in the sagittal plane.
- 2- The knee and hip joint kinematics and kinetics including knee and hip joints extension-flexion angles, moment and power during walking in the sagittal plane under the four known conditions barefoot, custom-made orthosis, Leaf Spring AFO, and shoes only
- 3- The plantar pressure characteristics during main phases of the gait; heel strike, midstance, and push off phase including the right and left foot contact area, contact pressure, peak pressure, and ground reaction force results for the three conditions; barefoot, custom-made-orthosis, and Leaf Spring AFO along with the entire stance phase of the gait.

5.2 KINEMATICS AND KINETICS

As previously explained, the patient has severe DDH and a stiff hyper-flexed knee, and has worn two types of ankle-foot orthoses for the past ten years to accommodate his daily life activities. This study can be considered as a new attempt to assess the gait of patients with untreated DDH as well as investigating the effect of the ankle-foot orthosis on gait kinematics and kinetics. Several studies have indicated that pathological individuals with untreated DDH differ to healthy people on such gait parameters; likely correlating to the pain, leg-length discrepancy (LLD), hip OA and

initial pathologic changes (Hurwitz et al. 1997; Eitzen et al. 2012; Meyer et al. 2015). To our knowledge, the hip joint motion identified clinically by the path of thigh displacement from the vertical, is considered the more clinically appropriate way to define joint motion. In the sagittal plane, describing the hip motion is affected by the displacement of both the femur and pelvis. As explained in the results from observation, the hip joint moved through two arcs of motion during the normal walking of a patient with DDH. The results of our studies represented greater and lesser degrees of flexion values, 20° to 120° , for the right limb unaffected by DDH, and from 10° to 75° for the left limb affected by DDH. However, the normal hip motion for healthy individuals reported in the literature ranges from -10° to 48° degrees considering the maximum hip flexion for normal adults ranges from 40° to 48° degrees during the swing phase of gait (Burnfield 2010). Therefore, the results of this study show that the excessive hyperflexion of the right knee is accompanied by extreme hyper-flexion hip angle while the patient is barefoot. As far as we know, the pathological deficiencies of severe hip dysplasia may highlight differences over the whole gait cycle when the patient is barefoot in comparison to that of moderate hip dislocation subjects and normal healthy subjects. Generally, the hip muscles produce a flexor moment of 1.06 Nm/kg during the late stance phase, which controls excessive extension of the hip (Burnfield 2010).

In our case, both the right hip and left hip affected by DDH produced an extensor moment of 0.5 Nm/kg during the push off portion of gait, which is half the peak value generated by healthy subject data stated in the literature (Burnfield 2010). The reason behind the reduction of the hip extensor moment during the late stance is that, in patients with severe DDH, the insufficient cover of the femoral head reduces the load-bearing surface in the hip joint. Therefore, the dislocated joint experiences more pain

when it is loaded (Chang et al. 2011). Our results indicated that both custom-made and Leaf Spring AFOs significantly reduce the left abnormal hip joint flexor moment during the pre-swing phase of gait. This reduction of the hip flexor moment while wearing the orthoses can be interpreted as an attempt to unload the hip joint and thereby lessen the pain as supported by the studies of Endo et al. (2003) and Hayashi et al. (2017). It seems likely that the patient with severe DDH has less propulsion of the abnormal limb, including less power generated due to the pathological change in the hip joint structure. It is worth noting that wearing both orthoses contributed to the forward progression of the hip by significantly increasing the amount of power generation in the second half of the stance phase in the left abnormal hip with DDH. The studies of Murray, Gore and Clarkson (1971) on walking patterns of patients with unilateral hip due to osteoarthritis support our current investigation. They pointed out that that the limited extension and the excessive flexion of the diseased hip during the stance phase, which was witnessed in many patients during walking, was an attempt to avoid the painful manoeuvre by reducing the load on the femoral head. In addition, the investigations of Romano et al. (1996b) on the gait cycle of 21 adults with residue congenital dysplasia of the hip, support our case as they reported that the range of extension of the affected hip in all patients was drastically reduced. Thus, our study indicated that both orthoses have made a positive effect on the hip kinetics of the gait cycle, especially in the second half of the stance phase by generating more power than that of barefoot condition and decreasing the amount of flexor moment to reduce the pain associated with loading during walking.

The other objective of this study was to prospectively study and evaluate the effect of using two types of AFO on kinematics and kinetics of the ankle and knee joints during walking in the sagittal plane for a patient with severe dysplasia of the left hip. Both

orthoses showed significant changes during walking in the sagittal plane, indicating gait improvements in some phases. It is worth noting that, at the terminal stance, the custom-made orthosis and “off-the-shelf” orthosis reduced the abnormal ankle dorsiflexion motion for the left limb with DDH. Some studies support our current research and have shown that the ankle dorsiflexion during the late stance phase is between 8° – 11.9° for patients with cerebral palsy, which is considerably closer than expected to healthy individuals (Carlson et al. 1997; Radtka et al. 1997; Rethlefsen et al. 1999). Therefore, our results show more improvements in the gait during the period between the push-off to toes off for the left abnormal foot affected by DDH while wearing both orthoses in comparison with the barefoot condition. Even though the Leaf Spring orthosis has the advantage of allowing a greater dorsi-flexion angle to occur during the midstance and terminal stance phases as the tibia transitions over the foot, the custom-made orthosis showed better maximum dorsiflexion results and was considerably closer to the healthy standard data observed in Radtka, Skinner and Johanson (2005) due to the polypropylene deformation that occurs even with the rigid custom-made orthosis. However, the maximum ankle dorsiflexion for the right unaffected limb increased significantly while using the custom-made orthosis and the Leaf Spring orthosis during the late stance in comparison to that of the barefoot condition. According to the studies of Burnfield et al (2010), the increase in the maximum dorsi angle reflected an improvement in gait over the excessive dorsiflexion while the patient is barefoot. The results showed similar values to the group of healthy persons. The positive increase in the right dorsiflexion angle might have occurred due to the enhancement in body stability while wearing the orthosis which allows the gastrocnemius muscle action to stabilize the dorsiflexion angle and also provide early heel arise (Burnfield 2010).

The corresponding ankle joint kinetics during the loading response phase while barefoot showed excessive ankle moments with extreme power generated. These findings indicate that the excessive dorsi-flexor eccentric contraction is occurring because the left affected limb with DDH excessively dorsiflexes during the weight-bearing portion of the gait. The abnormal ankle moments decreased with both orthoses during the LD however, the power absorption decreases excessively when wearing the custom-made orthosis. Few studies showed closer findings while using solid custom-made orthosis, but there is a lack of results regarding the Leaf Spring AFOs. In addition, the corresponding ankle joint kinetics while the patient is barefoot, showed a reduction in the abnormal left foot peak plantar flexor moment during the terminal stance phase of gait accompanying an excessive reduction in the power generated during the pre-swing portion of the late stance phase (Carlson et al. 1997). The custom-made orthosis produced larger peak ankle plantar flexor moments during the terminal stance as well as increasing power generation during the PSW portion of gait. However, the Leaf Spring orthosis did not decrease the power generated during the same phase. Moreover, the right limb unaffected by DDH generated more power during the pre-swing phase of gait while using the custom-made and Leaf Spring AFOs. These orthoses shifted the power generated value close to that of normal healthy subjects' values observed in the studies of Burnfield (2010). The findings of higher power generated for the abnormal left foot values with the solid AFO in comparison to that of the barefoot indicate that even the rigid material of the custom-made orthosis allows greater plantar flexor concentric contraction for push-off during the pre-swing phase, and is supported by the studies of Rethlefsen et al. (1999).

The corresponding knee joint kinematics and kinetics for the right limb not affected by DDH during walking in the sagittal plane while the patient is barefoot, showed an

excessive hyperflexion angle along the entire gait cycle. The results of our studies represented greater and lesser degrees of flexion values in the full range of 70° to 125° respectively. However, the normal knee motion for healthy individuals during walking in the sagittal plane had a full range of 0° to 60° as represented in the study of Burnfield (2010). At the instance of initial right heel contact with the floor while barefoot, the knee appears excessively flexed and the alignment of the body vector posterior to the knee axis causes less stable weight bearing with less power generated, resulting in exceptional flexor moment that modulates the rapid knee flexion. At the initiation of the mid-stance phase, the right knee flexion moment while barefoot had a flexion of almost 90°, a small amount of power generation, thus leading to lower the body towards the ground as the reference limb is shorter (the left limb affected by DDH), limiting the forward progression of the limb for the pre-swing phase providing less stable weight-bearing. The right showed a continuation of the progressive excessive flexion and reached the maximum value at the terminal stance, compromising weight-bearing stability. The studies of Rethlefsen et al. (1999) support our results, indicating that the abnormal knee motions of the crouch gait of cerebral palsy patients was not changed by the solid custom-made orthosis that was designed either specifically for each individual or the Hinged AFO. According to Rethlefsen et al. (1999), clinicians were concerned about the possibility of knee motion improvements over the pathological gait because the use of AFOs was not substantiated.

5.3 PLANTAR PRESSURE CHARACTERISTICS

The other objective of this research was to examine the effect of wearing two types of an ankle-foot orthosis (Leaf Spring AFO and custom-made AFO) on the plantar pressure characteristics of specific foot regions during walking for a patient with

severe developmental dysplasia of the left hip joint. We also examined the centre of pressure trajectory and its relationship to the lower limb movement during the whole gait cycle. To show the pressure trends under each anatomical region specified in this research, plantar peak pressure PP, pressure-time-integral PT, ground reaction force GRF, and contact areas CA values were measured under three conditions: barefoot, custom-made orthosis, and Leaf Spring AFO.

The patient was asked to walk at normal speed during the experiments. The data revealed that specific regions of both feet responded differently to changes in walking conditions. The new intention of this research was to point out the differences in plantar pressure readings at specific phases of gait using the mid-gait protocol. The observed pressure response may be related to the specific functions of each anatomic region specified in this study, taking into consideration the foot type, the effect of hip dislocation on plantar pressure readings, and the design of the AFOs.

The corresponding plantar pressure distribution results for the right foot unaffected by DDH showed that both orthoses had an impact on contact area, peak pressure, contact pressure, and pressure-time integral readings along the entire stance phase. During the heel strike phase, the custom-made orthosis had a greater contact area than the barefoot condition recording a value of $29.16 \pm 0.71 \text{ cm}^2$. Moreover, the contact area while wearing the Leaf Spring AFO increased to $35.89 \pm 0.38 \text{ cm}^2$, which is higher than the barefoot heel contact area by a mean difference of 11.63 cm^2 . Noticeably, the custom-made and Leaf Spring AFOs increased the contact area values significantly in both the lateral and medial heel regions of the right foot. Despite the increase in contact area values over the heel area, the custom-made orthosis kept showing a high value of contact pressure in contrast to the Leaf Spring AFO, which had larger area with less pressure distributed. Therefore, the risk of injury to the right heel risk could be

minimized by wearing the Leaf Spring AFO on the left side.

The corresponding results showed that, at the initiation of the midstance portion, the contact area was less than that of the barefoot by a mean difference of 15.46 cm², and included the mid-foot region only while wearing the custom-made orthosis. However, contact pressure increased significantly by a mean difference of 66.18 kPa, and peak pressure reached its second peak magnitude of 280.76±3.73 kPa. While wearing the Leaf Spring AFO, the results showed increases in contact pressure and peak pressure during the mid-stance phase of gait by a mean difference of 48.2 kPa and 124 kPa, respectively. The COP trace moved laterally along the entire midstance phase over the mid-foot region area of 29.56±1.26 cm², and the time spent to finish the phase was more than that of the barefoot by 0.1 sec. These increases in pressure readings over a smaller contact area of the mid-foot during the mid-stance phase can be interpreted in two ways. First, enhancing body balance and avoiding falling by putting more pressure under the right foot when the whole weight passes through it. Second, this could be a disadvantage as most of the pressure was recorded under the mid-foot area only, leading to increased mid-foot pain while loading and preparing for the progression of the limb. Thus, wearing high arch customized shoes can lead to a redistribution of the pressure under the heel and forefoot areas, including the first and fifth metatarsal regions, and can enhance foot comfort, as well as provide more shock absorption.

During the push-off the ground phase of the gait cycle, peak pressure and contact pressure reached their third and final peak magnitude of 283±3.109 kPa and 134±4.06 respectively, and the PP concentrated at a point between the third metatarsal and second toe which was significantly less than that of the barefoot by a mean difference of 285.99 kPa. The custom-made orthosis decreased the contact area by a mean difference of 7.47 cm², including the upper part of metatarsal regions and the lesser

toes regions. Similarly, while wearing the Leaf Spring AFO, peak pressure started increasing gradually until reaching its maximum value of 371 ± 2.08 kPa during the moment right foot pushed off the ground, concentrated on the significant and second toes regions, which was less than that of the barefoot by a mean difference of 198 kPa. The reduction in PP readings while wearing both AFOs was followed by a decrease in PT1 readings mainly under the big toe and the lesser toes regions and second, third, fourth, and fifth metatarsal regions, thus minimizing the pain in the forefoot and hallux regions during toe clearance, leading to a reduction in the risk of a hallux valgus injury. This finding is in line with another study that showed that decreasing the second peak pressure magnitude could minimize the risk of injury for an individual with painful pes cavus feet while wearing custom-made-foot orthosis (Najafi et al. 2012).

The results of the left foot affected with severe DDH and severe drop showed different outcomes. They revealed many changes in the plantar pressure distribution magnitudes and COP trace while wearing the custom-made orthosis and Leaf Spring AFO. When the left foot struck the ground, the peak pressure was concentrated at the middle of 16.99 ± 0.57 cm² heel area with a value of 483 ± 2.78 kPa. Noticeably, due to drop foot, the patient had to put more pressure on the heel area while barefoot, and the contact pressure and peak pressure values were 128 ± 1.31 kPa and 356 ± 4.04 kPa. Moreover, when the left foot pushed off the ground the patient had a greater contact area of 34.78 ± 0.99 cm², including the heel region and approximately half of the mid-foot region. Peak pressure was at its highest value of 563 ± 3.00 kPa. Also, there was no contact area recorded for the metatarsal regions except for the third metatarsal (M3) 2.59 ± 0.06 cm² while the patient was barefoot, indicating no pressure registering under the mentioned regions.

In conclusion, the patient had a severe drop left foot, and that explains why there were

no pressure readings under the metatarsal heads with the highest-pressure readings under the toes and the lateral heel. The centre of pressure was entirely under the lateral heel region along the entire stance phase, giving an indication that the forefoot area in the metatarsal regions can be considered as the most vulnerable part of the foot in our patient's case. The inclination of pressure towards the lateral heel and big toe can be related to the inadequate movement of the left limb due to the severe degree of dislocation of the left hip. In addition, these highest PP readings could be related to the anatomical structure of the foot, supported by the studies of De Doncker and Kowalski (1976). Noticeably, the smaller contact area readings recorded while walking barefoot were accepted due to the associated deformities of the left limb, supported by the studies of Franco (1987), Benedetti et al. (1997) and Williams III et al. (2001) who showed that the smaller contact area readings were structurally accepted due to the shape and characteristics of the feet. The research outcome of Sneyers et al. (1995) was in line with our current work. They reported that a greater area of contact between the foot and the ground during the initial strike phase could provide better distribution of the foot pressure under all specified regions. They also reported that the poorer distribution of the foot pressure under the mid-foot area was implied by decreasing the area of contact (Sneyers et al. 1995).

The corresponding results showed that the highest values of the pressure-time integral for the left foot barefoot condition were registered under the lateral heel (LH) 115.92 ± 2.91 kpa.sec, medial heel (MH) 101.66 ± 2.55 kpa.sec, first toe (T1) 73.79 ± 1.85 kpa.sec, fourth and fifth toes (T4, 5) 49.90 ± 1.25 kpa.sec and second toe (T2) 42.94 ± 1.08 kpa.sec. The mid-foot area and the five metatarsal regions had smaller recorded values of pressure-time integral along the whole stance phase of the gait. These highest PT1 readings resulted from the peak pressure under the heel regions and

big toe, and lesser toes regions. Therefore, such an increase in the PT1 under the hallux could be due to the lack of loading under the mid-foot area because of the lower limb weaknesses and the associated drop foot deformity. Burns et al. (2005) and Rosenbaum et al. (1994) found that the PT1 readings were higher in the pes cavus of neurological aetiology subject compared to the healthy normal individuals. Such findings are in line with the current investigation. Thus, the highest value of PTI and PP for a small contact area in the big toe can increase the possibility of hallux valgus incidence, which was supported by Putti et al. (2007).

The current work evaluated the influence of both AFOs on the redistribution of the pressure beneath the specified foot regions. The obtained results show that both orthotic devices had a positive effect on the peak pressure and pressure-time integral registered under the left foot during walking. When the left foot strikes the ground, the custom-made AFO increased the contact heel area by a mean difference of 8.11 cm². In contrast, contact pressure and peak pressure were drastically decreased by using the custom-made AFO. The results reveal decreases in both magnitudes in comparison with the barefoot condition by a mean difference of 31.02 kPa and 255 kPa, respectively. The results show a significant reduction in the peak pressure amount during the push-off phase. The pressure was concentrated on the medial part of the metatarsal regions, particularly on the fifth metatarsal. Also, the patient stepped off the ground using an area of 33.87±0.75 cm², which included most of the five metatarsal regions and a small part of the mid-foot region. Similarly, the Leaf Spring AFO increased the area of contact and decreased the PT1 and PP along the entire stance phase. The contact area, while wearing the Leaf Spring AFO, included the heel and the upper part of the fifth metatarsal region at the time the left foot stepped on the ground.

The improvement in pressure distribution beneath the left foot affected with DDH when wearing the custom-made AFOs can be attributed to a few factors. First, the COP trace during the initial strike was at a point on the medial-heel, and the trace was shifted medially towards the mid-foot and the five metatarsal regions during the late stance phase of the gait cycle. Therefore, readjusting the floor over the ground, giving the metatarsal region more time in contact with the floor and decreasing the risk of highest pressure under the toes. Second, the change of foot posture and its position inside the shoes while wearing the orthosis could enhance ankle joint ability when responding to such repetitive forces and stresses, and this is supported by Kwan, Zheng and Cheing (2010). It is worth noting that the associated decrease in forefoot peak pressure areas can be associated with a reduction in dorsiflexion angles during walking in the sagittal plane as previously explained in the kinematics and kinetics part of this current work, and which was mentioned and supported by the studies of Mueller et al. (1989) and Morag and Cavanagh (1999).

Importantly, the decrease in the pressure magnitude beneath the specified left foot regions while wearing the rigid custom-made orthosis could be due to the decrease in walking speed along the entire gait cycle. This is in line with the study of Burnfield et al. (2004), who examined the influence of walking velocity and footwear condition on plantar pressure variables in healthy older adults. The authors indicated that the higher-pressure magnitude in older adults resulted from faster barefoot walking due to the increase in peak force. Moreover, the results showed significant higher-pressure values under the heel, medial and central MTs, and toes just by increasing the walking speed from 57 m/min to 80 m/min. In addition, further significant pressure increases under the heel and hallux regions resulted from walking under the maximum speed of 97 m/min. These results were consistent with the findings of other studies documented in

young adults (Nilsson & Thorstensson 1989). The speed-pressure relationship documented by the reviews of Rosenbaum et al. (1994) on young adult individuals showed similar findings to the studies of Burnfield et al. (2004). The authors pointed out higher pressure readings registered under the heel, medial and central metatarsals, and the hallux just by increasing barefoot walking speed of the young adults (mean age 27) from 48 to 102 m/min. These results were also consistent with Hughes et al. (1991) who found an increase in the pressure readings under the same foot regions reported previously for ten young adults (mean age of 21 years) by increasing the barefoot walking speed. Thus, the findings of the current study are essential to understanding the behaviour of the foot effected with DDH and the effect could be made by different types of ankle foot orthoses on the planter pressure readings beneath the foot during walking. The current work is also important for understanding the risk ulceration, amputation and multiple foot injuries associated with inadequate distribution of pressure during the main phases of gait from heel strike to late stance. In general, a normal gait phase produced a COP trace from heel-strike to push-off for both feet. However, the scoliotic subject's gait phase produced three uniquely different COP trace configurations, depending on the type of AFO (custom-molded or Leaf AFO) or its absence (no-orthosis). Based on the alignment of these COP traces, the custom molded orthosis delivered continuous trace for both feet from heel-strike to push off and showed the closest COP displacement pattern to a normal healthy subject and the right foot gait phase. Thus, it appears that this orthosis provided sufficient stability for both feet from heel-strike to push-off.

The barefoot gait of the scoliotic subject showed the largest contact area in the left foot for the trial, but the shortest contact time. It appears that flattening of the plantar soft tissues resulted in a greater area of contact with the mat, particularly at the heel-strike,

while the rigid orthoses reduced the area of contact but improved the ability of the foot to support more body weight during gait. Observing the physical movement of the lower-limb and feet of the patient during the trials gave an impression that the left foot gait phase took longer however, the registered time was similar for these trials. Therefore, the loading of the dislocated hip was equivalent to the healthy hip thus, wearing orthoses did not alter the loading of each limb. As the loading distributed over the smaller surface area for the orthoses, the hard shell custom molded variety could be more beneficial than the soft-shell type.

Ankle-foot movement should be at its greatest during the barefoot gait as there was no orthosis to restrict any moments. Considering the size of displacement of COP trace, contact time and contact area of the trial, the left knee must have provided the majority of the rotational movement of the foot. Therefore, it is argued that the left ankle has limited movement in all three axes, as depicted by the COP trace at the heel in the barefoot trial. Thus, the design of the custom molded orthosis has encouraged more knee movements and provided better stability for the deformed left ankle and left foot.

CHAPTER 6: CONCLUSIONS

This thesis presents the first investigation into the effects of multiple types of AFOs on the gait characteristics of a patient with untreated DDH. It addresses a significant gap in the body of research studying the kinematics and kinetics of lower limb joints during walking in the sagittal plane for a DDH patient with and without orthoses. The work provides evidence that ankle-foot orthoses can produce specific biomechanical improvements in terms of range of motion, moments, and power generated by the lower limb joints during walking in the sagittal plane.

Although the gait cycle of the presented patient is unique, this investigation could be a useful resource for future investigations regarding people with severe hip dislocation. The application of the Oxford Leardini lower limb model to create a specific model for a patient with severe hip dislocation can be considered to be an innovative approach. This new approach can be used widely in research and clinical environments to obtain accurate data for ankle, knee and hip kinematics and kinetics, as well as measuring AFO suitability for specific cases. The current work concluded that both AFOs had a positive impact on hip joint kinetics by reducing the left abnormal hip joint flexor moment during the late stance phase of the gait, thus contributing to the reduction of pain associated with loading the hip during the late stance. Moreover, the current investigation proved that wearing AFOs increases the amount of generated power in the left hip joint during the second half of the stance phase, thus contributing to forward progression of the left hip.

The research concluded that the more appropriate of the two orthoses for the enhancement of ankle joint kinematics and kinetics for this patient is the rigid custom-

made AFO. Despite the higher cost of the custom-made AFO in comparison with the Leaf Spring AFO, the customised AFO produced better maximum dorsiflexion results, considerably closer to the data of healthy individuals observed in the literature. This result is due to the polypropylene deformation that occurs even with the rigid custom-made orthosis. The off-the-shelf Leaf Spring AFO allowed a smaller dorsiflexion angle during the midstance and terminal stance phases. Therefore, wearing the custom-made AFO contributed to better body stability giving the gastrocnemius muscle the ability to stabilise the dorsiflexion angle and provide early heel rise.

It should also be noted that a higher peak plantar flexor moment was produced during the terminal stance phase of gait, and higher power was generated during the pre-swing phase while wearing the custom-made-orthosis in comparison to the Leaf Spring orthosis. Thus, overall, both orthoses improved the same phases of gait. Still, wearing the custom-made orthosis on the left foot affected with DDH was the better option for the patient.

The research also aimed to determine the suitability of the custom-molded orthosis over The Leaf Spring AFO orthoses for an adult scoliotics subject who has left hip dislocation and severe scoliosis complications by studying the plantar pressure distribution beneath both feet. Plantar pressure during the gait phase were captured for three scenarios: barefoot, wearing custom-molded orthosis and wearing the Leaf Spring AFO orthosis. Four elements, COP trace displacement, contact time, contact area and orthoses design, were examined using the captured data. The evaluation showed that the custom-molded orthosis produced the best outcomes for all measures. Leaf Spring AFO orthoses permitted increased knee-joint movements and provided additional gait stability for the deformed left foot. The custom-made orthoses improved the gait of the left limb by allowing the KC trajectory within the footprint

on the ground, thus giving more body support. The orthoses also improved the right foot gait by shifting the COP at MS_F closer to the KC trajectory.

The 3D multi-stereo photogrammetric technique captured the high-accuracy positional change of the lower limbs and feet during normal gait speed. Multi-stereo limb/foot movement was valuable in the interpretation of knee joint activity and this unique feature enhanced the understanding of AFO performance. The developed correlation techniques permitted the development of new gait analysis methods to study the limb and plantar data in the case of a specific patient with severe DDH.

REFERENCES

Abbas, NS & Chong, AK 2018, '3D video imagery of the foot and plantar pressure to examine foot rotation and loading for older adults', *2018 IEEE Symposium on Computer Applications & Industrial Electronics (ISCAIE)*, IEEE, pp. 349-53.

Ahroni, JH, Boyko, EJ & Forsberg, RC 1999, 'Clinical correlates of plantar pressure among diabetic veterans', *Diabetes care*, vol. 22, no. 6, pp. 965-72.

Akiyama, M, Nakashima, Y, Fujii, M, Sato, T, Yamamoto, T, Mawatari, T, Motomura, G, Matsuda, S & Iwamoto, Y 2012, 'Femoral anteversion is correlated with acetabular version and coverage in Asian women with anterior and global deficient subgroups of hip dysplasia: a CT study', *Skeletal radiology*, vol. 41, no. 11, pp. 1411-8.

Arazpour, M, Ahmadi, F, Bahramizadeh, M, Samadian, M, Mousavi, ME, Bani, MA & Hutchins, SW 2016, 'Evaluation of gait symmetry in poliomyelitis subjects: Comparison of a conventional knee–ankle–foot orthosis and a new powered knee–ankle–foot orthosis', *Prosthetics and orthotics international*, vol. 40, no. 6, pp. 689-95.

Arvin, M, Kamyab, M, Moradi, V, Hajiaghaei, B & Maroufi, N 2013, 'Influence of modified solid ankle-foot orthosis to be used with and without shoe on dynamic balance and gait characteristic in asymptomatic people', *Prosthetics and orthotics international*, vol. 37, no. 2, pp. 145-51.

Benedetti, M, Catani, F, Ceccarelli, F, Simoncini, L, Giannini, S & Leardini, A 1997, 'Gait analysis in pes cavus', *Gait & Posture*, vol. 2, no. 5, p. 169.

Bernardi, M, Canale, I, Castellano, V, Di Filippo, L, Felici, F & Marchetti, M 1995, 'The efficiency of walking of paraplegic patients using a reciprocating gait orthosis', *Spinal Cord*, vol. 33, no. 7, p. 409.

Burnfield, JM, Few, CD, Mohamed, OS & Perry, J 2004, 'The influence of walking speed and footwear on plantar pressures in older adults', *Clinical Biomechanics*, vol. 19, no. 1, pp. 78-84.

Burnfield, M 2010, 'Gait analysis: normal and pathological function', *Journal of Sports Science and Medicine*, vol. 9, no. 2, p. 353.

Burns, J, Crosbie, J, Hunt, A & Ouvrier, R 2005, 'The effect of pes cavus on foot pain and plantar pressure', *Clinical Biomechanics*, vol. 20, no. 9, pp. 877-82.

Butler, P, Major, R & Patrick, J 1984, 'The technique of reciprocal walking using the hip guidance orthosis (hgo) with crutches', *Prosthetics and orthotics international*, vol. 8, no. 1, pp. 33-8.

Butterworth, PA, Urquhart, DM, Landorf, KB, Wluka, AE, Cicuttini, FM & Menz, HB 2015, 'Foot posture, range of motion and plantar pressure characteristics in obese and non-obese individuals', *Gait & Posture*, vol. 41, no. 2, pp. 465-9.

Carlson, WE, Vaughan, CL, Damiano, DL & Abel, MF 1997, 'Orthotic management of gait in spastic diplegia', *American journal of physical medicine & rehabilitation*, vol. 76, no. 3, pp. 219-25.

Carson, DW, Myer, GD, Hewett, TE, Heidt Jr, RS & Ford, KR 2012, 'Increased plantar force and impulse in American football players with high arch compared to normal arch', *The Foot*, vol. 22, no. 4, pp. 310-4.

Chang, CF, Wang, TM, Wang, JH, Huang, SC & Lu, TW 2011, 'Adolescents after Pemberton's osteotomy for developmental dysplasia of the hip displayed greater joint loading than healthy controls in affected and unaffected limbs during gait', *Journal of Orthopaedic Research*, vol. 29, no. 7, pp. 1034-41.

Chang, L, Su, F-c, Lai, K & Tsai, K 2005, 'Gait analysis after shoe lifts in adults with unilateral developmental dysplasia of the hip', *Journal of Medical and Biological Engineering*, vol. 25, no. 3, p. 137.

Cullell, A, Moreno, JC, Rocon, E, Forner-Cordero, A & Pons, J 2009, 'Biologically based design of an actuator system for a knee–ankle–foot orthosis', *Mechanism and Machine Theory*, vol. 44, no. 4, pp. 860-72.

Damiano, DL, Alter, KE & Chambers, H 2009, 'New clinical and research trends in lower extremity management for ambulatory children with cerebral palsy', *Physical Medicine and Rehabilitation Clinics*, vol. 20, no. 3, pp. 469-91.

De Doncker, E & Kowalski, C 1976, *Cinésiologie et rééducation du pied*, Masson.

De Sèze, M-P, Bonhomme, C, Daviet, J-C, Burguete, E, Machat, H, Rousseaux, M & Mazaux, JM 2011, 'Effect of early compensation of distal motor deficiency by the Chignon ankle-foot orthosis on gait in hemiplegic patients: a randomized pilot study', *Clinical rehabilitation*, vol. 25, no. 11, pp. 989-98.

Desloovere, K, Molenaers, G, Van Gestel, L, Huenaerts, C, Van Campenhout, A, Callewaert, B, Van de Walle, P & Seyler, J 2006, 'How can push-off be preserved during use of an ankle foot orthosis in children with hemiplegia? A prospective controlled study', *Gait & posture*, vol. 24, no. 2, pp. 142-51.

- Douglas, R, Larson, PF & McCall, RE 1983, 'The LSU reciprocation-gait orthosis', *Orthopedics*, vol. 6, no. 7, pp. 834-9.
- Eils, E, Nolte, S, Tewes, M, Thorwesten, L, Völker, K & Rosenbaum, D 2002, 'Modified pressure distribution patterns in walking following reduction of plantar sensation', *Journal of biomechanics*, vol. 35, no. 10, pp. 1307-13.
- Eitzen, I, Fernandes, L, Nordsletten, L & Risberg, MA 2012, 'Sagittal plane gait characteristics in hip osteoarthritis patients with mild to moderate symptoms compared to healthy controls: a cross-sectional study', *BMC musculoskeletal disorders*, vol. 13, no. 1, p.258.
- Elftman, H 1934, 'A cinematic study of the distribution of pressure in the human foot', *The Anatomical Record*, vol. 59, no. 4, pp. 481-91.
- Endo, H, Mitani, S, Senda, M, Kawai, A, McCown, C, Umeda, M, Miyakawa, T & Inoue, H 2003, 'Three-dimensional gait analysis of adults with hip dysplasia after rotational acetabular osteotomy', *Journal of orthopaedic science*, vol. 8, no. 6, pp. 762-71.
- Enzinger, C, Johansen-Berg, H, Dawes, H, Bogdanovic, M, Collett, J, Guy, C, Ropele, S, Kischka, U, Wade, D & Fazekas, F 2008, 'Functional MRI correlates of lower limb function in stroke victims with gait impairment', *Stroke*, vol. 39, no. 5, pp. 1507-13.
- Everett, T & Kell, C 2010, *Human Movement E-Book: An Introductory Text*, Elsevier health sciences.
- Fatone, S 2006, 'A review of the literature pertaining to KAFOs and HKAFOs for ambulation', *JPO: Journal of Prosthetics and Orthotics*, vol. 18, no. 7, pp. P137-P68.

Fatone, S, Gard, SA & Malas, BS 2009, 'Effect of ankle-foot orthosis alignment and foot-plate length on the gait of adults with poststroke hemiplegia', *Archives of physical medicine and rehabilitation*, vol. 90, no. 5, pp. 810-8.

Fernández-Seguín, LM, Mancha, JAD, Rodríguez, RS, Martínez, EE, Martín, BG & Ortega, JR 2014, 'Comparison of plantar pressures and contact area between normal and cavus foot', *Gait & Posture*, vol. 39, no. 2, pp. 789-92.

Fernando, M, Crowther, R, Lazzarini, P, Sangla, K, Cunningham, M, Buttner, P & Golledge, J 2013, 'Biomechanical characteristics of peripheral diabetic neuropathy: A systematic review and meta-analysis of findings from the gait cycle, muscle activity and dynamic barefoot plantar pressure', *Clinical biomechanics*, vol. 28, no. 8, pp. 831-45.

Franceschini, M, Massucci, M, Ferrari, L, Agosti, M & Paroli, C 2003, 'Effects of an ankle-foot orthosis on spatiotemporal parameters and energy cost of hemiparetic gait', *Clinical rehabilitation*, vol. 17, no. 4, pp. 368-72.

Franco, AH 1987, 'Pes cavus and pes planus: analyses and treatment', *Physical Therapy*, vol. 67, no. 5, pp. 688-94.

Frykberg, RG, Lavery, LA, Pham, H, Harvey, C, Harkless, L & Veves, A 1998, 'Role of neuropathy and high foot pressures in diabetic foot ulceration', *Diabetes care*, vol. 21, no. 10, pp. 1714-9.

Gök, H, Küçükdeveci, A, Altinkaynak, H, Yavuzer, G & Ergin, S 2003, 'Effects of ankle-foot orthoses on hemiparetic gait', *Clinical rehabilitation*, vol. 17, no. 2, pp. 137-9.

Gravante, G, Pomara, F, Russo, G, Amato, G, Cappello, F & Ridola, C 2005, 'Plantar pressure distribution analysis in normal weight young women and men with normal and claw feet: A cross-sectional study', *Clinical Anatomy: The Official Journal of the American Association of Clinical Anatomists and the British Association of Clinical Anatomists*, vol. 18, no. 4, pp. 245-50.

Guille, JT, Pizzutillo, PD & MacEwen, GD 2000, 'Developmental dysplasia of the hip from birth to six months', *JAAOS-Journal of the American Academy of Orthopaedic Surgeons*, vol. 8, no. 4, pp. 232-42.

Hartofilakidis, G & Lampropoulou-Adamidou, K 2016, 'Lessons learned from study of congenital hip disease in adults', *World journal of orthopedics*, vol. 7, no. 12, p. 785.

Hartofilakidis, G, Karachalios, T & Stamos, KG 2000, 'Epidemiology, demographics, and natural history of congenital hip disease in adults', *Orthopedics*, vol. 23, no. 8, pp. 823-7.

Hartofilakidis, G, Yiannakopoulos, CK & Babis, GC 2008, 'The morphologic variations of low and high hip dislocation', *Clinical orthopaedics and related research*, vol. 466, no. 4, pp. 820-4.

Hartofilakidis, G, Stamos, K, Karachalios, T, Ioannidis, TT & Zacharakis, N 1996, 'Congenital Hip Disease in Adults.: Classification of Acetabular Deficiencies and Operative Treatment with Acetabuloplasty Combined with Total Hip Arthroplasty', *JBJS*, vol. 78, no. 5, pp. 683-92.

Hayashi, K, Kako, M, Suzuki, K, Hattori, K, Fukuyasu, S, Sato, K, Kadono, I, Sakai, T, Hasegawa, Y & Nishida, Y 2017, 'Associations among pain catastrophizing, muscle strength, and physical performance after total knee and hip arthroplasty', *World journal of orthopedics*, vol. 8, no. 4, p. 336.

Hjorth, M, Stilling, M, Lorenzen, ND, Jakobsen, SS, Soballe, K & Mechlenburg, I 2014, 'Block-step asymmetry 5 years after large-head metal-on-metal total hip arthroplasty is related to lower muscle mass and leg power on the implant side', *Clinical biomechanics*, vol. 29, no. 6, pp. 684-90.

Hughes, J 1993, 'The clinical use of pedobarography', *Acta Orthop Belg*, vol. 59, no. 1, pp. 10-6.

Hughes, J, Clark, P & Klenerman, L 1990, 'The importance of the toes in walking', *The Journal of bone and joint surgery. British volume*, vol. 72, no. 2, pp. 245-51.

Hughes, J, Pratt, L, Linge, K, Clark, P & Klenerman, L 1991, 'Reliability of pressure measurements: the EM ED F system', *Clinical Biomechanics*, vol. 6, no. 1, pp. 14-8.

Hurwitz, D, Hulet, C, Andriacchi, T, Rosenberg, A & Galante, J 1997, 'Gait compensations in patients with osteoarthritis of the hip and their relationship to pain and passive hip motion', *Journal of Orthopaedic Research*, vol. 15, no. 4, pp. 629-35.

Hwang, S, Kang, S, Cho, K & Kim, Y 2008, 'Biomechanical effect of electromechanical knee-ankle-foot-orthosis on knee joint control in patients with poliomyelitis', *Medical & biological engineering & computing*, vol. 46, no. 6, pp. 541-9.

Irby, SE, Bernhardt, KA & Kaufman, KR 2005, 'Gait of stance control orthosis users: the dynamic knee brace system', *Prosthetics and orthotics international*, vol. 29, no. 3, pp. 269-82.

Jacobsen, JS, Nielsen, DB, Sørensen, H, Søballe, K & Mechlenburg, I 2013, 'Changes in walking and running in patients with hip dysplasia', *Acta orthopaedica*, vol. 84, no. 3, pp. 265-70.

Jacobsen, S, Rømer, L & Søballe, K 2005, 'Degeneration in dysplastic hips', *Skeletal radiology*, vol. 34, no. 12, pp. 778-84.

Jahss, MH, Kummer, F & Michelson, JD 1992, 'Investigations into the fat pads of the sole of the foot: heel pressure studies', *Foot & ankle*, vol. 13, no. 5, pp. 227-32.

Janeh, O, Langbehn, E, Steinicke, F, Bruder, G, Gulberti, A & Poetter-Nerger, M 2017, 'Walking in virtual reality: Effects of manipulated visual self-motion on walking biomechanics', *ACM Transactions on Applied Perception (TAP)*, vol. 14, no. 2, p. 12.

Jaspers, P, Van Petegem, W, Van der Perre, G & Peeraer, L 1995, 'Optimisation of a combined ARGO-FES system: adaptation of the knee mechanism to allow flexion of the knee during the swing phase', *Proceedings of 17th International Conference of the Engineering in Medicine and Biology Society*, IEEE, pp. 1143-4.

Kaufman, KR & Sutherland, DH 2006, 'Kinematics of normal human walking', *Human walking*, vol. 3, pp. 33-51.

Keller, TS, Weisberger, A, Ray, J, Hasan, S, Shiavi, R & Spengler, D 1996, 'Relationship between vertical ground reaction force and speed during walking, slow jogging, and running', *Clinical Biomechanics*, vol. 11, no. 5, pp. 253-9.

Kelly, V, Mueller, M & Sinacore, D 2000, 'Timing of peak plantar pressure during the stance phase of walking. A study of patients with diabetes mellitus and transmetatarsal amputation', *Journal of the American Podiatric Medical Association*, vol. 90, no. 1, pp. 18-23.

Kernozek, T, LaMott, E & Dancisak, M 1996, 'Reliability of an in-shoe pressure measurement system during treadmill walking', *Foot & ankle international*, vol. 17, no. 4, pp. 204-9.

Kim, G, Kang, S, Kang, S, Ryu, J, Mun, M & Kim, K 2009, 'Unlockable knee joint mechanism for powered gait orthosis', *International Journal of Precision Engineering and Manufacturing*, vol. 10, no. 3, pp. 83-9.

Klimiec, E, Zaraska, K, Piekarski, J, Guzdek, P, Kołasczyński, G & Jasiewicz, B 2016, 'Durable sensors for measurement of foot plantar pressure with piezoelectric polyvinylidene fluoride foil', *Sensors and Actuators A: Physical*, vol. 247, pp. 504-13.

Kwan, RL-C, Zheng, Y-P & Cheing, GL-Y 2010, 'The effect of aging on the biomechanical properties of plantar soft tissues', *Clinical Biomechanics*, vol. 25, no. 6, pp. 601-5.

Lai, K, Lin, C & Su, F 1997, 'Gait analysis of adult patients with complete congenital dislocation of the hip', *Journal of the Formosan Medical Association= Taiwan yi zhi*, vol. 96, no. 9, pp. 740-4.

Lawn, MJ, Takashima, M, Ninomiya, M, Yu, J, Soma, K & Ishimatsu, T 2015, 'Development of an actuation system for a rotary hydraulic brake on a low cost light weight knee-ankle-foot orthosis', *2015 IEEE SENSORS*, IEEE, pp. 1-4.

Leardini, A, Sawacha, Z, Paolini, G, Ingrosso, S, Nativo, R & Benedetti, MG 2007, 'A new anatomically based protocol for gait analysis in children', *Gait & posture*, vol. 26, no. 4, pp. 560-71.

Ledoux, WR, Shofer, JB, Cowley, MS, Ahroni, JH, Cohen, V & Boyko, EJ 2013, 'Diabetic foot ulcer incidence in relation to plantar pressure magnitude and measurement location', *Journal of Diabetes and Its Complications*, vol. 27, no. 6, pp. 621-6.

Lemaire, ED, Goudreau, L, Yakimovich, T & Kofman, J 2009, 'Angular-velocity control approach for stance-control orthoses', *IEEE Transactions on neural systems and rehabilitation Engineering*, vol. 17, no. 5, pp. 497-503.

Levangie, PK & Norkin, CC 2000, 'Joint Structure and function: a comprehensive analysis. 3rd', *Philadelphia: FA. Davis Company*.

Lewis, CL, Khuu, A & Marinko, LN 2015, 'Postural correction reduces hip pain in adult with acetabular dysplasia: A case report', *Manual therapy*, vol. 20, no. 3, pp. 508-12.

Liu, RY, Wang, KZ, Wang, CS, Dang, XQ & Tong, ZQ 2009, 'Evaluation of medial acetabular wall bone stock in patients with developmental dysplasia of the hip using a helical computed tomography multiplanar reconstruction technique', *Acta Radiologica*, vol. 50, no. 7, pp. 791-7.

Luo, Z-P, Berglund, LJ & An, K-N 1998, 'Validation of F-Scan pressure sensor system: a technical note', *Journal of rehabilitation research and development*, vol. 35, pp. 186-.

Machado, ÁS, Da Silva, CBP, Da Rocha, ES & Carpes, FP 2017, 'Effects of plantar foot sensitivity manipulation on postural control of young adult and elderly', *Revista Brasileira de Reumatologia (English Edition)*, vol. 57, no. 1, pp. 30-6.

Maeyama, A, Naito, M, Moriyama, S & Yoshimura, I 2009, 'Periacetabular osteotomy reduces the dynamic instability of dysplastic hips', *The Journal of bone and joint surgery. British volume*, vol. 91, no. 11, pp. 1438-42.

Marangoz, S, Atilla, B, Gök, H, Yavuzer, G, Ergin, S, Tokgözoğlu, AM & Alpaslan, M 2010, 'Gait analysis in adults with severe hip dysplasia before and after total hip arthroplasty', *Hip International*, vol. 20, no. 4, pp. 466-72.

Martin, A & Petruceac, D 2017, 'Developmental dysplasia of the hip (DDH)-review of major imaging techniques', European Congress of Radiology 2017.

McKay, MJ, Baldwin, JN, Ferreira, P, Simic, M, Vanicek, N, Wojciechowski, E, Mudge, A, Burns, J & Consortium, NP 2017, 'Spatiotemporal and plantar pressure patterns of 1000 healthy individuals aged 3–101 years', *Gait & Posture*, vol. 58, pp. 78-87.

McMillan, AG, Kendrick, K, Michael, JW, Aronson, J & Horton, GW 2004, 'Preliminary evidence for effectiveness of a stance control orthosis', *JPO: Journal of Prosthetics and Orthotics*, vol. 16, no. 1, pp. 6-13.

Mei, Q, Fernandez, J, Fu, W, Feng, N & Gu, Y 2015, 'A comparative biomechanical analysis of habitually unshod and shod runners based on a foot morphological difference', *Human Movement Science*, vol. 42, p. 38.

Meyer, CA, Corten, K, Fieuws, S, Deschamps, K, Monari, D, Wesseling, M, Simon, JP & Desloovere, K 2015, 'Biomechanical gait features associated with hip osteoarthritis: towards a better definition of clinical hallmarks', *Journal of Orthopaedic Research*, vol. 33, no. 10, pp. 1498-507.

Morag, E & Cavanagh, PR 1999, 'Structural and functional predictors of regional peak pressures under the foot during walking', *Journal of biomechanics*, vol. 32, no. 4, pp. 359-70.

Morton, DJ 1930, 'Structural factors in static disorders of the foot', *The American Journal of Surgery*, vol. 9, no. 2, pp. 315-28.

Mueller, MJ, Diamond, JE, Delitto, A & Sinacore, DR 1989, 'Insensitivity, limited joint mobility, and plantar ulcers in patients with diabetes mellitus', *Physical Therapy*, vol. 69, no. 6, pp. 453-9.

Mulroy, SJ, Eberly, VJ, Gronely, JK, Weiss, W & Newsam, CJ 2010, 'Effect of AFO design on walking after stroke: impact of ankle plantar flexion contracture', *Prosthetics and orthotics international*, vol. 34, no. 3, pp. 277-92.

Murphy, SB, Ganz, R & Müller, M 1995, 'The prognosis in untreated dysplasia of the hip. A study of radiographic factors that predict the outcome', *JBJS*, vol. 77, no. 7, pp. 985-9.

Murray, M, Gore, DR & Clarkson, B 1971, 'Walking patterns of patients with unilateral hip pain due to osteo-arthritis and avascular necrosis', *JBJS*, vol. 53, no. 2, pp. 259-74.

Najafi, B, Barnica, E, Wrobel, JS & Burns, J 2012, 'Dynamic plantar loading index: understanding the benefit of custom foot orthoses for painful pes cavus', *Journal of biomechanics*, vol. 45, no. 9, pp. 1705-11.

Nigg, BM, Cole, GK & Nachbauer, W 1993, 'Effects of arch height of the foot on angular motion of the lower extremities in running', *Journal of biomechanics*, vol. 26, no. 8, pp.909-16.

Nilsson, J & Thorstensson, A 1989, 'Ground reaction forces at different speeds of human walking and running', *Acta Physiologica Scandinavica*, vol. 136, no. 2, pp. 217-27.

Nix, SE, Vicenzino, BT, Collins, NJ & Smith, MD 2013, 'Gait parameters associated with hallux valgus: a systematic review', *Journal of foot and ankle research*, vol. 6, no. 1, p. 9.

Nurse, MA & Nigg, BM 2001, 'The effect of changes in foot sensation on plantar pressure and muscle activity', *Clinical Biomechanics*, vol. 16, no. 9, pp. 719-27.

Parvataneni, K, Olney, SJ & Brouwer, B 2007, 'Changes in muscle group work associated with changes in gait speed of persons with stroke', *Clinical biomechanics*, vol. 22, no. 7, pp. 813-20.

Pataky, TC, Bosch, K, Mu, T, Keijsers, NLW, Segers, V, Rosenbaum, D & Goulermas, JY 2011, 'An anatomically unbiased foot template for inter-subject plantar pressure evaluation', *Gait & Posture*, vol. 33, no. 3, pp. 418-22.

Patil, S, Thatte, MA & Chaskar, U 2009, 'Development of planter foot pressure distribution system using flexi force sensors', *Sensors & Transducers*, vol. 108, no. 9, p. 73.

Pedersen, E, Simonsen, E, Alkjær, T & Søballe, K 2004, 'Walking pattern in adults with congenital hip dysplasia 14 women examined by inverse dynamics', *Acta Orthopaedica Scandinavica*, vol. 75, no. 1, pp. 2-9.

Perry, JE, Ulbrecht, JS, Derr, JA & Cavanagh, PR 1995, 'The use of running shoes to reduce plantar pressures in patients who have diabetes', *JBJS*, vol. 77, no. 12, pp. 1819-28.

Powell, DW, Long, B, Milner, CE & Zhang, S 2011, 'Frontal plane multi-segment foot kinematics in high-and low-arched females during dynamic loading tasks', *Human Movement Science*, vol. 30, no. 1, pp. 105-14.

Putti, A, Arnold, G, Cochrane, L & Abboud, R 2007, 'The Pedar® in -shoe system: Repeatability and normal pressure values', *Gait & Posture*, vol. 25, no. 3, pp. 401-5.

Putti, AB, Arnold, GP, Cochrane, L & Abboud, RJ 2007, 'The Pedar.sup.[R] in -shoe system: Repeatability and normal pressure values.(Author abstract)', *Gait & Posture*, vol. 25, no. 3, p. 401.

Radtka, SA, Skinner, SR & Johanson, ME 2005, 'A comparison of gait with solid and hinged ankle-foot orthoses in children with spastic diplegic cerebral palsy', *Gait & posture*, vol. 21, no. 3, pp. 303-10.

Radtka, SA, Skinner, SR, Dixon, DM & Johanson, ME 1997, 'A comparison of gait with solid, dynamic, and no ankle-foot orthoses in children with spastic cerebral palsy', *Physical therapy*, vol. 77, no. 4, pp. 395-409.

Razak, A, Hadi, A, Zayegh, A, Begg, RK & Wahab, Y 2012, 'Foot plantar pressure measurement system: A review', *Sensors*, vol. 12, no. 7, pp. 9884-912.

Resch, S, Apelqvist, J, Stenström, A & Åström, I 1997, 'Dynamic plantar pressure measurement in 49 patients with diabetic neuropathy with or without foot ulcers', *Foot and Ankle Surgery*, vol. 3, no. 4, pp. 165-74.

Rethlefsen, S, Kay, R, Dennis, S, Forstein, M & Tolo, V 1999, 'The effects of fixed and articulated ankle-foot orthoses on gait patterns in subjects with cerebral palsy', *Journal of Pediatric Orthopaedics*, vol. 19, no. 4, pp. 470-4.

Romano, C, Frigo, C, Randelli, G & Pedotti, A 1996a, 'Analysis of the gait of adults who had residua of congenital dysplasia of the hip', *JBJS*, vol. 78, no. 10, pp. 1468-79.

Romano, C, Frigo, C, Randelli, G & Pedotti, A 1996b, 'Analysis of the gait of adults who had residua of congenital dysplasia of the hip', *JBJS*, vol. 78, no. 10, pp. 1468-79.

Rosenbaum, D, Hautmann, S, Gold, M & Claes, L 1994, 'Effects of walking speed on plantar pressure patterns and hindfoot angular motion', *Gait & Posture*, vol. 2, no. 3, pp. 191-7.

Rupérez, MJ, Martín-Guerrero, JD, Monserrat, C & Alcañiz, M 2012, 'Artificial neural networks for predicting dorsal pressures on the foot surface while walking', *Expert Systems with Applications*, vol. 39, no. 5, pp. 5349-57.

Sánchez-Rodríguez, R, Martínez-Nova, A, Escamilla-Martínez, E & Pedrera-Zamorano, JD 2012, 'Can the Foot Posture Index or their individual criteria predict dynamic plantar pressures?', *Gait & Posture*, vol. 36, no. 3, pp. 591-5.

Sarnow, MR, Veves, A, Giurini, JM, Rosenblum, BI, Chrzan, JS & Habershaw, GM 1994, 'In-shoe foot pressure measurements in diabetic patients with at-risk feet and in healthy subjects', *Diabetes care*, vol. 17, no. 9, pp. 1002-6.

Sawicki, GS & Ferris, DP 2009, 'A pneumatically powered knee-ankle-foot orthosis (KAFO) with myoelectric activation and inhibition', *Journal of neuroengineering and rehabilitation*, vol. 6, no. 1, p. 23.

Searle, A, Spink, M, Ho, A & Chuter, V 2017, 'Association between ankle equinus and plantar pressures in people with diabetes. A systematic review and meta-analysis', *Clinical Biomechanics*, vol. 43, pp. 8-14.

Segal, A, Rohr, E, Orendurff, M, Shofer, J, O'Brien, M & Sangeorzan, B 2004, 'The effect of walking speed on peak plantar pressure', *Foot & ankle international*, vol. 25, no. 12, pp. 926-33.

Shamaei, K, Napolitano, PC & Dollar, AM 2014, 'Design and functional evaluation of a quasi-passive compliant stance control knee-ankle-foot orthosis', *IEEE Transactions on neural systems and rehabilitation Engineering*, vol. 22, no. 2, pp. 258-68.

Shorter, D, Hong, T & Osborn, DA 2013, 'Cochrane Review: Screening programmes for developmental dysplasia of the hip in newborn infants', *Evidence-Based Child Health: A Cochrane Review Journal*, vol. 8, no. 1, pp. 11-54.

Simkin, A, Leichter, I, Giladi, M, Stein, M & Milgrom, C 1989, 'Combined effect of foot arch structure and an orthotic device on stress fractures', *Foot & ankle*, vol. 10, no. 1, pp. 25-9.

Simons, CD, van Asseldonk, EH, van der Kooij, H, Geurts, AC & Buurke, JH 2009, 'Ankle-foot orthoses in stroke: effects on functional balance, weight-bearing asymmetry and the contribution of each lower limb to balance control', *Clinical biomechanics*, vol. 24, no. 9, pp. 769-75.

Singh, A, Srivastava, RN, Shukla, P, Pushkar, A & Ali, S 2014, 'Management of Late Onset Perthes: Evaluation of Distraction by External Fixator—5-Year Follow-Up', *Advances in orthopedics*, vol. 2014.

Skopljak, A, Muftic, M, Sukalo, A, Masic, I & Zunic, L 2014, 'Pedobarography in diagnosis and clinical application', *Acta Informatica Medica*, vol. 22, no. 6, p. 374.

Sneyers, CJL, Lysens, R, Feys, H & Andries, R 1995, 'Influence of malalignment of feet on the plantar pressure pattern in running', *Foot & ankle international*, vol. 16, no. 10, pp. 624-32.

Soames, R 1985, 'Foot pressure patterns during gait', *Journal of biomedical engineering*, vol. 7, no. 2, pp. 120-6.

Statler, TK & Tullis, BL 2005, 'Pes cavus', *Journal of the American Podiatric Medical Association*, vol. 95, no. 1, pp. 42-52.

Stess, RM, Jensen, SR & Mirmiran, R 1997, 'The role of dynamic plantar pressures in diabetic foot ulcers', *Diabetes care*, vol. 20, no. 5, pp. 855-8.

Sucato, DJ, Tulchin-Francis, K, de La Rocha, A, Kulkarni, V & Podeszwa, DA 2015, 'Improved functional outcome with no decrease in hip strength 2 years following Ganz periacetabular osteotomies for adolescent hip dysplasia', *Journal of Pediatric Orthopaedics B*, vol. 24, no. 2, pp. 99-105.

Tian, F, Hefzy, MS & Elahinia, M 2015, 'State of the art review of Knee–Ankle–Foot orthoses', *Annals of biomedical engineering*, vol. 43, no. 2, pp. 427-41.

Vaughan, C, Du Toit, L & Roffey, M 1987, 'Speed of walking and forces acting on the feet', *Biomechanics XA*, pp. 349-54.

Wang, R-Y, Yen, L-L, Lee, C-C, Lin, P-Y, Wang, M-F & Yang, Y-R 2005, 'Effects of an ankle-foot orthosis on balance performance in patients with hemiparesis of different durations', *Clinical rehabilitation*, vol. 19, no. 1, pp. 37-44.

Warren, GL, Maher, RM & Higbie, EJ 2004, 'Temporal patterns of plantar pressures and lower-leg muscle activity during walking: effect of speed', *Gait & Posture*, vol. 19, no. 1, pp. 91-100.

Weinstein, SL 1997, 'Natural history and treatment outcomes of childhood hip disorders', *Clinical orthopaedics and related research*, no. 344, pp. 227-42.

Whittle, MW 1996, 'Clinical gait analysis: A review', *Human Movement Science*, vol. 15, no. 3, pp. 369-87.

Williams, G, Galna, B, Morris, ME & Olver, J 2010, 'Spatiotemporal deficits and kinematic classification of gait following a traumatic brain injury: a systematic review', *The Journal of head trauma rehabilitation*, vol. 25, no. 5, pp. 366-74.

Williams III, DS, McClay, IS, Hamill, J & Buchanan, TS 2001, 'Lower extremity kinematic and kinetic differences in runners with high and low arches', *Journal of applied biomechanics*, vol. 17, no. 2, pp. 153-63.

Woodburn, J & Helliwell, PS 1996, 'Observations on the F-Scan in-shoe pressure measuring system', *Clinical Biomechanics*, vol. 11, no. 5, pp. 301-4.

Xiong, S, Goonetilleke, RS, Rodrigo, WDAS & Zhao, J 2013, 'A model for the perception of surface pressure on human foot', *Applied Ergonomics*, vol. 44, no. 1, pp. 1-10.

Xu, H, Zhou, Y, Liu, Q, Tang, Q & Yin, J 2010, 'Femoral morphologic differences in subtypes of high developmental dislocation of the hip', *Clinical Orthopaedics and Related Research®*, vol. 468, no. 12, pp. 3371-6.

Yakimovich, T, Lemaire, ED & Kofman, J 2009, 'Engineering design review of stance-control knee-ankle-foot orthoses', *Journal of Rehabilitation Research & Development*, vol. 46, no. 2.

Zhang, S & Li, L 2013, 'The differential effects of foot sole sensory on plantar pressure distribution between balance and gait', *Gait & Posture*, vol. 37, no. 4, pp. 532-5.

Zhu, H, Wertsch, JJ, Harris, GF & Alba, HM 1995, 'Walking cadence effect on plantar pressures', *Archives of physical medicine and rehabilitation*, vol. 76, no. 11, pp. 1000-5.

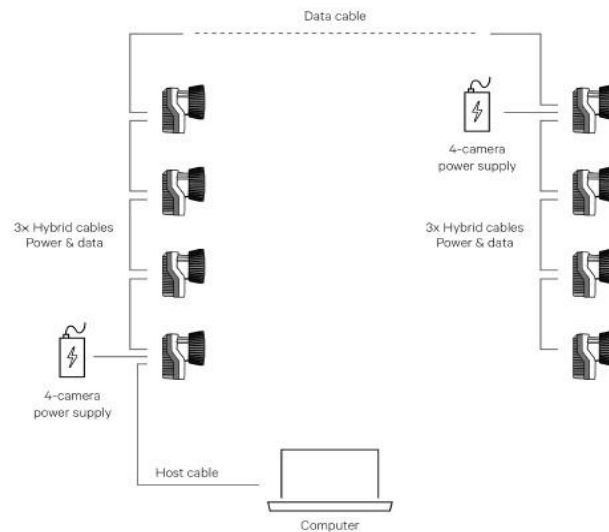
Zulkifli, SS & Ping, LW 2018, 'A state-of-the-art review of foot pressure', *Foot and Ankle Surgery*.

APPENDIX

Qualysis track manager setting up process and specifications

System setup

Note: When the cables have been connected correctly the LEDs on the back of the Oqus will be lit. The **EXT** LED will be lit green and the **ACT** LEDs will be blinking. However, the connection of the power adapters does require some attention. One power adapter can power up to 4 Oqus cameras. Therefore, the connection of a camera system comprising of more than four cameras must look something like the image below.



This means that you must use the following cables for an 8 camera system:

- 1 host cable between computer and camera.
- 6 bundled cables with power and data.
- 1 data cable connected between camera 4 and 5 in the setup, because one AC/DC adapter can only power 4 cameras.
- 2 AC/DC adapters, connected to for example camera 1 and 5.

Note: For more detailed information about the Oqus system, please refer to the QTM manual or the Oqus setup guide.

Oqus connectors

The back of the camera holds six connectors for power, data and control connections. The view differs slightly depending on the type of camera. The image below shows the standard version of the camera. The water protected version uses different connectors and lacks the LEDs found on the standard version.

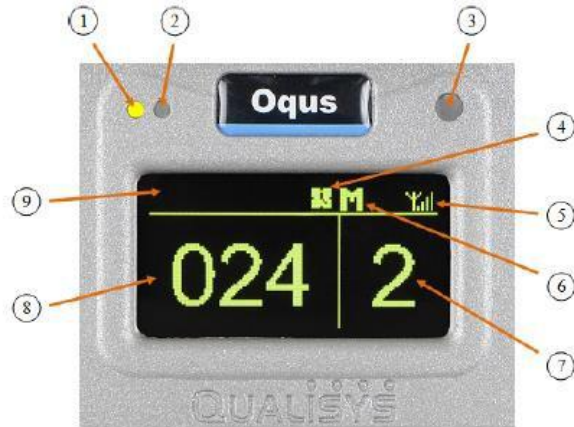


1. **Left Data port, Right Data port (light blue)**
 Ethernet connector. 100BaseTX/802.3i, 100 Mbps, Fast Ethernet. The two ports are identical.
2. **Left Ethernet activity indicator, Right Ethernet activity indicator**
 Shows the status of the Ethernet connection. Fixed green light means that a carrier signal has been detected and that the connection is up. Flashing green light indicates that data is received and/or transmitted.
3. **Battery port (white)**
 Used to supply the camera with power from an Oqus compatible battery.
4. **Battery status indicator**
 Lit green when the camera is supplied through the **BATTERY** port.
 Lit red when a voltage outside the specified range (10-16V) is connected to the port.
5. **Power supply status**
 Lit green when the camera is powered through one of the **POWER** ports. A red light indicates internal power supply error.
6. **Left power supply port, Right power supply port (black)**
 Daisy-chain power port. Supplies the camera with 48VDC and can be daisy chained to supply cameras further down the chain with power. The ports are identical there is no specific in-port or out-port.
7. **Control port (light grey)**
 The control port is used to synchronize the camera with external sources, and contains pins for e.g. external trigger in, external sync in and external sync out. Splitter cables are needed to connect one or more BNC cables to this port.
8. **Camera identification**
 This label provides information on:
 - The serial number of the camera
 - The product number
 - The Ethernet Mac address
 - The WLAN Mac address

Oqus camera display

The Oqus camera has a large graphical OLED display and three LEDs on the front to inform the user of the current status of the camera. The display shows, among other things, the camera number and the number of markers currently seen by the camera.

📌 Note: The display will be turned off when the camera enters stand-by mode, i.e. if the camera has not been in use for 2 hours. Start a preview in QTM to light up the display again.



1. **Measurement status indicator**
 Green light - The camera is ready to start a measurement
 Yellow light - The camera is measuring
 Flashing green light - Waiting for trigger to start measurement
 Flashing yellow light - Waiting for trigger to switch from pre-trigger to post-trigger measurement
2. **Error indicator**
 A red light indicates that an error has occurred. The LED is blinking when a software error occurs and is lit constantly if a hardware error occurs.
3. **IR receiver**
 The IR receiver is used for synchronization with certain active markers. It detects modulated light with a frequency of 33 kHz and is sensitive to light with wavelengths between 800 and 1100nm.
4. **Synchronization status**
 During the synchronization phase this symbol is flashing. When the camera is synchronized with the master camera in the system it becomes stable.
5. **WLAN indicator**
 This symbol is displayed when the WLAN of the camera is activated.
6. **Master/Slave indicator**
 An M indicates that the camera is master for the system and by that controls for example internal synchronization. An S indicates that the camera is a slave. The indicator can also be a rotating + sign, which means that the camera is looking for the Master camera.

7. **Camera number**

The area to the right usually shows the camera number that the camera has in QTM. The camera number can be changed with the **Reorder** tool in the 2D view window. This number is stored in the camera so it is shown at the next camera startup.

🔧 Note: If the camera has never been connected to QTM the last three digits of the serial number (upper part) and the last octet of the IP-number assigned to the camera (lower part) will be shown instead. This can also be activated from the QDS menu, see "QDS" on page 14.

8. **Marker area**

During a marker measurement this area shows the number of markers currently seen by the camera. When the camera is idle or is collecting video, this area shows '-----'.

9. **Text area**

This area is used for scrolling text messages, for example during startup.

Setting the aperture and focus (Oqus)

For Oqus it is very important to set the aperture and focus correctly for your measurement volume. If these are not set correctly the cameras will not reach their full potential in detecting markers. Follow this procedure to set the aperture and focus.

1. For cameras with manual lens control, turn the strobe part of the camera counterclockwise to expose the lens for adjustment. For Oqus 7+ cameras with motorized lenses the aperture and focus can be controlled in QTM via the Lens Control interface in the Camera Settings sidebar in the 2D View window (see "Camera settings sidebar" in the QTM manual).

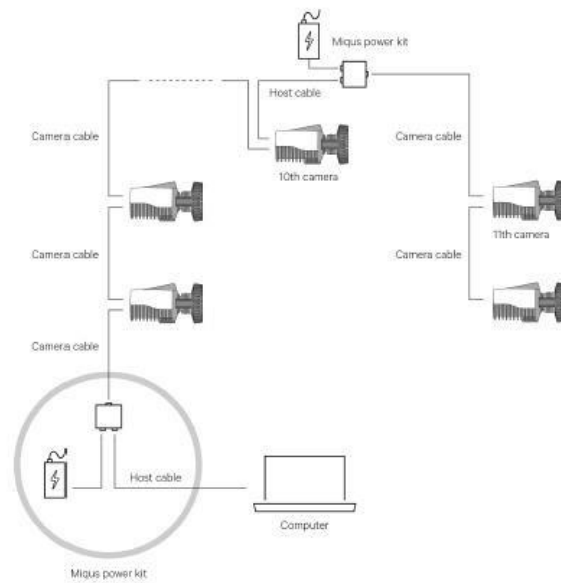


2. Set the aperture. The recommended value is 2.8 (or the lowest value if 2.8 is not available).

🔧 Note: If a larger focal depth is needed, the aperture can be set at a higher value. You can use the **Marker intensity** mode in the 2D view in QTM to check if the markers are bright enough. Note that by increasing the aperture by one f-stop (e.g., from 2.8 to 4) the light intensity is reduced by half.

🔧 Note: At larger distance a lower aperture value may help to increase the light intensity of the markers. However, note that this may lead to deformation of the markers, especially in the vicinity of the corners.

System setup

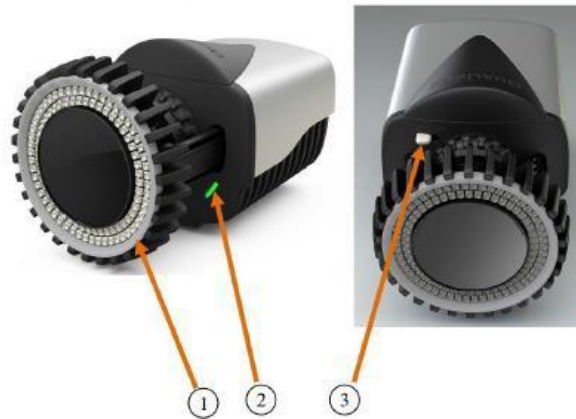


When the cables have been connected correctly, the indicator LEDs at the Miquis data/power ports will be lit as indicated in the illustration below. For more information about the connectors and the function of the indicators, see the Sections "Miquis camera: front side" on the facing page and "Miquis camera: back side" on page 12.



 **Note:** For more detailed information about the Miquis system, please refer to the QTM manual or the Miquis setup guide.

Miqus camera: front side



1. LED ring

LED ring for camera identification and indication of status during startup sequence.

- Green light: Active camera indicator (see “Identifying the cameras (Miqus)”)
- Pulsing green light: Camera system being calibrated
- Amber light: Camera is booting
- Pulsing amber light: Camera is waiting for IP address

2. Measurement status indicator

- Green light: The camera is ready to start a measurement
- Yellow light: The camera is measuring
- Flashing green light: The camera is synchronizing to the master camera
- Flashing red light: Error signal

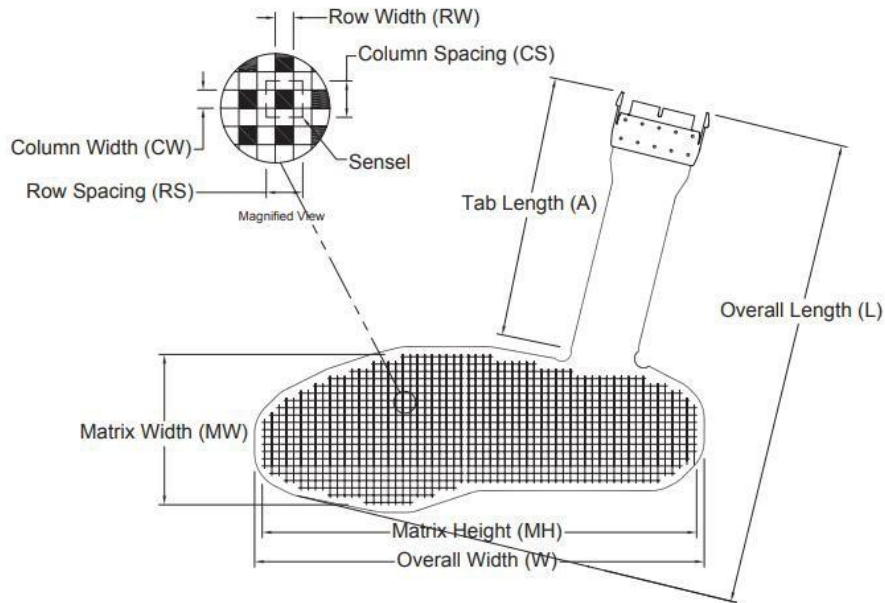
3. Lock lever

- Lock/unlock the strobe mechanics

7.1 2-IN SOLE SHOES F-SCAN SYSTEM SPECIFICATIONS



PRESSURE MAPPING, FORCE MEASUREMENT, AND TACTILE SENSORS



General Dimensions			Sensing Region Dimensions						Summary			
Overall Length <i>L</i>	Overall Width <i>W</i>	Tab Length <i>A</i>	Matrix Width <i>MW</i>	Matrix Height <i>MH</i>	Columns			Rows			Total No. of Sensels	Sensel Spatial Resolution (sensels per sq-cm)
(mm)	(mm)	(mm)	(mm)	(mm)	Pitch <i>CW</i>	Pitch <i>CS</i>	<i>Qty.</i>	<i>RW</i>	Pitch <i>RS</i>	<i>Qty.</i>		
327.2	313.7	182.6	106.7	304.8	2.5	5.1	21	2.5	5.1	60	954	3.9
12.88	12.35	7.19	4.20	12.00	0.100	0.200	21	0.100	0.200	60	954	25.0

Pressure Ranges		
kPa	517	862
psi	75	125